Master's thesis

NTNU
Norwegian University of Science and Technology
Faculty of Information Technology and Electrical Engineering
Department of Electric Power Engineering

Emilie Bøe Surdal

Robust Control of Nonlinear Wind Energy Conversion Systems:

A scalable and adaptive energy-based approach for cascaded interconnections

Master's thesis in Energy and Environmental Engineering
Supervisor: Gilbert Bergna-Diaz
June 2023

NTNU
Norwegian University of Science and Technology

Emilie Bøe Surdal

Robust Control of Nonlinear Wind Energy Conversion Systems:

A scalable and adaptive energy-based approach for cascaded interconnections

Master's thesis in Energy and Environmental Engineering
Supervisor: Gilbert Bergna-Diaz
June 2023

Norwegian University of Science and Technology
Faculty of Information Technology and Electrical Engineering
Department of Electric Power Engineering

NTNU
Norwegian University of
Science and Technology

Abstract

This master thesis aims to provide a large-signal stability certificate for a wind energy conversion system consisting of a wind turbine (WT) connected to a permanent magnet synchronous generator (PMSG), followed by a full-scale back-to-back two-level voltage source converter (2L-VSC) connected to the grid.

A fundamental step towards our goal is to first *force* a cascaded structure in the dynamical system of interest, such that the overall system is decomposed as a cascade connection of two subsystems, with a leader-follower composition. Under this configuration, the leader subsystem is unaffected by the rest of the system, while the follower considers the leader as input or disturbance. In this way, the two subsystems can be considered almost separately, making the stability analysis and control design arguably less complex. Second, both subsystems are modeled using the *port-Hamiltonian* framework as a useful starting point for the control design while preserving the challenging non-linearities in the generator dynamics, power converters, and between wind speed and mechanical torque. The leader subsystem, consisting of the wind turbine, PMSG, and a converter, must extract maximum power from the wind. Towards this end, the chosen controller for the closed loop is the proportional-integral current controller, which we show via *passivity* arguments to have prominent plug-and-play features, provided sufficient mechanical damping is available. Analyzing the system stability through Lyapunov's direct method shows that global asymptotic stability is guaranteed.

To address the issue of inaccurate wind speed knowledge, which affects the optimal operation of the conversion system, we design an adaptive control law based on Immersion and Invariance (I&I). We applied this methodology with three different degrees of model complexity; i.e., we first utilize the I&I procedure to estimate the mechanical torque when considered as a constant, then by rewriting $T_m = \frac{P}{\omega_m}$ and estimating the mechanical power, and finally to estimate the wind speed, accounting for all the non-linearities. All three I&I estimators demonstrate high convergence speed and provide accurate results. Additionally, when confronted with the non-linearities between wind and torque, it is observed that there are multiple solutions for the rotor speed given a specific torque. Consequently, an outer loop is added to the simulations, although it has not been included in the stability proof, and further investigation is necessary to establish its formal validation.

Similarly, perfect information of the equilibrium to be stabilized is not available for the follower system comprised of the grid-side converter and the grid. With the goal of *practically* regulating the dc voltage of the 2L-VSC to *approximately* a desired reference, a proportional-leaky- integrator (PLI) passivity-based controller (PBC) is implemented as the controller for the grid-side converter. The aim is to design the integral action in such a way that when having inaccuracies in the model, the leakage term acts similar to a *droop* controller, consequently limiting deviations while guaranteeing global asymptotic stability. Initially, a PLI-PBC (a PI with an additional leakage term in the integral channel) was considered. However, this resulted in poor performance characterized by high peaks and oscillations when the leakage was significant. As a result, the controller was modified to only include the passive output in one of the controller inputs, giving the possibility of indirectly doing voltage control while performing q-axis current control with the other control input. Interestingly, this modification did not affect the stability properties of the controller, and its proof is considered to be one of the main contributions of the manuscript.

Simulations are carried out for the leader system (WT, PMSG, machine side 2L-VSC) and follower (grid-side 2L-VSC, grid) system separately. When including an outer loop controller for the mechanical rotor speed, the system is observed to have characteristics associated with a non-minimum-phase system. To address this, the outer loop is designed sufficiently slow to mitigate the consequences associated with such a system. Finally, the two systems are combined, and simulations are performed for the entire system to validate the theoretical results obtained.

Sammendrag

Denne masteroppgaven har som mål å utlede et stabilitetssertifikat for et konverteringssystem bestående av en vindturbin (WT) koblet til en permanentmagnet-synkron generator (PMSG), etterfulgt av en fullskala to-nivå spenningskildeomformer (2L-VSC) koblet til strømnettet.

Et grunnleggende trinn mot vårt mål er å først *tvinge* en kaskade-struktur i det dynamiske systemet, slik at det overordnede systemet blir dekomponert som en kaskadekobling av to delsystemer med en leder-følger-sammensetning. Under denne konfigurasjonen påvirkes ikke lederdelen av resten av systemet, mens følgerdelen betrakter lederen som input/forstyrrelse. På denne måten kan de to delsystemene betraktes nesten separat, noe som gjør stabilitetsanalyse og kontrollutforming mindre komplekst. Videre modelleres begge delsystemene ved hjelp av *port-Hamiltonian* rammeverket som et nyttig utgangspunkt for kontrollutformingen samtidig som de utfordrende ikke-linearitetene i generatordynamikk, kraftomformere og mellom vindhastighet og mekanisk dreiemoment opprettholdes. Lederdelen, bestående av en vindturbinen, PMSG og en omformer, må utvinne maksimal effekt fra vinden. Til dette er den valgte kontrolleren for lukket sløyfe en proporsjonal-integrerende strømregulator, som vi viser via *passivitets*-argumenter har fremtredende plug-and-play-egenskaper, forutsatt at tilstrekkelig mekanisk demping er tilgjengelig. Analyse av systemets stabilitet gjennom Lyapunovs metode viser at global asymptotisk stabilitet er garantert.

For å håndtere problemet med unøyaktig kunnskap om vindhastighet, som påvirker optimal drift av konverteringssystemet, designer vi en adaptiv kontrolllov basert på Immersion and Invariance (I&I). Vi bruker denne metodikken med tre ulike grader av modellkompleksitet; det vil si, vi bruker først I&I-prosedyren for å estimere det mekaniske momentet når det betraktes som konstant, deretter ved å omskrive $T_m = \frac{P}{\omega_m}$ og estimere den mekaniske effekten, og til slutt for å estimere vindhastigheten med hensyn til alle ikke-lineariteter. Alle tre I&I-estimatene viser høy konvergenshastighet og gir nøyaktige verdier. I tillegg, når vi står overfor ikke-lineariteten mellom vindhastighet og mekanisk dreiemoment, observeres det at det finnes flere løsninger for rotasjonshastigheten gitt et spesifikt dreiemoment. Som et resultat blir det lagt til en kontroller i en ytre sløyfe i simuleringene, selv om den ikke er inkludert i stabilitetsbeviset. Videre undersøkelser er derfor nødvendig for å etablere stabilitetsbeviset med denne inkludert.

På samme måte forventes det ikke perfekt informasjon om likevektspunktet for følgersystemet bestående av nettsideomformeren og resten av nettet. Med målet om å *praktisk talt* regulere likestrømspenningsnivået til 2L-VSC *tilnærmet* en ønsket referanse, implementeres en passivitets-basert proporsjonal-lekkasje integrator (PLI-PBC) som kontroller for nettside-omformeren. Målet er å utforme integralaksjonen slik at når det er unøyaktigheter i modellen, fungerer lekkasjetermen lignende en *droop*-kontroller og begrenser avvik samtidig som global asymptotisk stabilitet garanteres. I utgangspunktet ble en PLI-PBC (PI med en lekkasje i integralkanalen) vurdert. Imidlertid resulterte dette i dårlig ytelse preget av høye topper og oscillasjoner når lekkasjen var betydelig. Som et resultat ble kontrolleren endret for å bare inkludere den passive utgangen i en av kontrollerinngangene, noe som gir muligheten for indirekte spenningsregulering samtidig som q-aksestrømregulering utføres med den andre kontrollerinngangen. Interessant nok påvirket ikke denne endringen stabilitetsegenskapene til kontrolleren, og dens bevis betraktes som en av hovedbidragene i manuskriptet.

Simuleringer utføres både for lederdelen (WT, PMSG, maskinside 2LVSC) og følgerdelen (nettside 2LVSC, nett) separat. Når en ytterligere løkkekontroller for den mekaniske rotasjonshastigheten inkluderes, observeres det at systemet har karakteristika assosiert med et ikke-minimumsfase-system. For å takle dette utformes den ytre løkken til å operere tilstrekkelig sakte for å begrense konsekvensene forbundet med et slikt system. Til slutt kombineres de to systemene, og simuleringer utføres for hele systemet for å validere de teoretiske resultatene som er oppnådd.

Acknowledgement

I would like to express my sincere gratitude to my supervisor, Professor Gilbert Bergna-Diaz, for all his support and guidance throughout my final year at university. His expertise, passion for the field, and ability to make every subject interesting have been a huge motivation for me.

I would also like to thank my fellow students who have made this year the most memorable and rewarding period of my education. I would like to give a special thanks to "the corner office" for all the laughter and countless moments of joy. The engaging discussions and assistance provided by this group have been truly invaluable.

Table of Contents

List of Figures

List of Tables

List of Abbreviations

d-axis	-	Direct axis
EIA	-	Energy Information Administration
IEA	-	International Energy Agency
LCF	-	Lyapunov candidate function
P controller	-	Proportional controller
PBC	-	Passivity-based controller
pH	-	Port-Hamiltonian
PI controller	-	Proportional integral controller
PMSG	-	Permanent magnet synchronous generator
PnP	-	Plug-and-Play
q-axis	-	Quadrature axis
WECS	-	Wind energy conversion systems
2L-VSC	-	Two-level voltage source converter
VRE	-	variable input renewable energies
RoCoF	-	rate of change of frequency

Chapter 1

Introduction

1.1 Introduction

As our world urgently needs to transition to renewable energy, wind power has emerged as a critical player in achieving a more sustainable future. This type of energy source has seen a rapid increase in popularity due to its ability to provide clean, reliable, and cost-effective energy [1]. However, with this growth comes the challenge of integrating large amounts of wind power into the existing electrical grid, where advanced control strategies are in high demand to manage the power output of the wind turbines. The International Energy Agency's (IEA) report from 2021 found a 5% rise in electricity demand in 2021, where renewable energy sources only cover about half of the increase.[2] Further, Energy Information Administration (EIA) projects a nearly 50% increase in energy demand by 2050, driven by growth in both population and economy. A rapid growth in fossil fuels, notably coal power, is therefore threatening record levels of emissions in the electricity sector [3]. Already, wind energy fulfills 15% of Europe's total electricity demand, with 17.4 GW of new installations in 2021, but the rise in installations will need to accelerate to keep up with the demand.

The integration of variable input renewable energies (VRE) poses several security of supply problems, and inverter-based sources - mainly wind and solar PV - are especially challenging due to the variable and uncertain power generation and the non-synchronous interface with the grid. In the analysis "Technical Shortfalls for Pan European Power System with High Levels of Renewable Generation" [4] concluded in 2020, they identified significant challenges with the rapid growth of VREs. They observed a general trend towards lower frequency nadirs, that is, the minimum value the frequency reaches during a transient period. Regarding frequency stability, one of the most critical problems is that synchronous inertia falls as the share of VRE increases, which leads to faster frequency dynamics. Synchronous inertia is the energy stored in the rotating masses synchronized to the system and acts to resist any imbalance between supply and demand. If a system inherits high synchronous inertia, it will have a lower rate of change of frequency (RoCoF) after an imbalance, which hinders the power system frequency from leaving the predefined range for which the system can operate securely.

In regards to voltage stability, it is observed that as the VRE-share increases and the conventional generation is replaced, there will be a significant lack of steady-state reactive capability, which leads to degradation in dynamic voltage performance. Lastly, for the transient stability, having fewer synchronous generators online led to lower synchronous torque on the system, and some localized scarcities were identified, but no system-wide scarcities were observed. [4] [5]

One of the primary objectives in the evolution of wind energy conversion systems is the aim of obtaining plug-and-play solutions where wind energy can easily be integrated into the existing infrastructure. Plug-and-play (PnP) solutions hold significant importance as they offer adaptability to various systems and networks with minimal modifications, easing the transition to a high proportion of renewable energy. This requires control strategies that can respond to real-time changes in demand. The race to find optimal solutions to the new challenges is intensifying as the world seeks to rapidly transition to a more sustainable energy future.

In this thesis, we investigate PMSGs connected to wind turbines in the context of increasing the integration of renewable energy sources, especially sources that have less contribution of inertia to the grid, such as wind power, due to being separated from the grid via converters. We examine the theoretical foundation of nonlinear control theory and the practical implementation of these in wind power conversion systems. The goal, in general, is to obtain stability certificates for the power systems to optimize production and contribute to accelerating the energy transition.

Many of the studies done on WECS are based on double-fed induction generators due to the economic aspect. These have high efficiency and good controllability and require lower converter ratings. [6] Nevertheless, in the last few years, the permanent magnet synchronous generator (PMSG) has become more popular. There are several advantages of using this generator instead of an induction generator. One of these is that the PMSG does not require a gearbox, giving higher overall efficiency and reliability, little need for maintenance, and reduced weight. In addition, external excitation is not needed [7].

Control theory plays a critical role in the optimization of wind turbines with permanent magnet synchronous generators (PMSG). The ability to adjust the torque and power output of the generator in response to changing wind speeds is crucial for maximizing the stability and efficiency of the system. Nonlinear control theory, such as Lyapunov's direct method, provides powerful frameworks for designing control strategies to achieve the desired performance objective while still ensuring stability in the face of disturbance and uncertainty.

Load flow calculations are used to model and analyze the behavior of power systems in steady-state. These calculations involve solving a set of algebraic equations describing the dynamics of a network of interconnected components such as generators, transmission lines, and loads. The load flow study aims to determine the steady-state operation conditions, such as currents and voltages. However, it is impossible to implement a perfect mathematical model of a physical system in a load flow calculation due to parametric uncertainties and/or unexpected disturbances. This means there will always be some degree of error or approximation in the model. As a result, the reference value for the calculated equilibrium point may deviate from the actual equilibrium point in the real world, and any load flow calculation based on an imperfect mathematical model will only provide an approximation of the real-world operating conditions.

Various techniques can be used to mitigate the error in load flow calculations. One technique is to conduct detailed measurements and analyses of the physical system. Another technique is to perform sensitivity analysis to identify the most significant factors that affect the accuracy of the model and adjust the model accordingly. In this thesis, two distinct methods will be investigated; each applied to different aspects of the system. An adaptive control viewpoint based on *immersion and invariance* (I&I) is explored for one part of the system. This will be used to estimate the wind speed and to make the estimated equilibrium point eventually converge to the real-world equilibrium point. For another section of the system, the proportional-integral passivity-based controller (PI-PBC) is modified to include leakage in the integral action to limit deviations in the presence of imperfect knowledge of the system.

In summary, we aim to contribute, if modestly, to the development of plug-and-play solutions

for integrating wind energy into the existing infrastructure. By deriving large-signal stability certificates, we ensure the stability of the wind energy conversion system, even under significant changes in power flow. This is of particular interest to make the renewable energy transition more seamless.

1.1.1 Objectives

The objective of this thesis is to derive a large-signal stability certificate for a wind turbine connected to a PMSG, followed by a full-scale back-to-back two-level voltage source converter connected to the grid. This will be done by taking into consideration the inaccurate knowledge of the equilibrium to be stabilized. The Immersion & Invariance methodology will be utilized to derive a wind speed estimator, while a PI- Passivity-based controller will be modified to mitigate the error induced by possessing inaccurate information about the system. More precisely, the objectives are to

i: Force the overall system to have a cascade connection of two subsystems with a leader-follower composition
ii: Derive a shifted port-Hamiltonian model for both the leader and follower system.
iii: Create a wind speed estimator using the I&I estimation technique.
iv: Design a controller with large signal stability guarantees for the WT side 2L-VSC, capable of extracting maximum power from the wind.
v: Similarly, design a controller with large signal stability guarantees for the grid side converter capable of regulating the voltage within an acceptable range under parametric uncertainties and the presence of unexpected disturbances.
vi: Simulate the overall system in Matlab/Simulink.

1.2 Limitation of Scope

This thesis is subject to certain limitations imposed by various assumptions. The following limitations should be considered:

1. **Grid Model**: The grid is modeled as a stiff grid, assuming ideal conditions. However, in real-world scenarios, the grid may exhibit varying degrees of impedance and behavior. The simplification of a stiff grid may not capture the full dynamics and interactions with the wind energy conversion system.
2. **Synchronous Generator Model**: The model of the synchronous generator employed in this thesis is a simplified version. It neglects hysteresis losses and magnetic saturation effects due to their relative magnitude. Additionally, assumptions are made regarding the even distribution of the magnetic field and the sinusoidal distribution of the magnets' field. Furthermore, the inductances and resistances are assumed to be independent of frequency. These simplifications may not fully capture the behavior of the generator under certain operating conditions.
3. **Damper Windings**: The damper windings on the rotor of the generator are considered only in terms of their damping effect. Neglecting the effect of flux linkages simplifies the model but may not provide a fully representative picture of the generator's behavior under specific operating conditions. However, proper design of the control system can help mitigate this limitation.

4. **Losses and Switching Effects**: While physical components inherently incur losses, a conductance term (G') is added to the capacitor to account for these losses. However, the modeling of switching losses is neglected, even though it can be argued that they could be incorporated into the parameter G'.

5. **Synchronisation to the grid via PLL**: It is assumed that the converters are synchronized to the grid via a Phase-locked loop (PLL). However, for the purposes of this thesis, the PLL is not explicitly considered, but the synchronous reference frame (SRF) for PLL is considered to align the d-axis with the voltage vector; hence V_q^G is zero. [8] This decision is justified for two reasons: firstly, the main focus of the thesis is on its own contribution rather than complementary features; and secondly, the synchronization process is assumed to have faster dynamics compared to the control of the system itself. Therefore, to some extent, it can be argued that the PLL can be neglected.

These limitations should be acknowledged and taken into account when interpreting the results and conclusions of this thesis. They present opportunities for future research and further refinement of the modeling and control strategies employed in wind energy conversion systems.

1.3 Thesis Structure

The outline of the thesis is structured as follows. Chapter two presents the theoretical framework required to understand the concepts presented in the thesis. In addition, the overall system and its configuration are presented.

In chapter three, the subsystem consisting of a wind turbine, PMSG, and machine side 2L-VSC is modeled using the port-Hamiltonian framework, and the stability is investigated using Lyapunov direct method under a standard PI current control. Three distinct estimators based on Immersion and Invariance are proposed, and simulations are performed to validate both the stability of the system and the estimators.

Similarly, in chapter four, the stability of the subsystem comprised of the grid-side 2L-VSC and the grid is investigated using Lyapunov direct method. Several controllers are proposed, ending with a modified version of the PLI-PBC. The section concludes by presenting the simulation results for the subsystem.

Furthermore, chapter five gives the simulation results when the complete system is modeled in order to demonstrate the effectiveness of our proposal. The thesis is finalized with some concluding remarks and suggestions for further work in chapter six, before the appendix, which in turn contains an attempt to find an estimator for the flux parameter.

Chapter 2

Preliminaries and System Configuration

2.1 Preliminaries for Non-linear Control Theory

The theory that is presented in this section is theory essential for the understanding of the work that will be presented. The preliminaries about port-Hamiltonian and Lyapunov stability are taken from the project thesis [9] completed prior to this master's thesis.

2.1.1 Port-Hamiltonian Modeling

The port-Hamiltonian (pH) modeling framework is a mathematical approach for representing physical systems described by first-order differential equations. This framework is based on the principle of energy conservation, which is a fundamental physical principle that applies to both linear and nonlinear systems. The pH modeling framework views a system as the interconnection of several energy-storing subsystems, which generally are represented by three types of ideal components: energy-storing, energy-dissipating, and energy-routing elements.

One of the key advantages of using the pH modeling framework is its ability to compactly and intuitively model nonlinear networks. The use of the port Hamiltonian framework allows for a unified description of the system's dynamics, and facilitates the integration of different energy domains in a modular and scalable way. This makes it a useful tool for studying complex, nonlinear systems in fields such as engineering. In addition, an important feature is that a power-preserving interconnection of pH systems again gives a pH system, where the total Hamiltonian is the sum of the Hamiltonian functions. [10]

It is further known that nonlinear systems can be written in the general form $\dot{x} = f(x, u)$, $y = h(x, u)$. Such a system, where $x \, \epsilon \, \mathcal{X}$ and u, $y \, \epsilon \, \mathbb{R}^m$, is called passive if there exist a storage function $\mathcal{S}(x) \geq 0 : \mathcal{X} \rightarrow \mathbb{R}$, which satisfy the inequality in equation (2.1.1).

$$\frac{d}{dt}\mathcal{S}(x(t)) \leq u^T(t)y(t) \tag{2.1.1}$$

The right-hand side of the above equation can be interpreted as the supplied power and $\mathcal{S}$ as the stored energy. If the equation also holds for equality, the system is called lossless. A passive system

will never be able to store more energy than what is being supplied. [10] It is well known that port Hamiltonian systems take the same form as in (2.1.1), hence being passive with respect to the port variables and storage function.

If, for a system, there are 1) no algebraic constraints between the state variables, 2) the external port variables can be split into input and output variables, and 3) the resistive structure is linear and on the input-output form, then the subclass input-state-output port-Hamiltonian systems occur. This class of systems provides a valuable starting point for establishing a Lyapunov function used in developing control strategies, where passivity is intimately related to Lyapunov stability.

2.1.2 Lyapunov Stability Analysis

Stability theory is essential in control theory and engineering. For linear time-invariant systems, $\dot{x}(t) = Ax(t)$, stability can be investigated through eigenvalues of A and linearization around the equilibrium point. [11] This is disadvantageous for nonlinear systems because linearization will only be valid for the exact point of operation and only for minor disturbances. This results in the stability conclusion being highly dependent on the initial values for the linearization. An alternative would be to simulate the system and check for stability. Still, in theory, this would correspond to infinite simulations since the initial values are constantly changing.

The Lyapunov stability method is based on the concept of a Lyapunov function; a mathematical function used to determine a system's stability. The Lyapunov stability method avoids integration and linearization, therefore independent of the initial conditions. This function is defined over the entire phase space of the system rather than a single point, giving a global view of the system's stability. Furthermore, since this method works with the vector field instead of the integral of the vector field, it can be applied to a wide range of systems, both linear and nonlinear. This makes it a more versatile and general method for stability analysis. On the other hand, there seems to be no systematic method to establish a Lyapunov function. Nevertheless, there are natural function candidates, like energy functions in electrical and mechanical systems. This latter method will be utilized in this thesis.

To investigate if the system is globally asymptotically stable, some criteria need to be fulfilled. $\mathcal{V}$ is a strict Lyapunov function if $\mathcal{V}$ is continuously differentiable, and:

i: $\mathcal{V}(\bar{x}) = 0$
ii: $\mathcal{V}(x) > 0$ in $\mathbb{R}^n \backslash \{\bar{x}\}$
iii: $\dot{\mathcal{V}}(\bar{x}) = 0$
iv: $\dot{\mathcal{V}}(x) < 0$ in $\mathbb{R}^n \backslash \{\bar{x}\}$

Where $\bar{x}$ describes the states at the equilibrium point. If instead of being defined for all $x \in \mathbb{R}$, the conditions is defined for all $x \in \mathbb{D}$, then the system will be regionally (in $\mathbb{D}$) asymptotically stable. Furthermore, it should also be noted that if a system is Lyapunov stable, and the Lyapunov function $\mathcal{V}(x, x_c)$ is the sum of two positive definite functions, $\mathcal{V}_1(x) + \mathcal{V}_2(x_c)$, then there exist two passive functions connected in feedback. This will be relevant for the implementation of PI-PBC. [12]

2.1.3 Immersion and Invariance

To determine the steady-state operation conditions of a system, load flow calculations are performed. However, in real-life applications, perfect information of the system is rarely available.

This lack of accurate information can lead to slight deviations between the calculated equilibrium and the actual equilibrium point, thereby affecting the optimal operation of the system. Several factors contribute to the error in load flow calculations, including the accuracy of the data used in the model, such as the parameters of the network components. Other factors can be external factors such as weather conditions, equipment failures, and operating temperatures. In addition, the complexity of the model itself, which can range from a simple representation to a highly detailed and comprehensive model that includes a large number of components and operating conditions is also a factor. Such systems, as e.g. power systems, can be difficult to imitate. To address these challenges, the immersion and invariance (I&I) technique can be employed to estimate the uncertain parameters, converging to the actual values and achieving global asymptotic stability. [13] The use of this approach can remove the need for sensors and provide more accurate information about the parameters.

I&I is a method to design asymptotically stabilizing and adaptive control laws for nonlinear systems. The approach does not invoke certainty equivalence nor requires a linear parameterization. A shortcoming with the classical adaptive control is that the estimation error only guarantees to be bounded and converge to an unknown constant, and the dynamical behavior can be hard to foresee. In addition, there is a strong coupling between the plant and the estimator dynamics, resulting in an inherent limitation on the achievable performance. However, I&I overcomes these limitations and introduces techniques for shaping the estimation error's dynamic response while still guaranteeing global asymptotic stability. [14]

This technique of estimating uncertain parameters is already used in several applications. In [15], the Immersion and Invariance theorem is presented for glucose regulation in type-I diabetes patients. The glucose-insulin metabolism is often considered to be an uncertain parameter in other studies, but by utilizing I&I, the study can estimate the uncertain parameters. In [16], the methodology is used to obtain an estimator that guarantees to converge to the true value, to estimate the mass of a VTOL(Vertical Take-Off and Landing) vehicle. In addition to utilizing I&I for stabilization of equilibrium points, in [17], they demonstrates the effectiveness of also utilizing I&I for achieving orbital stabilization. Their results are validated by several examples, e.g for a 3-phase DC-AC converter with a pure resistive load, and for a cart-pendulum system.

A general example of the method, found in [18], will be provided, having a single uncertain parameter. Consider the system

$$\dot{x} = f(x) + g(x)u \tag{2.1.2}$$

with $u = u(x, \theta)$ and an equilibrium point in $\bar{x}$. Having a single uncertain parameter θ, the error between the estimation parameter and its true parameter value is defined as:

$$e_\theta := \theta^E - \theta, \tag{2.1.3}$$

where the estimator for the unknown parameter can be defined as in the expression below.

$$\begin{aligned} &\theta^E := \beta(x) + \zeta \\ &\Rightarrow \theta = \theta^E - e_\theta = \beta(x) + \zeta - e_\theta \end{aligned} \tag{2.1.4}$$

$\beta(\cdot)$ is a function yet to be specified and contains an adaption gain that impacts the speed of convergence of the estimation process, which you select yourself. The specific form of these laws and equations depends on the particular I&I control strategy used. The time derivative of ζ, $\dot{\zeta}$ is called the update law, and a key step is to find an update law that renders the manifold $\mathcal{M}$ in

(2.1.5) invariant.

$$\mathcal{M} = \{(x, \zeta) \in \mathbb{R}^2 | e_\theta = 0\}. \tag{2.1.5}$$

The update law is typically chosen so that all terms, except for the one containing the error parameter, cancel out in the dynamics of the off-the-manifold coordinates, given in equation (2.1.6).

$$\dot{e}_\theta = \dot{\theta}^E - \dot{\theta} = \dot{\theta}^E = \frac{\partial \beta(x)}{\partial x}\dot{x} + \dot{\zeta} \tag{2.1.6}$$

Further, Lyapunov stability analysis will be applied. One example of a Lyapunov function candidate is the quadratic, positive definite function defined in (2.1.7), and its derivative in (2.1.8). $\beta(\cdot)$ is then selected to ensure that the system has a globally stable equilibrium point and that the error converges to zero.

$$V(e_\theta) = \frac{1}{2}e_\theta^2 \tag{2.1.7}$$

$$\begin{aligned} \dot{V}(e_\theta) &= e_\theta \dot{e}_\theta \\ &= e_\theta \cdot (\frac{\partial \beta(x)}{\partial x}\dot{x} + \dot{\zeta}) \end{aligned} \tag{2.1.8}$$

It is important to note that the specific I&I control strategy employed will determine the precise form of the laws and equations discussed. Details regarding these strategies will be elaborated in subsequent chapters of this thesis.

2.2 System Under Consideration

The wind energy conversion system considered in this thesis consists of a wind turbine connected to a permanent magnet synchronous generator (PMSG), followed by a full-scale back-to-back two-level voltage source converter connected to the grid as illustrated in Figure 2.1.

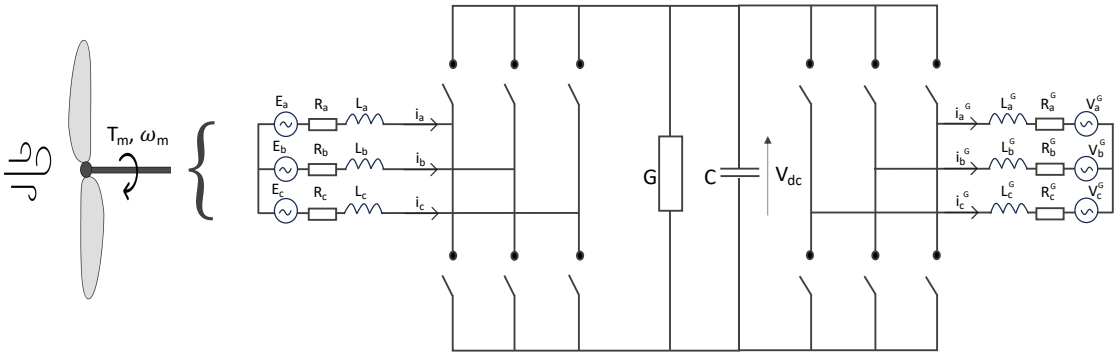

Figure 2.1: The full wind energy conversion system, comprising of the PMSG followed by a full-scale back-to-back 2L-VSC.

This entire system is described by the dynamical expressions below. The two first equations relate to the electrical behaviour of the generator dynamics, while the third equation describes the rotational dynamics of the wind turbine. The expression in (2.2.1d) describes the machine side 2L-VSC and the capacitor, while the two last expressions represent the electrical behavior of the grid side converter connected to the grid.

$$\dot{\Psi}_d = L\dot{i}_d^{(1)} = -ri_d^{(1)} + Li_q^{(1)}\frac{p}{2}\omega_m - u_1^{(1)}v_{dc} \tag{2.2.1a}$$

$$\dot{\Psi}_q = L\dot{i}_q^{(1)} = -ri_q^{(1)} - Li_d^{(1)}\frac{P}{2}\omega_m + \phi\frac{P}{2}\omega_m - u_2^{(1)}v_{dc} \tag{2.2.1b}$$

$$\dot{\rho} = J\dot{\omega}_m = T_m - T_e = T_m - \frac{3}{2}\frac{P}{2}\phi i_q^{(1)} + d(\omega_{ref} - \omega_m) \tag{2.2.1c}$$

$$\dot{q}_{dc} = C\dot{v}_{dc} = -Gv_{dc} + \frac{e_d i_d^{(1)}}{v_{dc}} + \frac{e_q i_q^{(1)}}{v_{dc}} - u_1^{(2)}i_d^{(2)} - u_2^{(2)}i_q^{(2)} \tag{2.2.1d}$$

$$\dot{\Psi}_d^G = L_G\dot{i}_d^{(2)} = -r_G i_d^{(2)} + L_G i_q^{(2)}\omega_G + u_1^{(2)}v_{dc} - V_d^G \tag{2.2.1e}$$

$$\dot{\Psi}_q^G = L_G\dot{i}_q^{(2)} = -r_G i_q^{(2)} - L_G i_d^{(2)}\omega_G + u_2^{(2)}v_{dc} - V_q^G \tag{2.2.1f}$$

The rotating dq-reference frame is used to provide a time-invariant model [19]. It allows for independent control of the active (d-axis) and the reactive (q-axis) components of the currents. Similarly, the operator can adjust the torque and flux separately, which is particularly important in applications where precise control is needed, such as in electric vehicles or wind turbines [20].

The three first equations can be traced back to their derivation in [21]. Kirchhoff's voltage law is responsible for the formation of Equation (2.2.1a) and (2.2.1b), while Newton's law of rotation gives rise to Equation (2.2.1c). The variables used in these equations include L, the inductance of the stator windings, i_d and i_q, the direct and quadrature axis currents, respectively, and r, the machine resistance. Additionally, p represents the number of poles in the PMSG, ω_m is the rotor's angular velocity, and ω_{ref} is the reference angular velocity. The magnetic flux from the magnets is denoted by ϕ, while V represents the constant voltage source on the DC side. The duty cycle for the d- and q-axes in the machine side 2L-VSC are defined by $u_1^{(1)}$ and $u_2^{(1)}$, respectively. Finally, J is the machine's inertia, while T_m and T_e represent the mechanical and electrical torque, respectively.

To make the model more realistic, an additional damping term is included in Equation (2.2.1c), inspired by the master thesis on scalable stability certificates for entire wind parks in [22]. The damping coefficient, denoted by d, is chosen during the machine's design process. At steady-state, the damper winding does not affect the system but contributes to the pull-in torque of the PMSG and damps the sub-transient oscillations that may arise during a fault. The pull-in torque represents the torque needed to pull the connected total inertia into synchronism and is produced when transitioning from slip speed to synchronous speed. This period is usually the most critical phase for such a generator during grid connection, making it practical to include the damping coefficient in the model equations [23].

Further on, to make the system skew-symmetric, which helps simplify the control design and analysis, Equation (2.2.1c) is multiplied with a factor of $\frac{2}{3}$:

$$\dot{\rho^*} = J^*\dot{\omega}_m = T_m^* - T_e^* = T_m^*(\omega_m) - \frac{P}{2}\phi i_q + d^*(\omega_{ref} - \omega_m) \tag{2.2.2}$$

In the above expression, $(\cdot)^* = \frac{2}{3}(\cdot)$, but for simplicity, this thesis will further use the simple notation ρ, J, T_m and d for ρ^*, J^*, T_m^* and d^*. The nonlinear behavior between torque and speed is also accounted for, where the mechanical torque is as

$$T_m(\omega_m) = \frac{1}{2}\rho A v^3 C_p(\lambda)\frac{1}{\omega_m}, \tag{2.2.3}$$

where the air density is represented by ρ, A denotes the area swept by the turbine blades, and v represents the wind speed. The wind power coefficient, denoted by C_p, is defined as $C_p = e^{-\frac{C_1}{\lambda}}\left(\frac{C_2}{\lambda} - C_5\right) + C_6\lambda$, where $\lambda = \frac{r_b\omega_m}{v}$ is the tip speed ratio. Here, C_1, C_2, C_5, C_6 are specified constant values [21]. It is interesting to investigate the impact of this non-linearity on the system's stability.

The expression in (2.2.1d) results from Kirchhoff's current law, while the two equations below can be found using Kirchhoff's voltage law. Here, q_{dc} is the charge in the capacitor C with voltage v_{dc}. $u_1^{(2)}$ and $u_2^{(2)}$ can be interpreted as the duty cycle for the d- and q-axis components for the grid-connected VSC using PWM, respectively. These control variables can take values in the range of $u \in [-\frac{1}{2}, \frac{1}{2}]$. The currents $i_d^{(2)}$ and $i_q^{(2)}$ are the direct- and quadrature currents from the grid side converter, respectively. r_G is the grid resistance, L_G is the grid inductance, and the angular grid frequency is denoted ω_G. Lastly, V_d^G and V_q^G are the direct and quadrature grid voltages, modeling the grid as a stiff voltage source.

Via control action, the overall system is forced to behave as a cascade connection of two subsystems, constructing a leader-follower structure. The leader, further on also referred to as the primary side, consists of a wind turbine, PMSG, and the machine side converter, as shown in Figure 2.2. The figure illustrates the resulting circuit after the feedback linearization procedure is applied to the

machine-side converter: in particular that the control now enters linearly into the current dynamics. The follower, or secondary side, comprises of a capacitor and the grid side voltage source converter. This subsystem is shown in Figure 2.3. The fundamental property of this construction is that the leader states are decoupled and unaffected by the rest of the system. In contrast, the follower states see the leader as input or disturbance. Consequently, the overall eigenvalues are the union of the eigenvalues of the two subsystems. This is also interesting in terms of performance since the eigenvalues do not influence each other dynamically.

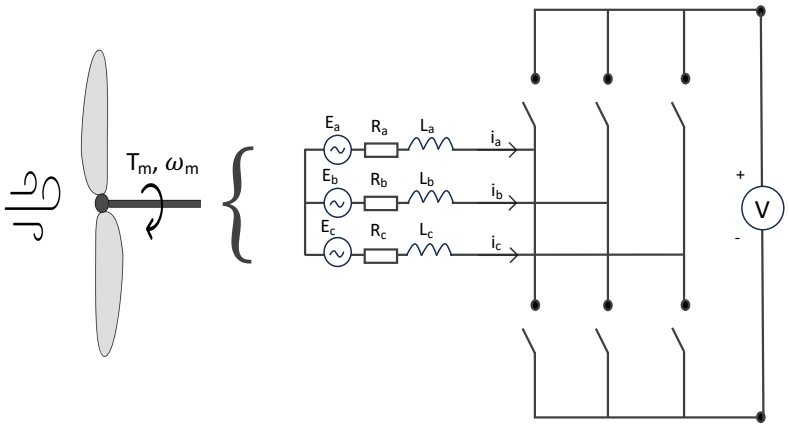

Figure 2.2: The leader subsystem.

For this thesis, Equation (2.2.4) corresponds to the leader, while Equation (2.2.5) corresponds to the follower. Starting first with the leader:

$$\dot{\Psi}_d = L\dot{i}_d^{(1)} = -ri_d^{(1)} + Li_q^{(1)}\frac{P}{2}\omega_m - e_d \tag{2.2.4a}$$

$$\dot{\Psi}_q = L\dot{i}_q^{(1)} = -ri_q^{(1)} - Li_d^{(1)}\frac{P}{2}\omega_m + \phi\frac{P}{2}\omega_m - e_q \tag{2.2.4b}$$

$$\dot{\rho} = J\dot{\omega}_m = T_m - T_e = T_m - \frac{3}{2}\frac{P}{2}\phi i_q^{(1)} + d(\omega_{ref} - \omega_m) \tag{2.2.4c}$$

Now, the terms in (2.2.1) containing $u_1^{(1)}$ and $u_2^{(1)}$ are rewritten using the direct axis voltage $e_d = u_1^{(1)} \cdot v_{dc}$ and the quadrature axis voltage $e_q = u_2^{(1)} \cdot v_{dc}$ to force the system to behave as a cascade connection of the subsystems.

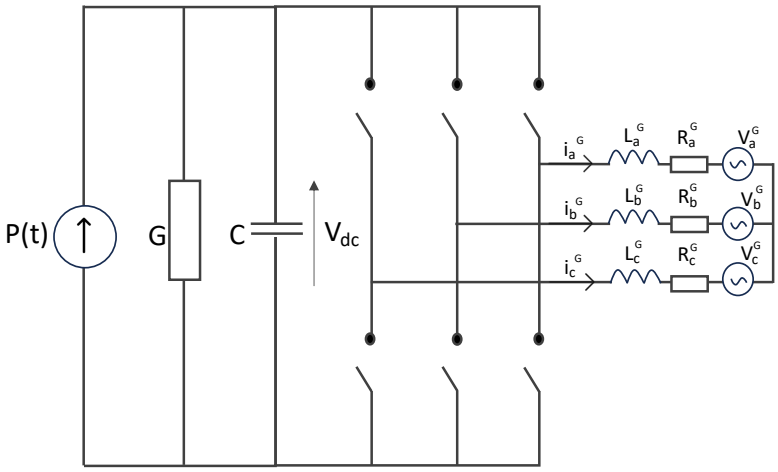

Figure 2.3: The Follower subsystem.

Moreover, the follower-subsystem (grid-side 2L-VSC, grid) can be expressed in terms of the three following equations:

$$\dot{q}_{dc} = C\dot{v}_{dc} = -Gv_{dc} + \frac{P(t)}{v_{dc}} - u_1^{(2)} i_d^{(2)} - u_2^{(2)} i_q^{(2)} \tag{2.2.5a}$$

$$\dot{\Psi}_d^G = L_G \dot{i}_d^{(2)} = -r_G i_d^{(2)} + L_G i_q^{(2)} \omega_G + u_1^{(2)} v_{dc} - V_d^G \tag{2.2.5b}$$

$$\dot{\Psi}_q^G = L_G \dot{i}_q^{(2)} = -r_G i_q^{(2)} - L_G i_d^{(2)} \omega_G + u_2^{(2)} v_{dc} - V_q^G \tag{2.2.5c}$$

The grid side converter now views the machine side as a current source, which is transformed into a power source, where $P(t) = P + \delta_p(t)$. This source will eventually stabilize after a time t and be viewed as a constant power source.

Chapter 3

Stability Analysis of the Leader Subsystem

Prior to this master thesis, a specialization project was completed aiming to discover a stability certificate for a wind turbine connected to a generator, primarily focusing on a standard current controller [9]. The procedure in the following section was presented in the specialization project but has been modified and updated to include the nonlinear behavior between wind speed and mechanical torque.

3.1 System Modeling

The port Hamiltonian (pH) of the system shown in Figure 2.2 is established using the equations in (2.2.4) for a permanent magnet synchronous generator (PMSG) connected to a wind turbine and a converter with a voltage source on the DC-side. As a result, the system can be represented in matrix form as shown below, known as the port Hamiltonian form, an energy-based description of the system:

$$\dot{x} = \begin{bmatrix} \dot{\Psi}_d \\ \dot{\Psi}_q \\ \dot{\rho} \end{bmatrix} = \left(\underbrace{\begin{bmatrix} 0 & L\frac{P}{2}\omega_m & 0 \\ -L\frac{P}{2}\omega_m & 0 & \frac{P}{2}\phi \\ 0 & -\frac{P}{2}\phi & 0 \end{bmatrix}}_{\mathcal{J}} - \underbrace{\begin{bmatrix} r & 0 & 0 \\ 0 & r & 0 \\ 0 & 0 & d - \frac{T_m(\omega_m)}{\omega_m} \end{bmatrix}}_{\mathcal{R}(\omega_m)} \right) \underbrace{\begin{bmatrix} i_d \\ i_q \\ \omega_m \end{bmatrix}}_{\nabla\mathcal{H}(x)} + \underbrace{\begin{bmatrix} -1 & 0 \\ 0 & -1 \\ 0 & 0 \end{bmatrix}}_{G} \underbrace{\begin{bmatrix} v_d \\ v_q \end{bmatrix}}_{u} + \underbrace{\begin{bmatrix} 0 \\ 0 \\ d\omega_{ref} \end{bmatrix}}_{E} \tag{3.1.1}$$

where $x = [\Psi_d \ \Psi_q \ \rho]^\top$ denotes the energy variables, $\nabla\mathcal{H}(x)$ is the Hamiltonian gradient, $u = [v_d \ v_q]^\top$ is the control vector, and $E = [0 \ 0 \ d\omega ref]^\top$ is the vector containing the external sources. The interconnection matrix, denoted by $\mathcal{J}$, is an $n \times n$ skew-symmetric matrix with elements in the set of real numbers $\mathbb{R}$. This matrix represents the connections and interactions between different subsystems, such as the mechanical and electrical subsystems in this case, and contains all the

connections related to power preservation. The interconnection matrix J can be divided into two matrices, as shown below:

$$\mathcal{J} = \underbrace{\begin{bmatrix} 0 & 0 & 0 \\ 0 & 0 & \frac{P}{2}\phi \\ 0 & -\frac{P}{2}\phi & 0 \end{bmatrix}}_{\mathcal{J}_0} + \underbrace{\begin{bmatrix} 0 & L\frac{P}{2}\omega_m & 0 \\ -L\frac{P}{2}\omega_m & 0 & 0 \\ 0 & 0 & 0 \end{bmatrix}}_{\mathcal{J}(\omega_m)} \tag{3.1.2}$$

Further on, the dissipation matrix $\mathcal{R} \in \mathbb{R}^{n\times n}$ is symmetric and represents the damping of the system, where $\mathcal{R}(x) > 0$. Furthermore, $G \in \mathbb{R}^{n\times m}$ is the control input matrix, where $m \leq n$. Lastly, $\mathcal{H}(x)$ is the Hamiltonian or stored energy of the system, which is a scalar given by Equation (3.1.3), where $Q = Q^\top \in \mathbb{R}^{n\times n}$ is a positive definite matrix with entries given by the inverse of the energy-storing element parameters.

$$\mathcal{H}(x) = \frac{1}{2}x^\top Q x \tag{3.1.3}$$

Moreover, Equation (3.1.4) provides a compact expression for the dynamics of the system:

$$\dot{x} = (\mathcal{J}_0 + \mathcal{J}(\omega_m) - \mathcal{R}(\omega_m))\nabla\mathcal{H}(x) + Gu + E, \tag{3.1.4}$$

By utilizing Equation (3.1.3), the Hamiltonian of the system can be calculated as in (3.1.5), and subsequently, the gradient of the Hamiltonian is found in (3.1.6).

$$\mathcal{H}(x) = \frac{1}{2}\begin{bmatrix} \Psi_d & \Psi_q & \rho \end{bmatrix}\begin{bmatrix} \frac{1}{L} & 0 & 0 \\ 0 & \frac{1}{L} & 0 \\ 0 & 0 & \frac{1}{J} \end{bmatrix}\begin{bmatrix} \Psi_d \\ \psi_q \\ \rho \end{bmatrix} = \frac{1}{2}[\frac{1}{L}\Psi_d^2 + \frac{1}{L}\Psi_q^2 + \frac{1}{J}\rho^2], \tag{3.1.5}$$

$$\nabla\mathcal{H}(x) = \begin{bmatrix} \frac{\partial\mathcal{H}}{\partial\Psi_d} \\ \frac{\partial\mathcal{H}}{\partial\Psi_q} \\ \frac{\partial\mathcal{H}}{\partial\rho} \end{bmatrix} = \begin{bmatrix} \frac{1}{L}\Psi_d \\ \frac{1}{L}\Psi_q \\ \frac{1}{J}\rho \end{bmatrix} = \begin{bmatrix} \frac{1}{L} & 0 & 0 \\ 0 & \frac{1}{L} & 0 \\ 0 & 0 & \frac{1}{J} \end{bmatrix}\begin{bmatrix} \Psi_d \\ \psi_q \\ \rho \end{bmatrix} = Qx \tag{3.1.6}$$

Having established the port Hamiltonian of the system, Lyapunov's direct method can be used to investigate the global asymptotic stability. This requires an equilibrium point at the origin. Still, since this corresponds to having turned off the generator, it is desirable to use a model that allows an equilibrium point different from zero. To address this issue, the incremental model is introduced. Starting with the compact model in (3.1.4), its equilibrium point can be found as

$$\dot{\bar{x}} = 0 = (\mathcal{J}_0 + \mathcal{J}(\bar{\omega}_m) - \mathcal{R}(\bar{\omega}_m))\nabla\mathcal{H}(\bar{x}) + G\bar{u} + E \tag{3.1.7}$$

We can introduce a new incremental model that uses the notation:

$$\tilde{(\cdot)} = (\cdot) - \bar{(\cdot)}, \tag{3.1.8}$$

where $\tilde{(\cdot)}$ represents the new equilibrium point shifted to the origin, and $\bar{(\cdot)}$ represents the actual equilibrium point of the model. By adopting this notation and subtracting Equation (3.1.7) from Equation (3.1.4), we obtain:

$$\begin{aligned}\dot{\tilde{x}} = \dot{x} - \dot{\bar{x}} &= \mathcal{J}_0(\nabla\mathcal{H}(x) - \nabla\mathcal{H}(\bar{x})) + G(u - \bar{u}) + (\mathcal{J}(\omega_m) - \mathcal{R}(\omega_m))\nabla\mathcal{H}(x) \\ &- (\mathcal{J}(\bar{\omega}_m) - \mathcal{R}(\bar{\omega}_m))\nabla\mathcal{H}(\bar{x}) \\ &= \mathcal{J}_0\nabla\mathcal{H}(\tilde{x}) + G\tilde{u} + (\mathcal{J}(\omega_m) - \mathcal{R}(\omega_m))\nabla\mathcal{H}(x) - (\mathcal{J}(\bar{\omega}_m) - \mathcal{R}(\bar{\omega}_m))\nabla\mathcal{H}(\bar{x}).\end{aligned} \tag{3.1.9}$$

3.2 Stability Analysis of the System

To analyze passivity using Lyapunov's direct method, the incremental model dynamics are investigated. It is well-known that any port-Hamiltonian systems are passive with respect to the port variables and the storage function [10]. This property is a fundamental property of port-Hamiltonian systems and is derived from the underlying physical principles that govern these systems. One way to initiate passivity-based control design is, therefore, to set the LCF equal to the Hamiltonian, as in the following equation:

$$\mathcal{V}(x) = \frac{1}{2}\tilde{x}^\top Q\tilde{x}. \tag{3.2.1}$$

It is evident from Equation (3.1.6) that the gradient is given as below:

$$\nabla\mathcal{V}(x) = Q\tilde{x}, \tag{3.2.2}$$

leading to the following relationship:

$$\nabla H(x) - \nabla H(\bar{x}) = Qx - Q\bar{x} = Q\tilde{x} = \nabla\mathcal{V}(x). \tag{3.2.3}$$

It can be observed that the expression contains a new energy-like Hamiltonian $\mathcal{V}(x) = H(\tilde{x})$. This Hamiltonian does not represent the actual energy in the physical system but instead reflects how far the system is from reaching equilibrium.

Since the Lyapunov function candidate presented in (3.2.1) and subsequent candidates in this thesis are quadratic functions (or sums of quadratic functions), they are all continuously differentiable. The first Lyapunov condition gives:

$$\mathcal{V}(\bar{x}) = \frac{1}{2}(\bar{x} - \bar{x})^\top Q(\bar{x} - \bar{x}) = 0. \tag{3.2.4}$$

In addition, the function must be positive definite in $\mathbb{R}$, as stated in condition *ii* in section 2.1.2. This condition is satisfied since $\mathcal{V}(x)$ in Equation (3.2.1) is a quadratic function, and Q is positive definite by definition.

The remaining two conditions require finding the time derivative of $\mathcal{V}(x)$. Using the chain rule, we obtain the following expression:

$$\begin{aligned}\dot{\mathcal{V}}(x) = \frac{\partial\mathcal{V}(x)}{\partial t} = \nabla^\top\mathcal{V}\dot{x} &= \underbrace{\nabla^\top\mathcal{V}(x)\mathcal{J}_0\nabla\mathcal{V}(x)}_{=0} + \underbrace{\nabla^\top\mathcal{V}(x)G}_{\tilde{y}^\top}\tilde{u} \\ &+ \nabla^\top\mathcal{V}(x)(\mathcal{J}(\omega_m) - \mathcal{R}(\omega_m))Qx - \nabla^\top\mathcal{V}(x)(\mathcal{J}(\bar{\omega}_m) - \mathcal{R}(\bar{\omega}_m))Q\bar{x} \\ &= \tilde{y}^\top\tilde{u} + \nabla^\top\mathcal{V}(x)(\mathcal{J}(\omega_m) - \mathcal{R}(\omega_m))Qx - \nabla^\top\mathcal{V}(x)(\mathcal{J}(\bar{\omega}_m) - \mathcal{R}(\bar{\omega}_m))Q\bar{x}.\end{aligned} \tag{3.2.5}$$

A port-Hamiltonian system comprises ports that represent input-output relations within the system. The power at a given port is determined by the product of its input and output quantities. Hence, the portion of the equation that multiplies the input provides the passive output of the system. This observation is also evident from the definition of a passive system in Equation (2.1.1). For instance, if speed is the input, torque will be the output such that their product equals the power at the input-output port. From the above equation, we can conclude that the passive output of the system, denoted by $\tilde{y}$, can be expressed as $G^\top \nabla \mathcal{V}(x)$ for this specific system. Furthermore, notice also that the first term in the equation equals zero because J_0 is a skew-symmetric matrix.

Additionally, inspired by the method presented in [24], the term $\tilde{x}^\top Q\mathcal{J}(\omega_m))Q\bar{x}$ is added and subtracted in the expression below.

$$\dot{\mathcal{V}}(x) = \tilde{y}^\top \tilde{u} + \nabla^\top \mathcal{V}(x)(\mathcal{J}(\omega_m) - \mathcal{R}(\omega_m))Qx - \nabla^\top \mathcal{V}(x)(\mathcal{J}(\bar{\omega}_m) - \mathcal{R}(\bar{\omega}_m))Q\bar{x} + \underbrace{\tilde{x}^\top Q\mathcal{J}(\omega_m)Q\bar{x} - \tilde{x}^\top Q\mathcal{J}(\omega_m)Q\bar{x}}_{\text{added}} \tag{3.2.6}$$

Which can be rearranged to:

$$\dot{\mathcal{V}}(x) = \tilde{y}^\top \tilde{u} + \tilde{x}^\top Q \underbrace{(\mathcal{J}(\omega_m)Qx - \mathcal{J}(\omega_m)Q\bar{x})}_{\mathcal{J}(\omega_m)Q\tilde{x}} - \tilde{x}^\top Q\mathcal{J}(\bar{\omega}_m)Q\bar{x} + \tilde{x}^\top Q\mathcal{J}(\omega_m)Q\bar{x} - \tilde{x}^\top Q\mathcal{R}(\omega_m)Qx + \tilde{x}^\top Q\mathcal{R}(\bar{\omega}_m)Q\bar{x}. \tag{3.2.7}$$

The third term vanishes in the expression above due to skew symmetry. To ensure passivity in the system, output feedback is added in the following equation, where γ is a tunable scalar control parameter constant [24]. Output feedback allows for monitoring and adjustment of the system's output to keep it within the passive domain, preventing it from becoming active and unstable. An active output fails to satisfy the conditions for passivity, i.e., it does not have a non-negative storage function and dissipated power [25].

$$\dot{\mathcal{V}}(x) = \tilde{y}^\top \tilde{u} - \tilde{x}^\top Q\mathcal{J}(\bar{\omega}_m)Q\bar{x} + \tilde{x}^\top Q\mathcal{J}(\omega_m)Q\bar{x} - \tilde{x}^\top Q\mathcal{R}(\omega_m)Qx + \tilde{x}^\top Q\mathcal{R}(\bar{\omega}_m)Q\bar{x} + \underbrace{\tilde{x}^\top Q[\gamma GG^\top - \gamma GG^\top]Q\tilde{x}}_{\text{added}} \tag{3.2.8}$$

If rearranging, and the definition for the passive output, $\tilde{y}^\top = \nabla^\top \mathcal{V}(x)g(x)$, is utilized, Equation (3.2.9) is obtained.

$$\dot{\mathcal{V}}(x) = \underbrace{\tilde{y}^\top \tilde{u}}_{i} + \underbrace{\gamma \tilde{y}^\top \tilde{y}}_{ii} + \underbrace{\tilde{x}^\top Q[\mathcal{J}(\omega_m)Q\bar{x} - \mathcal{R}(\omega_m)Qx - \mathcal{J}(\bar{\omega}_m)Q\bar{x} + \mathcal{R}(\bar{\omega}_m)Q\bar{x} - \gamma GG^\top Q\tilde{x}]}_{iii}. \tag{3.2.9}$$

When a generator is included in the pH model, the $\mathcal{J}(\omega_m)$ matrix is introduced, making the stability analysis more complicated. Therefore, further steps involving monotonicity are utilized to prove that the term *iii* of Equation (3.2.9) is negative definite. The definition in 1 will be helpful for further derivations.

Definition 1. *Given a function f, the function will be monotonically decreasing if and only if, for all $a, b \in \mathbb{R}$, $(b-a)[f(b) - f(a)] < 0$. This corresponds to the derivative of the function f being*

negative since the derivative at a point is given by

$$\frac{df(x)}{dx}\Big|_x = \frac{f(b)-f(a)}{b-a} = \frac{(b-a)(f(b)-f(a))}{(b-a)^2} < 0. \tag{3.2.10}$$

Inspired by [24], we now define a new variable $z := \nabla\mathcal{H}(x) = Qx$, and a function $M(z) := \mathcal{J}(z)\bar{z} - \mathcal{R}(z)z$. The reason for this is a desire to express the last term in Equation (3.2.9) in the form mentioned above so that evaluating the derivative of f is the only requirement. With this notation, Equation (3.2.9) can be rewritten:

$$\dot{\mathcal{V}}(x) = \tilde{y}^\top\tilde{u} + \gamma\tilde{y}^\top\tilde{y} + \underbrace{(z-\bar{z})}_{b-a}^\top[\underbrace{M(z) - M(\bar{z}) - \gamma GG^\top(z-\bar{z})}_{f(b)-f(a)}], \tag{3.2.11}$$

giving the possibility of formulating the function f as follows:

$$f(z) := M(z) - \gamma GG^\top z. \tag{3.2.12}$$

The expression on the form $(b-a)[f(b)-f(a)]$ is negative if the derivative of the function $f(x)$ for all $x\epsilon\mathbb{R}$ is negative. Therefore, checking if the function in Equation (3.2.12) is constantly decreasing is enough to confirm that the third term in Equation (3.2.11) is negative definite. According to [26], an $n \times n$ matrix is positive definite if and only if its symmetrical part is positive definite. The symmetrical part of a matrix A can be found as $A_{sym} = \frac{1}{2}(A + A^\top)$, and the gradient of f becomes

$$\nabla f(z) = \frac{1}{2}(\nabla M(z) + \nabla^\top M(z)) - \gamma GG^\top \tag{3.2.13}$$

with the terms calculated in Equation (3.2.14), (3.2.15), and (3.2.16).

$$\begin{aligned} M(z) = J(z)\bar{z} - Rz = &\begin{bmatrix} 0 & L\frac{P}{2}\omega_m & 0 \\ -L\frac{P}{2}\omega_m & 0 & 0 \\ 0 & 0 & 0 \end{bmatrix}\begin{bmatrix} \frac{1}{L} & 0 & 0 \\ 0 & \frac{1}{L} & 0 \\ 0 & 0 & \frac{1}{J} \end{bmatrix}\begin{bmatrix} \bar{\Psi}_d \\ \bar{\Psi}_q \\ \bar{\rho} \end{bmatrix} - \\ &\begin{bmatrix} r & 0 & 0 \\ 0 & r & 0 \\ 0 & 0 & d - \frac{T_m(\omega)}{\omega} \end{bmatrix}\begin{bmatrix} \frac{1}{L} & 0 & 0 \\ 0 & \frac{1}{L} & 0 \\ 0 & 0 & \frac{1}{J} \end{bmatrix}\begin{bmatrix} \Psi_d \\ \Psi_q \\ \rho \end{bmatrix} = \\ &\begin{bmatrix} 0 & L\frac{P}{2}\omega_m & 0 \\ -L\frac{P}{2}\omega_m & 0 & 0 \\ 0 & 0 & 0 \end{bmatrix}\underbrace{\begin{bmatrix} \bar{i}_d \\ \bar{i}_q \\ \bar{\omega}_m \end{bmatrix}}_{\bar{z}} - \begin{bmatrix} r & 0 & 0 \\ 0 & r & 0 \\ 0 & 0 & d - \frac{T_m(\omega)}{\omega} \end{bmatrix}\underbrace{\begin{bmatrix} i_d \\ i_q \\ \omega_m \end{bmatrix}}_{z} \end{aligned} \tag{3.2.14}$$

$$\begin{aligned} \nabla M(z) = \begin{bmatrix} \frac{\partial M(z)}{\partial i_d} \\ \frac{\partial M(z)}{\partial i_q} \\ \frac{\partial M(z)}{\partial \omega_m} \end{bmatrix} = &\begin{bmatrix} 0 & 0 & L\frac{P}{2}\bar{i}_q \\ 0 & 0 & -L\frac{P}{2}\bar{i}_d \\ 0 & 0 & 0 \end{bmatrix} - \begin{bmatrix} r & 0 & 0 \\ 0 & r & 0 \\ 0 & 0 & d - \frac{\partial T_m(\omega)}{\partial \omega} \end{bmatrix} = \\ &\begin{bmatrix} -r & 0 & L\frac{P}{2}\bar{i}_q \\ 0 & -r & -L\frac{P}{2}\bar{i}_d \\ 0 & 0 & -d + \frac{\partial T_m(\omega)}{\partial \omega} \end{bmatrix} \end{aligned} \tag{3.2.15}$$

$$\gamma GG^\top = \gamma \begin{bmatrix} -1 & 0 \\ 0 & -1 \\ 0 & 0 \end{bmatrix} \begin{bmatrix} -1 & 0 & 0 \\ 0 & -1 & 0 \end{bmatrix} = \begin{bmatrix} \gamma & 0 & 0 \\ 0 & \gamma & 0 \\ 0 & 0 & 0 \end{bmatrix} \tag{3.2.16}$$

The gradient of f can now be calculated using Equation (3.2.13), and the following expression is obtained:

$$\begin{aligned} 2 \cdot \nabla f(z) = &\begin{bmatrix} -r & 0 & L\frac{P}{2}\bar{i}_q \\ 0 & -r & -L\frac{P}{2}\bar{i}_d \\ 0 & 0 & -d + \frac{\partial T_m(\omega)}{\partial \omega} \end{bmatrix} + \begin{bmatrix} -r & 0 & 0 \\ 0 & -r & 0 \\ L\frac{P}{2}\bar{i}_q & -L\frac{P}{2}\bar{i}_d & -d + \frac{\partial T_m(\omega)}{\partial \omega} \end{bmatrix} \\ -2 &\begin{bmatrix} \gamma & 0 & 0 \\ 0 & \gamma & 0 \\ 0 & 0 & 0 \end{bmatrix} = \begin{bmatrix} -2r - 2\gamma & 0 & L\frac{P}{2}\bar{i}_q \\ 0 & -2r - 2\gamma & -L\frac{P}{2}\bar{i}_d \\ L\frac{P}{2}\bar{i}_q & -L\frac{P}{2}\bar{i}_d & -2d + 2\frac{\partial T_m(\omega)}{\partial \omega} \end{bmatrix}. \end{aligned} \tag{3.2.17}$$

Optimal operation of a PMSG is achieved when it operates at maximum torque per ampere, also known as optimal α_p control. By aligning the angle α_p of the current vector with respect to the q-axis, maximum torque can be obtained while minimizing ohmic losses in the stator winding, resulting in $\bar{i}_d = 0$ [27]. Assuming the use of this operation, the following matrix is obtained.

$$\begin{bmatrix} -2r - 2\gamma & 0 & L\frac{P}{2}\bar{i}_q \\ 0 & -2r - 2\gamma & 0 \\ L\frac{P}{2}\bar{i}_q & 0 & -2d + 2\frac{\partial T_m(\omega)}{\partial \omega} \end{bmatrix} = \begin{bmatrix} A_{2\times 2} & B_{2\times 1} \\ C_{1\times 2} & D_{1\times 1} \end{bmatrix} \tag{3.2.18}$$

The Schur complement can be used to determine whether a matrix is positive definite without explicitly computing its eigenvalues. Checking whether $\nabla f(z)$ is negative definite is equivalent to checking whether $-\nabla f(z)$ is positive definite. By using the definition of the Schur complement in [28], it is possible to determine $\nabla f/A$.

$$\begin{aligned} -\nabla f/A = 2d - 2\frac{\partial T_m(\omega)}{\partial \omega} - \begin{bmatrix} -L\frac{P}{2}\bar{i}_q & 0 \end{bmatrix} &\begin{bmatrix} \frac{1}{2r+2\gamma} & 0 \\ 0 & \frac{1}{2r+2\gamma} \end{bmatrix} \begin{bmatrix} -L\frac{P}{2}\bar{i}_q \\ 0 \end{bmatrix} \\ &= 2d - 2\frac{\partial T_m(\omega)}{\partial \omega} - \frac{(L\frac{P}{2}\bar{i}_q)^2}{2(r+\gamma)} \end{aligned} \tag{3.2.19}$$

If now both Equation (3.2.20) and (3.2.21) hold, the matrix in (3.2.18) is a negative definite matrix.

$$d - \frac{\partial T_m(\omega)}{\partial \omega} - \frac{(L\frac{P}{2}\bar{i}_q)^2}{4(r+\gamma)} > 0 \tag{3.2.20}$$

$$-A = \begin{bmatrix} 2r + 2\gamma & 0 \\ 0 & 2r + 2\gamma \end{bmatrix} > 0 \tag{3.2.21}$$

Condition (3.2.21) is satisfied if

$$\gamma > -r. \tag{3.2.22}$$

By choosing a sufficiently large value for γ, condition (3.2.22) can be satisfied. In practical applications, it is recommended to choose a value for γ that accounts for the worst-case value of $\bar{i}_q$.

We further investigate the condition in Equation (3.2.20), which involves the derivative of the torque with respect to the mechanical rotor speed. The calculation of the required size of the damper windings is a crucial step in the design of this wind turbine generator. Hence, the expression for the derivative of the torque is considered, given by Equation (3.2.23):

$$\frac{\partial T_m(\omega)}{\partial \omega} = \frac{1}{2} \frac{A\rho v^3 e^{-c_1 \frac{v}{r\omega}} \left(c_2 v(c_1 v - 2r\omega) + c_3 r\omega(r\omega - c_1 v)\right)}{r^2\omega^4}. \tag{3.2.23}$$

However, it is not immediately clear how the derivative affects the stability condition. Therefore, the stability condition as a function of the rotor speed for different values of the damper coefficient is plotted. This plot is presented in Figure 3.1, where the wind speed is set to 15 m/s and $\gamma = 6$, while the other parameters, such as the current, are assumed constant.

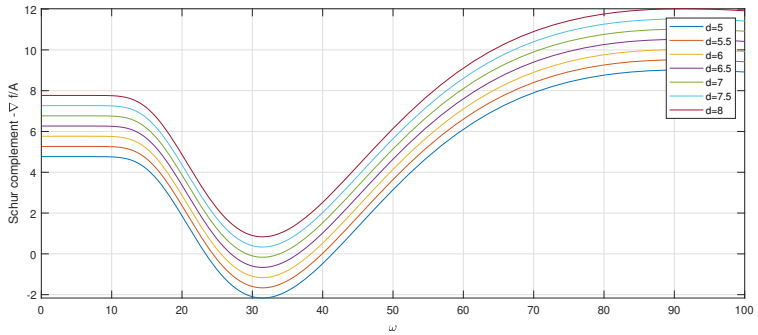

Figure 3.1: The stability criteria in (3.2.20) for different values of the damper coefficient.

From Figure 3.1, it is observed that the Schur complement is positive for all rotor speeds when the damper coefficient is 7.5 or higher. This implies that the generator needs to be constructed with enough damper windings to satisfy the stability criterion. However, note that the stability criterion is easily satisfied for the optimal operating point, $\omega_m = \frac{\lambda v}{r_b} = \frac{8.1 \cdot 15}{1.84} = 66 rad/s$, but problems may arise during acceleration or deceleration. Therefore, it is essential to carefully choose the damper coefficient to ensure stable operation of the wind turbine generator.

Assuming both the conditions are met, Equation (3.2.11) becomes as:

$$\dot{\mathcal{V}}(x) \leq \tilde{y}^\top \tilde{u} + \gamma \tilde{y}^\top \tilde{y} \tag{3.2.24}$$

Further, the controllers utilize the passive output from the system as input. For example, for a proportional controller, the control vector u is defined as $u = -K_p y$, where K_p is a diagonal 2×2 matrix representing the proportional gain and contains only diagonal elements. Using this definition of the control vector, Equation (3.2.25) can be obtained.

$$\dot{\mathcal{V}}(x) \leq -\tilde{y}^\top K_p \tilde{y} + \gamma \tilde{y}^\top \tilde{y} = \tilde{y}^\top [\gamma - K_p] \tilde{y} \tag{3.2.25}$$

It is evident from the equation above that if $K_p > \gamma$, the Lyapunov condition iv is satisfied. For the third condition in 2.1.2, the passive output is investigated, where

$$\tilde{y} = G^\top \nabla \mathcal{V}(x) = \begin{bmatrix} -1 & 0 & 0 \\ 0 & -1 & 0 \end{bmatrix} \begin{bmatrix} \tilde{i}_d \\ \tilde{i}_q \\ \tilde{\omega}_m \end{bmatrix} = \begin{bmatrix} -(i_d - \bar{i}_d) \\ -(i_q - \bar{i}_q) \end{bmatrix}, \tag{3.2.26}$$

which will be zero at the system's equilibrium point:

$$\tilde{y}(\bar{x}) = \begin{bmatrix} -(\bar{i}_d - \bar{i}_d) \\ -(\bar{i}_q - \bar{i}_q) \end{bmatrix} = \begin{bmatrix} 0 \\ 0 \end{bmatrix}. \tag{3.2.27}$$

Consequently, condition *iii* is satisfied:

$$\dot{\mathcal{V}}(\bar{x}) = -\tilde{y}(\bar{x})^\top K_p \tilde{y}(\bar{x}) + \gamma \tilde{y}(\bar{x})^\top \tilde{y}(\bar{x}) = 0. \tag{3.2.28}$$

Given that all the Lyapunov conditions are met, the function $\mathcal{V}(x)$ is asymptotically stable in $\mathbb{R}$. However, in practice, the P-controller is often not used, and therefore it is desirable to obtain a stability certificate for the PI-controller. This will be implemented next.

3.3 Lyapunov Candidate for PI-PBC-control

This first paragraph is a reproduction from the specialization project in [9], included to provide some background information. In the industry today, it is often standard to control the current in the inner control loop using a PI controller. This type of control combines two control actions: the proportional action represented by "P" and the integral action represented by "I". These controllers are relatively easy to design and implement, making them a popular choice in the industry. On the other hand, a PI-PBC controller combines a PI controller with the concept of passivity. The idea behind PBC is based on bringing the stored energy to its minimum, rooted in Lyapunov's theory. This makes the PI-PBC controllers powerful tools for controlling complex systems, but it also adds an additional layer of complexity to the control system. Unlike traditional PI controllers that typically operate directly on error signals, the PI-PBC acts on the passive output of the system. By doing so, the controller can often provide both a fast response and the accuracy of a PI controller, in addition to ensuring that the system is stable [29] [30]. This control strategy has been proven effective in many practical applications, such as in [31] and [32]. However, it has been observed in both [31] and [33] that the P(I)-PBC may have slightly poorer control performance in some cases.

This new, novel nonlinear control design approach that capitalizes on the system's physical characteristics has recently gained popularity. Adjusting the stored energy function makes it possible to establish a new energy balance and convert the closed-loop system into a passive state [10], which has significant Plug-and-Play capabilities.

Proposition 2. Given the system represented by Equation (3.1.2), if expanding the Lyapunov candidate to incorporate the "energy" from the controller, the resulting system can be described as:

$$\mathcal{W}_1(x, x_c) := \underbrace{\frac{1}{2}\tilde{x}^\top Q \tilde{x}}_{\mathcal{V}(x)} + \frac{1}{2}\tilde{x}_c^\top K_I \tilde{x}_c, \tag{3.3.1}$$

The stability condition obtained will be equivalent to that of the P controller:

$$\dot{\mathcal{W}}_1(x) \leq \tilde{y}^\top[\gamma - K_p]\tilde{y}. \tag{3.3.2}$$

Proof. For a PI controller, the control input, denoted by u, can be defined as shown in Equation (3.3.3). In steady state, the controller output $\bar{u}$ will be given by Equation (3.3.4).

$$u = -K_p y + K_I x_c, \tag{3.3.3}$$

$$\bar{u} = -K_p \bar{y} + K_I \bar{x}_c. \tag{3.3.4}$$

K_p and K_I are the proportional and integral gains, respectively. Both are 2×2 matrices, only containing diagonal elements. The diagonal entries are responsible for scaling the error between the setpoint and the system output.

When a PI controller is used, the additional state variable, x_c, is introduced to the system. This state represents the desired setpoint of the system. The time derivative of x_c, denoted by $\dot{x}_c$, is defined as in Equation (3.3.5).

$$\dot{x}_c = -(y - y^{\text{ref}}) \tag{3.3.5}$$

However, simply using the previous Lyapunov function candidate for the system would not be sufficient to ensure asymptotic stability at equilibrium since the behavior of the new state variable is not accounted for. To address this, the Lyapunov function candidate is updated to include the new state variable. The updated Lyapunov candidate is presented in Equation (3.3.1). By using the new candidate function, the time derivative can be established.

$$\dot{\mathcal{W}}_1 = \dot{\mathcal{V}} + \nabla^\top(\frac{1}{2}\tilde{x}_c^\top K_I \tilde{x}_c) \begin{bmatrix} \dot{\tilde{x}} \\ \dot{\tilde{x}}_c \end{bmatrix} = \dot{\mathcal{V}} + \frac{\partial}{\partial \tilde{x}_c}(\frac{1}{2}\tilde{x}_c^\top K_I \tilde{x}_c)\dot{\tilde{x}}_c = \dot{\mathcal{V}} - \tilde{x}_c^\top K_I \tilde{y} \tag{3.3.6}$$

If rewriting Equation (3.3.6) knowing that each term is a scalar, the first line in Equation (3.3.7) is obtained. In the last equality, Equation (3.3.3) and (3.3.4) for $K_I x_c$ and $K_I \bar{x}_c$, respectively.

$$\begin{aligned} \dot{\mathcal{W}}_1 &= \dot{\mathcal{V}} - \tilde{y}^\top[K_I x_c - K_I \bar{x}_c] \\ &= \dot{\mathcal{V}} - \tilde{y}^\top[u + K_p \tilde{y} - \bar{u}] \end{aligned} \tag{3.3.7}$$

The equation in (3.2.24) can further be substituted into the above expression, and after rearranging, the candidate can be expressed as:

$$\dot{\mathcal{W}}_1 \leq \tilde{y}^\top \tilde{u} + \gamma \tilde{y}^\top \tilde{y} - \tilde{y}^\top \tilde{u} - \tilde{y}^\top K_p \tilde{y}, \tag{3.3.8}$$

The resulting stability criteria obtained in Equation (3.3.2) for the PI-PBC controller is the same as that of a P controller. It's worth noting that in this case, the PI-PBC controller takes the same form as the standard PI current controller since $\dot{x}_c$ is chosen equal to the passive output, which contains the error in the current.

■

3.4 Control of the System

When the theoretical stability certificate is derived, simulations can be performed to validate the results. The primary side of the system described in this thesis has two degrees of freedom. As already described in section 3.2, it is desired to operate at maximum torque per ampere, requiring $\bar{i}_d = 0$. The direct-axis current is therefore chosen as the first control objective. Additionally, a wind turbine should optimally operate in accordance with the torque-speed characteristics of the system. For this to be achieved, the mechanical rotor speed needs to be adjusted continuously to follow the calculated reference speed; hence it is preferable to choose this parameter as the second control objective [34]. In this way, MPPT can be performed.

For simulations conducted on the primary side of the system through this thesis, the parameter values used are obtained from [21] and are shown in Table 3.1.

Parameters	Symbol	Nominal values
Synchronous resistance	r	0.3676 [Ω]
Synchronous inductance	L	3.55[mH]
Number of poles	p	28
Permanent magnet flux	ϕ	0.2867 [Wb]
Damping	d	0.5 $[\frac{Nm}{rad/s}]$
Inertia	J	7.856 $[kgm^2]$
Direct current	i_d^{ref}	0 [A]

Table 3.1: WECS parameters

The gain γ is chosen to fulfill the criteria in (3.2.22). Since a larger γ require a smaller damping while also a higher proportional gain constant, a value of 6 is chosen. It should further be mentioned that since this thesis is more concerned with finding a viable stability certificate rather than performance, it is only needed to show that there exist some values that give the possibility of guaranteed stability. Optimization of control parameter selection and performance are left for future work.

3.4.1 Equilibrium Analysis

When deriving the stability certificates, it depends on the fact that an equilibrium point exists for the system to obtain. An equilibrium is a state in which all forces or influences acting on a system are balanced, and the system remains unchanged unless some external disturbance is introduced. In the following sections, $\bar{(\cdot)}$ describes the physical system actual equilibrium point. $(\cdot)^{\text{ref}}$ represents the requested reference for the equilibrium point, while $(\cdot)^*$ is the reference, calculated by a load flow, that the system is given. The latter may differ from $(\cdot)^{\text{ref}}$ because of the inaccuracies that may appear in the load flow calculations.

The primary side has three coenergy variables, i_d, i_q, and ω_m, while the control variables are v_d and v_q. At the equilibrium, both the coenergy variables i_d and ω_m are known, in addition to the two inputs ω^{ref} and v^E. It is further assumed that the control objectives are achieved for the equilibrium calculations, where i_q and the two control variables v_d and v_q are calculated. This is done using the equations describing the system in (2.2.4), where the derivatives are zero at steady state.

To find the equilibrium for the quadrature current, the derivatives in Equation (2.2.4c) are put to

zero and $\omega = \omega^{\text{ref}}$. Rearranged, an expression for the quadrature current is obtained:

$$i_q^* = \frac{T_m}{\frac{3}{2}\frac{P}{2}\phi} \tag{3.4.1}$$

The equations in (2.2.4a) and (2.2.4b) are utilized and rearranged to derive the values of e_d and e_q at equilibrium, respectively. The resulting equations describing the variables at steady state are presented below.

$$e_d^* = -ri_d^{\text{ref}} + Li_q^* \frac{P}{2}\omega_m^{\text{ref}} \tag{3.4.2}$$

$$e_q^* = -ri_q^* - Li_d^{\text{ref}} \frac{P}{2}\omega_m^{\text{ref}} + \phi \frac{P}{2}\omega_m^{\text{ref}} \tag{3.4.3}$$

3.5 Estimation of Wind Speed Using Immersion and Invariance Adaptive Control

Since an outer loop is not included in our stability proof, the system depends on getting accurate information about the parameters to achieve the right control objectives. It is desired to operate the wind turbine at the point of maximum power extraction [35] [36], which requires the wind speed to be known. The knowledge of the time-varying wind speed signal is often used to improve the overall performance of the controller, using, e.g., gain scheduling and feedback techniques, as discussed in [37]. The turbine top wind speed measurement is often imprecise as it can only provide pointwise information, while it, in reality, varies over the rotor plane. Since this is insufficient to obtain the optimal power extraction, the speed often must be estimated. Several estimators have been proposed, such as in [17] and [38], while the Immersion and Invariance (I&I) wind speed estimator found in [39] is widely used to date, e.g., in [40] and [41]. Anyway, in [42], the latter wind speed estimator is revisited, and the paper claims that the estimator hinders the extension of the method and proof to time-delayed or uncertain systems. They propose a new estimator using the circle criterion and propose to include an additional integrator to the correction term to improve the estimator's performance. However, for simplicity, and to stay within the field of expertise, we will take the thoughts in [39] as a starting point.

Other parameters, such as the flux, could also be estimated. Knowing that the rotor flux angle has a significant impact on various aspects of a PMSG, such as output voltage, frequency, and power extraction, it is of great interest to possess an accurate estimation of this parameter. This becomes particularly relevant when considering cost-effective approaches, eliminating the need for additional measurement instruments. An attempt to find an estimator for the flux can be found in Appendix A.1, but it was unsuccessful in obtaining a valid β function. Further on, the objective of this section is to estimate wind speed. Still, since it is a highly nonlinear relationship between the torque and the speed, the torque is firstly estimated while viewed as a constant.

3.5.1 Designing an Adaptive Control Law for the Mechanical Torque T_m

For the estimation of the torque parameter, the differential equation of $\dot{\rho}$ will be considered. Let the estimation parameter be defined as in Equation (3.5.1), and the error between the estimated and real value of the parameter as in Equation (3.5.2).

$$T_m^E := \beta(\rho) + \zeta \tag{3.5.1}$$

$$e_{T_m} := T_m^E - T_m \tag{3.5.2}$$

This gives:

$$\begin{aligned} T_m &= T_m^E - e_{T_m} \\ &= \beta(\rho) + \zeta - e_{T_m}. \end{aligned} \tag{3.5.3}$$

It is desired to have the error converge to 0, and knowing that the actual torque will be constant in relation to time, the derivative of the error can be written using the chain rule, as below, when inserting the expression for $\dot{\rho}$ defined in (2.2.4c). The β- function can be interpreted as the proportional part of the control, while the ζ-function as the integral part.

$$\begin{aligned}\dot{e}_{T_m} &= \dot{T}_m^E = \beta'(\rho)\cdot\dot{\rho} + \dot{\zeta} \\ &= \beta'(\rho)\cdot(T_m^E - e_{T_m} - \frac{P}{2}\phi i_q + d(\omega_{ref} - \omega_m)) + \dot{\zeta}\end{aligned} \tag{3.5.4}$$

Since the objective is for ζ to cancel out as much as possible from the error expression above except the error itself, $\dot{\zeta}$ can be given as in Equation (3.5.5). The resulting error dynamics are described by Equation (3.5.6).

$$\dot{\zeta} = -\beta'(\rho)\cdot(T_m^E - \frac{P}{2}\phi i_q + d(\omega_{ref} - \omega_m)) \tag{3.5.5}$$

$$\dot{e}_{T_m} = -\beta'(\rho)\cdot e_{T_m} \tag{3.5.6}$$

It is now required to define a $\beta(\rho)$-function that will guarantee asymptotic stability. One method is to use Lyapunov stability analysis. Choosing the quadratic function in Equation (3.5.7), the derivative will be given by Equation (3.5.8).

$$\mathcal{V}(e_{T_m}) = \frac{1}{2}e_{T_m}^2 \tag{3.5.7}$$

$$\begin{aligned}\dot{\mathcal{V}}(e_{T_m}) &= e_{T_m}\dot{e}_{T_m} \\ &= -\beta'(\rho)e_{T_m}^2\end{aligned} \tag{3.5.8}$$

There are several possibilities for how to define β, and Equation (3.5.9) is one example, where $\nu > 0$ is an adaptation gain, impacting the speed of convergence.

$$\beta'(\rho) = \nu \Rightarrow \beta(\rho) = \nu\rho \tag{3.5.9}$$

If this β is chosen, the error dynamics are described by (3.5.10). As a result, the derivative of the Lyapunov candidate will be negatively defined, and the system will consequently be exponentially stable.

$$\begin{aligned}&\dot{e}_{T_m} = -\nu e_{T_m} \\ &\Rightarrow e_{T_m}(t) = e^{-\nu t}\end{aligned} \tag{3.5.10}$$

Consequently, the I&I estimator is asymptotically consistent; that is,

$$\lim_{t\to\infty} T_m^E(t) = T_m$$

for all $(\rho(0), \zeta(0)) \in \mathbb{R}\times\mathbb{R}$, and $T_e(t)$ such that $(\rho(t), T_m^E(t))$ exists for all $t \geq 0$.

Simulations

To validate the theoretical results concerning the stability certificates, the control strategies developed in this thesis will be simulated and executed using the Matlab/Simulink software package. The system will be tested by simulating step changes in the wind speed. The gain values used in control are selected using trial and error while fulfilling the stability criteria developed. The simulations will be carried out for a small wind turbine featuring a blade radius of merely $1.43m$. In this way, it allows for the potential validation of results in a laboratory setting at a later stage. However, the simulation results are valid irrespective of the scaling of the numbers and will also be applicable for large wind turbines in the MW range.

The parameter ν, which essentially impacts the convergence speed for the estimator, was selected using trial and error.

Implementing the estimator in Simulink and using an adaption gain of 40 with the control parameters described in Table 3.2, the response in Figure 3.2 is obtained.

Parameters	value
$k_{p,1}$	500
$k_{p,2}$	5
$k_{i,1}$	5000
$k_{i,2}$	5000
k_p, outer-loop	0.1
$k_{i,\text{outer-loop}}$	0.003

Table 3.2: Control parameters used for Figure 3.2.

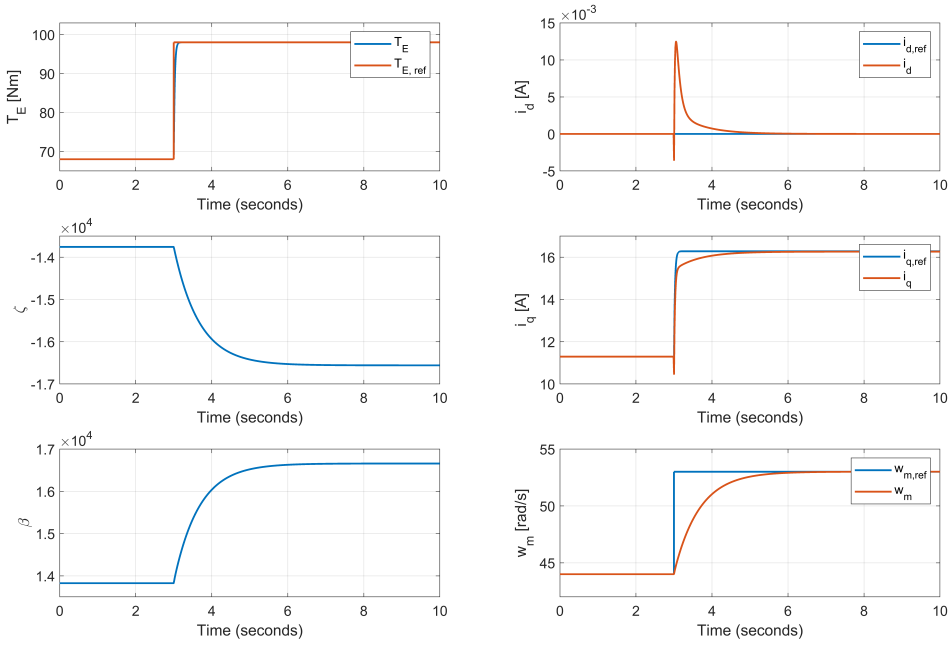

Figure 3.2: Simulating the system with the torque estimator doing a step in torque from 68 to $98Nm$.

The estimator finds the correct value after only one tenth of a second, and it should be mentioned that the estimator could be tuned to obtain an even faster convergence rate. Anyhow, the physical system finds the steady state values, and the system is observed to be stable.

3.5.2 Designing an Adaptive Control Law for the Mechanical Power P

The next step is to investigate if we can rewrite $T_m = \frac{P}{\omega_m}$ and estimate P to account for the additional nonlinearity. The same procedure as above will be repeated, starting with defining the estimator in (3.5.11) and the error in (3.5.12). Introducing P^E into Equation (3.5.12) and rearranging, the expression given in (3.5.13) is obtained.

$$P^E := \beta(\rho) + \zeta \tag{3.5.11}$$

$$e_P := P^E - P \tag{3.5.12}$$

$$\begin{aligned} P &= P^E - e_P \\ &= \beta(\rho) + \zeta - e_P \end{aligned} \tag{3.5.13}$$

The error dynamics can further be described by Equation (3.5.14) when inserting the expression for $\dot{\rho}$ given in (2.2.4c).

$$\begin{aligned} \dot{e}_P = \dot{P}^E &= \beta'(\rho) \cdot \dot{\rho} + \dot{\zeta} \\ &= \beta'(\rho) \cdot (\frac{P^E - e_P}{\omega_m} - \frac{P}{2}\phi i_q + d(\omega_{ref} - \omega_m)) + \dot{\zeta} \end{aligned} \tag{3.5.14}$$

To render the error dynamics attractive, that is, by removing the less interesting terms, the expression below is selected,

$$\dot{\zeta} = -\beta'(\rho) \cdot (\frac{P^E}{\omega_m} - \frac{P}{2}\phi i_q + d(\omega_{ref} - \omega_m)) \tag{3.5.15}$$

resulting in the error dynamics on the form as in (3.5.16). As noted from the equation below, the error dynamics depend on both the $\beta'(\rho)$-function and ω_m, which implies a nonlinear behavior where the speed act as a non-constant disturbance.

$$\dot{e}_P = -\beta'(\rho) \cdot \frac{e_P}{\omega_m} \tag{3.5.16}$$

The $\beta(\rho)$-function will need to be constructed, and also here, there are several possibilities for this function. Having the Lyapunov candidate in (3.5.17), the derivative is given in (3.5.18).

$$V(e_P) = \frac{1}{2}e_P^2 \tag{3.5.17}$$

$$\begin{aligned} \dot{V}(e_P) &= e_P \dot{e}_P \\ &= -\beta'(\rho)\frac{e_P^2}{\omega_m} \end{aligned} \tag{3.5.18}$$

If now, the following function is chosen for β

$$\beta_0'(\rho) = \nu \frac{1}{J\omega} = \nu \frac{1}{\rho} \Rightarrow \beta_0(\rho) = \nu \ln \rho, \tag{3.5.19a}$$

it will correspond to having a $\dot{\mathcal{V}}(e_p) < 0 \; \forall \; e_p \in \mathbb{R}$. However, major drawbacks are observed if using this β-function, since it will give a problem when the mechanical rotor speed is zero, for example, during generator start-up. A series of β candidates are proposed below, and it is interesting to investigate how the different functions impact the convergence speed. Such simulations are performed in the following subsection.

i: $\beta_1'(\rho) = \nu\rho$
$\Rightarrow \beta_1(\rho) = \frac{1}{2}\nu\rho^2$

ii: $\beta_2'(\rho) = \nu \cdot 0.01 \cdot \rho^3$
$\Rightarrow \beta_2(\rho) = \frac{1}{4}\nu \cdot 0.01 \cdot \rho^4$

iii: $\beta_3'(\rho) = \arctan(\nu\rho)$
$\Rightarrow \beta_3(\rho) = \rho \arctan(\nu\rho) - \frac{ln(\nu^2\rho^2+1)}{2\nu}$

Simulations of different choices of β-functions for the estimator

The form of the different candidates in the above section, when divided on the mechanical speed, is shown in Figure 3.3 for $\nu = 1$. The second β-function is multiplied with 0.01 to slow it down for practical purposes.

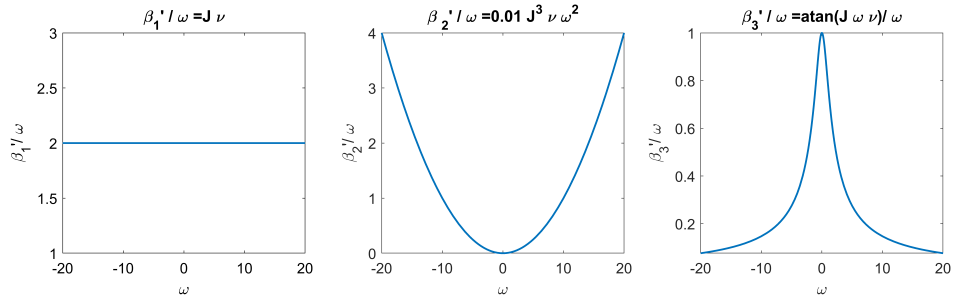

Figure 3.3: Different choices for β-functions.

It is evident that all candidates will give $\dot{\mathcal{V}} \leq 0$, resulting in a passive system. It can further be investigated how the choice of β will influence the convergence speed of the estimator. The performance of the three estimators is depicted in Figure 3.4, 3.5, and 3.6.

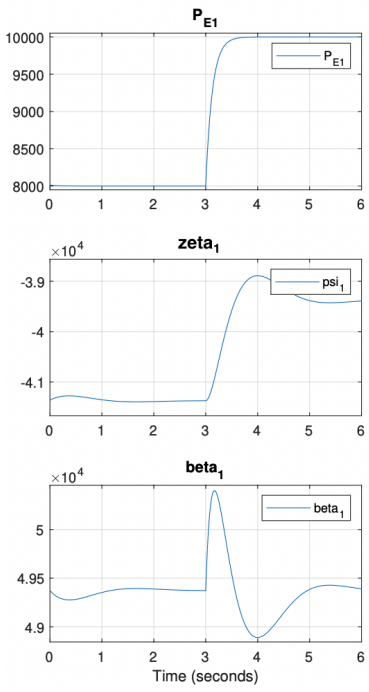

Figure 3.4: P_{E1} using $\beta_1(\rho)$.

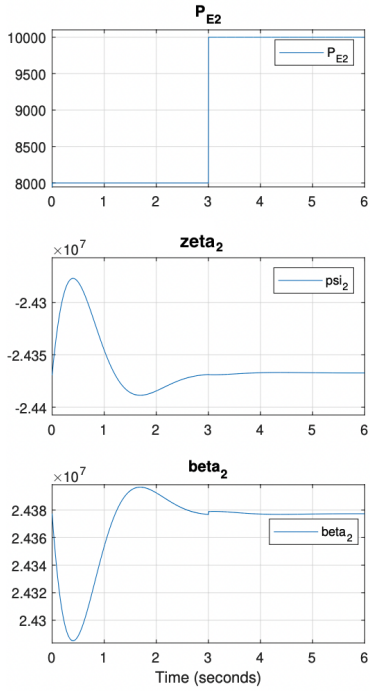

Figure 3.5: P_{E2} using $\beta_2(\rho)$.

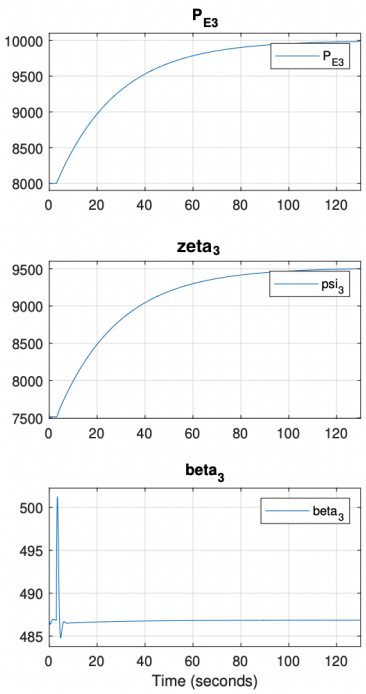

Figure 3.6: P_{E3} using $\beta_3(\rho)$.

It is observed that the first and second estimators are relatively fast compared to the third estimator. The third estimator takes more than 120 seconds to converge to the correct estimated value, which is unacceptably slow. On the other hand, the second option is extremely fast. However, it should be noted that the first alternative can be fine-tuned by using a higher adaption gain, resulting in reaching the desired value in a reasonable amount of time. In addition, it can sometimes be beneficial to slow down the estimator to increase the performance of the rest of the system. Hence, the first estimator which uses $\beta_1(\rho) = \frac{1}{2}\nu\rho^2$, is a viable option.

Using the selected β-function, the designed estimator can be incorporated into the system model described in (2.2.4). If the control parameters are as described in Table 3.3, the response to a step in mechanical power from 1900 to 2900W is shown in Figure 3.7.

Parameters	value
$k_{p,1}$	1000
$k_{p,2}$	5
$k_{i,1}$	50000
$k_{i,2}$	500
$k_{p,\text{outer-loop}}$	1
$k_{i,\text{outer-loop}}$	0.005

Table 3.3: Control parameters used for Figure 3.7.

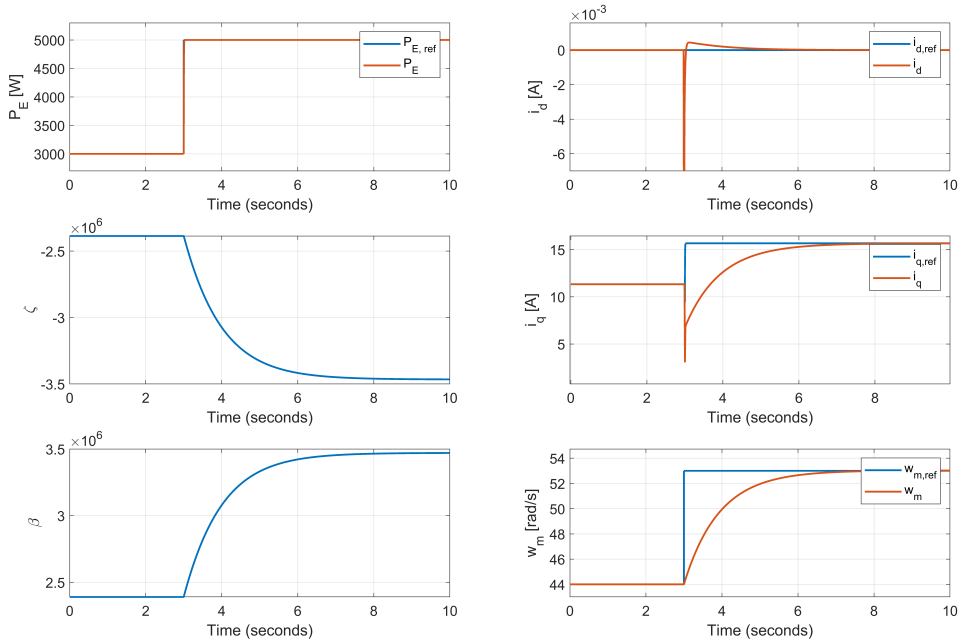

Figure 3.7: Simulating the system with the power estimator doing a step in power from 3000 to $5000W$.

Also here, the adaption gain used is $\nu = 40$. The estimator only requires $0.02s$ to obtain the actual power input, and the rest of the system is observed to be stable. The theoretical results are therefore validated.

3.5.3 Designing an Adaptive Control Law for the Wind Speed

We are in a position to estimate the actual wind speed, and the same dynamic equation will be used as in the former subsection. For simplicity, this thesis has so far not considered the nonlinear relation between angular velocity and mechanical torque, given in (2.2.3).

The following method of procedure is inspired by [39], and the reader is referred to [43] and [44] for further proof and details of the proposition. The expression for $\dot{\rho}$ is divided by J, and introducing the new notation $\Phi(\omega_m, v_w)$, $F(t)$ and $G(\omega)$.

$$\dot{\omega}_m = \frac{T_m - T_e}{J} = \underbrace{\frac{\rho A}{2J} v^3 C_p(\lambda) \frac{1}{\omega_m}}_{\Phi(\omega_m, v_w)} - \underbrace{\frac{P}{2J}\phi i_q}_{F(t)} + \underbrace{\frac{d}{J}(\omega_{ref} - \omega_m)}_{G(\omega)} \tag{3.5.20}$$

The form of the wind power coefficient is depicted in the following figure:

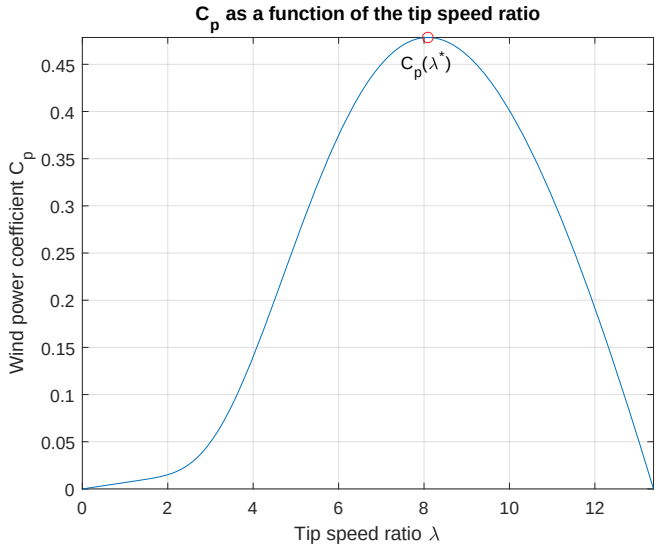

Figure 3.8: The wind power coefficient as a function of the tip speed ratio.

Since C_p is now included, additional comments regarding this function will be discussed. A typical shape for this function is shown in Figure 3.8, where the operating region is restricted to $\lambda \in [0, \lambda_M]$, giving:

$$C_p(\lambda) \begin{cases} = 0 \text{ for } \lambda = 0 \\ > 0 \text{ for } \lambda \in (0, \lambda_M) \\ = 0 \text{ for } \lambda = \lambda_M \end{cases} \tag{3.5.21}$$

Further, it is assumed that the power coefficient is a smooth function that verifies

$$C_p'(\lambda) \begin{cases} > 0 \text{ for } \lambda \in [0, \lambda^*) \\ = 0 \text{ for } \lambda = \lambda^* \\ < 0 \text{ for } \lambda \in (\lambda^*, \lambda_M], \end{cases} \tag{3.5.22}$$

where $(\cdot)'$ denotes differentiation. In addition, the wind speed is assumed to be a positive constant, and the flux, current, and rotor speeds are measurable. Note that C_p is also a function of the blade pitch angle, typically denoted β. However, we are interested in the operation regime where this angle is constant, typically zero, since this corresponds to operating at maximum aerodynamic efficiency [21].

The estimator and error are defined in (3.5.23) and (3.5.24), respectively, giving the expression for the wind speed in (3.5.25).

$$v_w^E := \beta(\omega_m) + \zeta \tag{3.5.23}$$

$$e_{v_w} := v_w^E - v_w \tag{3.5.24}$$

$$\begin{aligned} v_w &= v_w^E - e_{v_w} \\ &= \beta(\omega) + \zeta - e_{v_w} \end{aligned} \tag{3.5.25}$$

The error dynamics can be found in (3.5.26), while ζ is defined using the speed estimator, as in (3.5.27).

$$\begin{aligned} \dot{e}_{v_w} &= \dot{v_w}^E = \beta'(\omega) \cdot \dot{\omega} + \dot{\zeta} \\ &= \beta'(\omega) \cdot (\Phi(\omega_m, v_w) + F(t) + G(\omega)) + \dot{\zeta} \end{aligned} \tag{3.5.26}$$

$$\dot{\zeta} = -\beta'(\omega) \cdot (\Phi(\omega_m, v_w^E) - F(t) + G(\omega)) \tag{3.5.27}$$

Inserting $\dot{\zeta}$ into the expression for the error, the following equation is obtained. Here, a new parameter called the tip speed ratio is defined as $\lambda = \frac{r\omega}{v_w}$.

$$\begin{aligned} \dot{e}_{v_w} &= -\beta'(\omega_m) \cdot (\Phi(\omega_m, v_w) - \Phi(\omega_m, v_w^E)) \\ &= -\beta'(\omega_m) r \frac{1}{2J} \rho A \cdot (v^2 \frac{v}{r\omega_m} C_p(\frac{r\omega}{v_w}) - (v_w^E)^2 \frac{v_w^E}{r\omega_m} C_p(\frac{r\omega}{v_w^E})) \\ &= -\beta'(\omega_m) r \frac{1}{2J} \rho A \cdot (v^2 \frac{1}{\lambda} C_p(\lambda) - (v_w^E)^2 \frac{1}{\lambda^E} C_p(\lambda^E)) \end{aligned} \tag{3.5.28}$$

Now, the β function will need to be constructed. If the Lyapunov candidate is defined as the error between the estimated and the actual speed, such as in Equation (3.5.29), then its derivative will take the form as in Equation (3.5.30).

$$V(e_{v_w}) = \frac{1}{2} e_{v_w}^2 = \frac{1}{2} (v_w^E - v_w)^2 \tag{3.5.29}$$

$$\begin{aligned} \dot{V}(e_{v_w}) &= e_{v_w} \dot{e}_{v_w} \\ &= \beta'(\omega_m)(v_w^E - v_w)(\Phi(\omega_m, v_w) - \Phi(\omega_m, v_w^E)) \\ &= -(v_w - v_w^E)[\beta'(\omega_m)\Phi(\omega_m, v_w) - \beta'(\omega_m)\Phi(\omega_m, v_w^E)] \end{aligned} \tag{3.5.30}$$

The key step will be to construct the β-function so that the function $\varrho = \beta'(\omega_m)\Phi(\omega_m, v_w)$ is strictly monotonically increasing. The latter is true if and only if its derivative, expressed below, is positive.

$$\varrho' = \beta'(\omega_m) \cdot \frac{\partial \Phi}{\partial v_w} = \beta'(\omega_m) \frac{\rho A}{2J} r v_w [\frac{3 v_w}{r\omega} C_p(\frac{r\omega}{v_w}) - C_p'(\frac{r\omega}{v_w})]$$

Since the wind speed is a positive constant and β is a function we construct ourselves; it is evident that the monotonicity proof relies on the sign of $\Phi'(\omega_m, v_w)$. To investigate, the term in brackets above can be written in a more compact form, shown below.

$$\mathcal{K}(\lambda) = \frac{3}{\lambda} C_p(\lambda) - C_p'(\lambda) \tag{3.5.31}$$

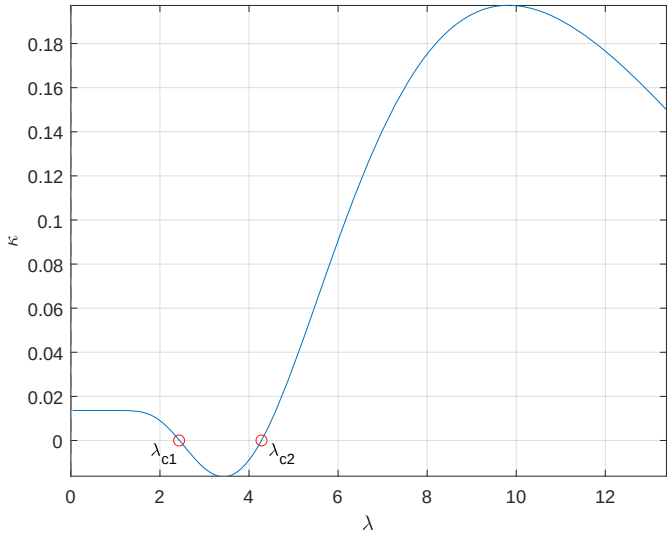

Figure 3.9: $\kappa(\lambda)$-condition when the function changes sign, introducing λ_{c1} and λ_{c2}.

The following lemma will further be of great relevance, and its proof can be found in [39].

Lemma 1. *There exist two constants, λ_{c1} and λ_{c2}, marked in Figure 3.9, where*

$$0 < \lambda_{c1} < \lambda_{c2} < \lambda^*$$

such that

$$\mathcal{K}(\lambda) > 0 \text{ for } \lambda \in [0, \lambda_{c1}) \cup (\lambda_{c2}, \lambda_M].$$

Further, if β is defined as:

$$\beta'(\omega_m) = \nu \Rightarrow \beta(\omega_m) = \nu\omega_m \tag{3.5.32}$$

where ν is a positive constant, the derivative of β is positive regardless of the rotor speed. We are then left with two cases:

1. If
$$\frac{3}{\lambda}C_p(\lambda) > C_p'(\lambda) \tag{3.5.33}$$
for all $\lambda \in (0, \lambda^*)$, then ϱ is monotonically increasing for all ω_m.

2. On the other hand, if there exists an $\omega_m^{c2} < \omega_m^*$, where ω_m^{c2} defines the rotor speed for which $\mathcal{K}(\lambda^{c2}) = 0$, and where w_m^*, corresponding to the point of maximum power extraction, is defined as:
$$\omega_m^* = \frac{v_w}{r}\lambda^*, \tag{3.5.34}$$
then ζ is monotonically increasing as long as
$$\lambda > \lambda_{c2} \Rightarrow \omega_m(t) > \omega_m^{c2} \tag{3.5.35}$$
for all $t \geq 0$.

If either of these cases holds, the I&I estimator is asymptotically consistent.

It is further observed that the model used has some drawbacks and is, in principle, not suited for this type of control scheme. For the previous master thesis in [22], they included the simplified damping term, which was a possibility since they also had an outer loop for speed regulation, which was not a part of the stability proof. This was defended by the assumption that the dynamics of the wind are sufficiently slow; hence the output of the outer loop controller could be viewed as a constant. In that case, they decided the reference speed themselves, and this parameter could therefore be included in the machine model. However, in our case, the reference speed for the rotor is calculated as a function of the wind speed and only provided to the load flow, and an outer loop was initially not included. To avoid including the reference term for the rotor speed in the machine model, the model should be updated to describe the short-circuited copper bars (the damper winding) more realistically. This is left for future work. In addition to the problem concerning the damper term, there is also observed an additional problem when excluding the outer loop. Looking at Equation (2.2.4c) at steady state while assuming $\omega_m = \omega^{\text{ref}}$, the following relation is obtained:

$$\begin{aligned} 0 = T_m - T_e = \Gamma(\bar{v})\frac{C_p(\bar{\lambda})}{\bar{\omega}_m} - T_e \\ \Rightarrow T_e = \Gamma(\bar{v})\frac{C_p(\bar{\lambda})}{\bar{\omega}_m} = T_m \end{aligned} \tag{3.5.36}$$

If C_p and $\Gamma(\bar{v})$ are constant, it's obvious that one rotor speed corresponds to a unique electrical torque value (thus a specific current) and vice versa. If, on the other hand, C_p is not a constant but represents the figure in 3.8, one mechanical rotor speed will indeed give a unique electric torque value. However, if given quadrature current as input (proportional to electric torque), as done in the model, two different rotor speeds will provide the torque value.

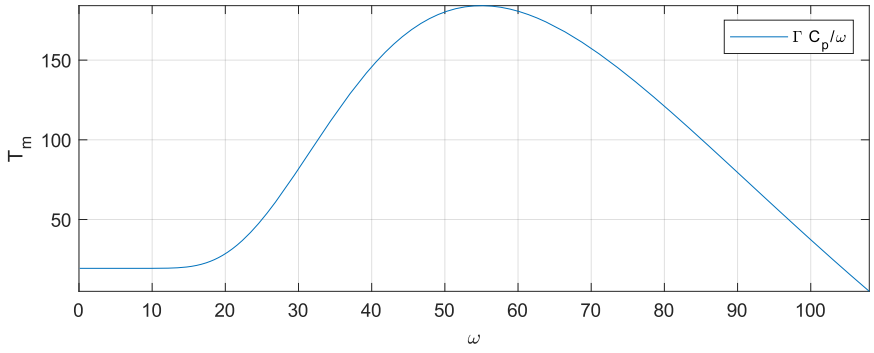

Figure 3.10: Demonstration of the torque equation, where two rotor speeds give the same torque.

One potential solution to address this issue is to explore the possibility of including an outer loop in the stability certificate or utilizing alternative control methods, where one integrates the mechanical speed error. The latter approach was examined in the pre-project phase leading up to this thesis, involving controlling the rotor speed in the integral channel of one of the inner loop controllers. Unfortunately, it was not successful in satisfying the conditions found for stability. Another possibility that was investigated was to introduce a leaky integrator to control the mechanical rotor speed in one of the integral channels. However, in the presence of an imperfect model of the system, such an approach would result in deviation from the desired equilibrium point. Since no other viable solutions were found, this thesis will adopt a speed controller in the outer loop.

This approach is justified by assuming that the wind's dynamics are sufficiently slow, enabling the output of the speed controller to be considered constant. However, under certain operating conditions, this may not be guaranteed, posing a potential risk to stability. To maintain some consistency with the existing stability certificate, this thesis will define the new reference value as $\hat{i}_q^{\text{ref}} = i_q^{\text{ref}} - e_\omega$, where e_ω represents the difference between the measured and reference value of rotor speed. Including an outer loop will also contribute to justifying the use of the damper term. For future work, singular perturbation theory could be an exciting research topic. This is a mathematical tool used to analyze systems with multiple time scales. Due to time scale separation between the outer loop and the remaining system, the outer loop could potentially be included in the stability proof.

Simulations

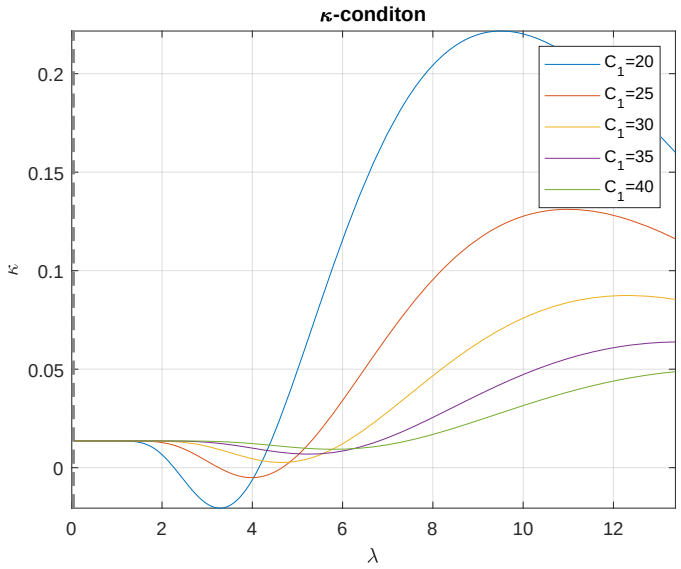

Figure 3.11: $\kappa(\lambda)$-function for different values of C_1.

The wind power coefficient (C_p) curve used in this thesis has a constant value of $C_1 = 21$. However, the corresponding κ-function exhibits sign changes, and as a result, the system does not achieve global asymptotic stability as proposed in [39]. Nevertheless, the system remains stable, provided that the mechanical rotor speed (ω_m) is greater than the second zero crossing for the tip speed ratio, corresponding to (ω_{c2}), as discussed in section 3.5.3. Since the maximum power point tracking (MPPT) algorithm employed in this study operates at the optimal tip speed ratio, there should be no issues with steady-state operation. However, under changing wind speeds, the angular rotor speed may deviate from the optimal operating point, resulting in potential stability issues. One potential solution is to modify one of the constants in the C_p function, such as C_1. Figure 3.11 illustrates the $\kappa(\lambda)$-function for different C_1 values. Notably, a value of $C_1 \geq 30$ satisfies the condition for global asymptotic stability. Note that the shape of $C_p(\lambda)$ depends on the wind turbine's design, and the curve is obtained from simulations and/or experimental data. Consequently, the options available are to continue using the current C_p curve and rely on operating within the safe region, use an alternative C_p curve (hence, another wind turbine), or inquire with the manufacturer regarding the feasibility of building a wind turbine that satisfies $C_1 \geq 30$. Due to the limitations in scope and time constraints, this thesis will continue using the existing wind power coefficient curve.

Notably, when the κ-function falls below zero, the system becomes immediately unstable. In many

cases, stability analysis using Lyapunov candidate functions involves several state variables, as demonstrated in the candidate function presented in (3.3.1). When determining whether the candidate matrix is positive or negative using Schur complement or eigenvalue analysis, the matrix is only negative if all eigenvalues are negative or positive if all eigenvalues are positive. If the eigenvalues have both positive and negative values, making them sign-indefinite, it is unclear how the system will behave. However, in the case of having only one state variable, such as that presented in (3.5.29), a negative value of the κ-function in (3.5.31) results in the Lyapunov candidate function in (3.5.30) not being monotonically increasing. Consequently, the system becomes unstable, as demonstrated later in the simulations.

The estimator for the wind speed will now be tested through simulations. The control structure used to simulate the system is shown in the figure below.

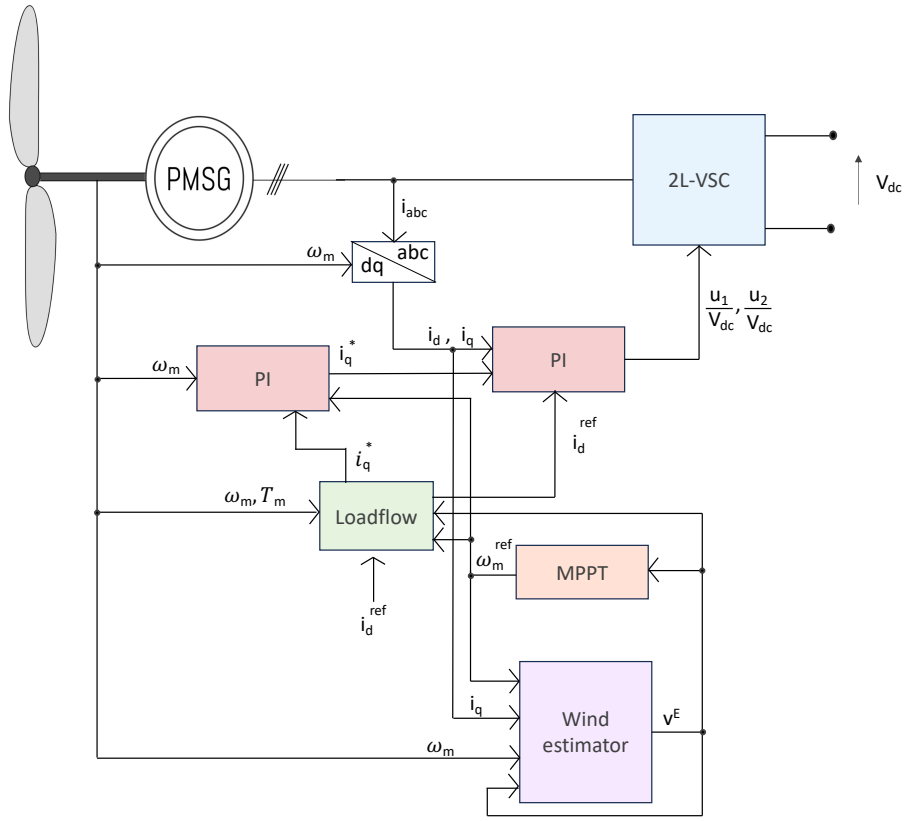

Figure 3.12: Control structure of primary side with an outer speed loop and wind speed estimation.

The control variables are given in Table 3.4, and the response to a step in wind speed from $7m/s$ to $9m/s$, when $\nu = 40$, is shown in Figure 3.13.

Parameters	value
$k_{p,1}$	6
$k_{p,2}$	500
$k_{i,1}$	5000
$k_{i,2}$	500
$k_{p,\text{outer-loop}}$	4
$k_{i,\text{outer-loop}}$	10

Table 3.4: Control parameters used for Figure 3.13.

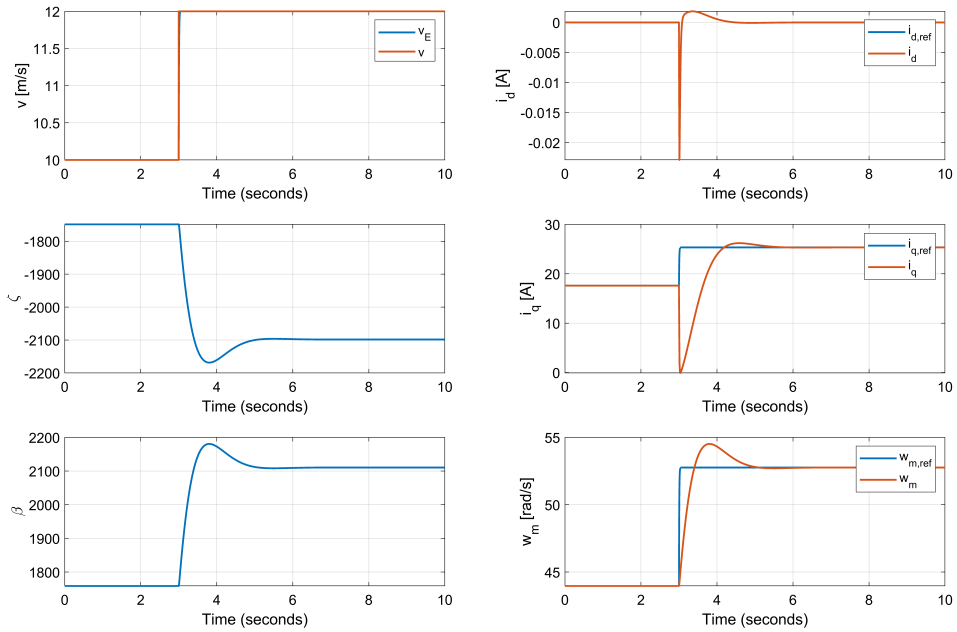

Figure 3.13: Simulating the system with the wind speed estimator doing a step in wind speed from $10m/s$ to $12m/s$.

The estimator finds the correct value after just $0.05s$, and the system is observed to be stable. When the step is performed and the speed is moving toward the new reference value, there is a temporary phenomenon where the currents initially move in the opposite direction of the reference. However, shortly after, they adjust and reach a new equilibrium. Notably, it is observed that the q-axis current drops below zero, indicating that the generator acts as a motor for a short amount of time. This operation mode is less than ideal. From the simulations above, preliminary observations suggest that the system may have the characteristics of a non-minimum phase system. For nonlinear systems, a minimum phase system is a system that has stable zero dynamics. The analysis of zero dynamics is a theoretical approach where the error of the regulated output is forced to zero. [45] To this end, any current errors in the equations are artificially put to zero, even though in reality it takes time for this to happen. This enables us to enter the zero dynamics manifold where the passive output is zero and explore the behavior of the rest of the variables. If the resulting artificial system is stable, the system is a minimum-phase system. On the other hand, if it possesses unstable zero dynamics, the other variables, in this case, the rotor speed, exhibit a counteractive response to changes in the currents. This results in an oscillatory behavior until eventual stabilization, with one variable moving up while the other moves down, creating an alternating pattern.

Since the type of control resembles a PI-control of the currents, and it is assumed that i_d and i_q went to i_d^{ref} and i_q^{ref}, we are now only interested in the dynamics of the mechanical rotor speed. We can first examine the easy case of T_m being a constant. If introducing the incremental model, where constants are eliminated, the following result is obtained:

$$\dot{\tilde{\omega}} = -\frac{d}{J}\tilde{\omega} \Rightarrow \tilde{\omega} = c_1 e^{-\frac{d}{J}t} \tag{3.5.37}$$

which obviously is a linear, stable system. If, on the other hand the mechanical torque is not stable, zero dynamics of the rotor speed is described in (3.5.38).

$$\dot{\tilde{\omega}} = -\frac{d}{J}\tilde{\omega} + \frac{T_m(\omega)}{J} - \frac{T_m(\bar{\omega})}{J} \tag{3.5.38}$$

The stability can further be investigated using the quadratic Lyapunov candidate

$$\mathcal{V}(\omega) = \frac{1}{2}J\tilde{\omega}^2, \tag{3.5.39}$$

where the time derivative can be calculated as follows:

$$\begin{aligned}\dot{\mathcal{V}} &= -(\omega - \bar{\omega})d(\omega - \bar{\omega}) + (\omega - \bar{\omega})\left(T_m(\omega) - T_m(\bar{\omega})\right) \\ &= -(\omega - \bar{\omega})\left[d(\omega - \bar{\omega}) - (T_m(\omega) - T_m(\bar{\omega}))\right] \\ &= -(\omega - \bar{\omega})\left[\hat{M}(\omega) - \hat{M}(\bar{\omega})\right].\end{aligned} \tag{3.5.40}$$

In the above expression, $\hat{M}$ is defined as

$$\hat{M} := d\omega - T_m(\omega).$$

As we already know, monotonicity can be investigated for an expression on the form as in (3.5.40) by calculating the derivative of the function $\hat{M}$. This results in the following condition being required to obtain a minimum phase system.

$$\frac{\partial \hat{M}}{\partial \omega} > 0 \Rightarrow d - \frac{\partial T_m(\omega)}{\partial \omega} > 0 \tag{3.5.41}$$

An interesting observation is that this condition is already satisfied as long as the condition in (3.2.20) is satisfied. Since the damper coefficient used in the simulation was deliberately chosen to fulfill the latter condition, it can be concluded that the system is indeed a minimum-phase system. However, in the simulations performed, an outer loop was included that was not incorporated into the stability proof. This may cause the total system now to be a non-minimum phase system. Due to the complexity of the zero dynamics analysis when incorporating the outer loop, the proof is left for future work. However, such systems are difficult to control, and due to the inherent tendency of "undershooting" in its step response, the control objective should often be to bound the error rather than perfect tracking. The reader is referred to [46] for a deeper understanding of non-minimum-phase nonlinear systems. There have been proposed different solutions to these problems, and in [47], they design a feedback control law based on the approximated minimum-phase system for slightly non-minimum phase systems, while in [48], they propose a new approach of using input-output linearization to control a single input-output non-minimum phase nonlinear system. Anyhow, this thesis will satisfy by making the outer loop sufficiently slow, thereby minimizing its influence on the system. If now using the parameters for a slow outer loop given in Table 3.5, the response is given in Figure 3.14.

Parameters	value
$k_{p,1}$	1000
$k_{p,2}$	5
$k_{i,1}$	50000
$k_{i,2}$	500
$k_{p,outerloop}$	1.2
$k_{i,outerloop}$	0.005

Table 3.5: Control parameters used for Figure 3.14.

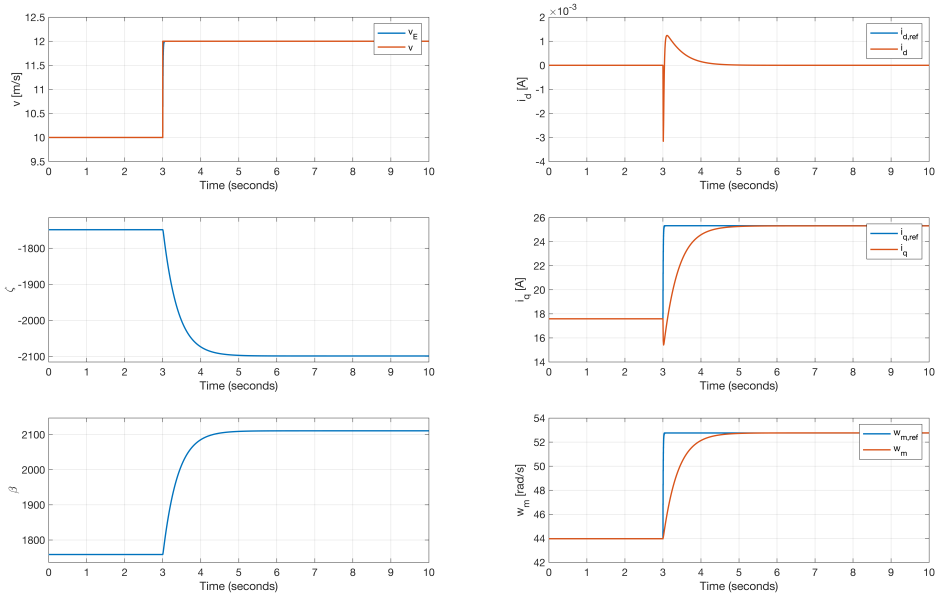

Figure 3.14: Simulating the system with the wind speed estimator doing a step in wind speed from $10m/s$ to $12m/s$.

By comparing Figure 3.14 and Figure 3.13, it is clear that a slower outer loop controller contributes to significantly reducing the undershoot of the currents. All the state variables find their equilibrium, and the system is observed to be stable. The estimator can further be checked for when the $\kappa > 0$-condition in (3.5.31) is not satisfied, and an unstable estimator is expected. From Figure 3.9, it is clear that $\lambda = 3$ will be in the range of negative κ-values, hence achieving instability. If the parameters in Table 3.6 are used, the response is shown in Figure 3.15.

Parameters	value
$k_{p,1}$	6
$k_{p,2}$	5
$k_{i,1}$	500
$k_{i,2}$	500
$k_{p,outerloop}$	4
$k_{i,outerloop}$	10

Table 3.6: Control parameters used for Figure 3.15.

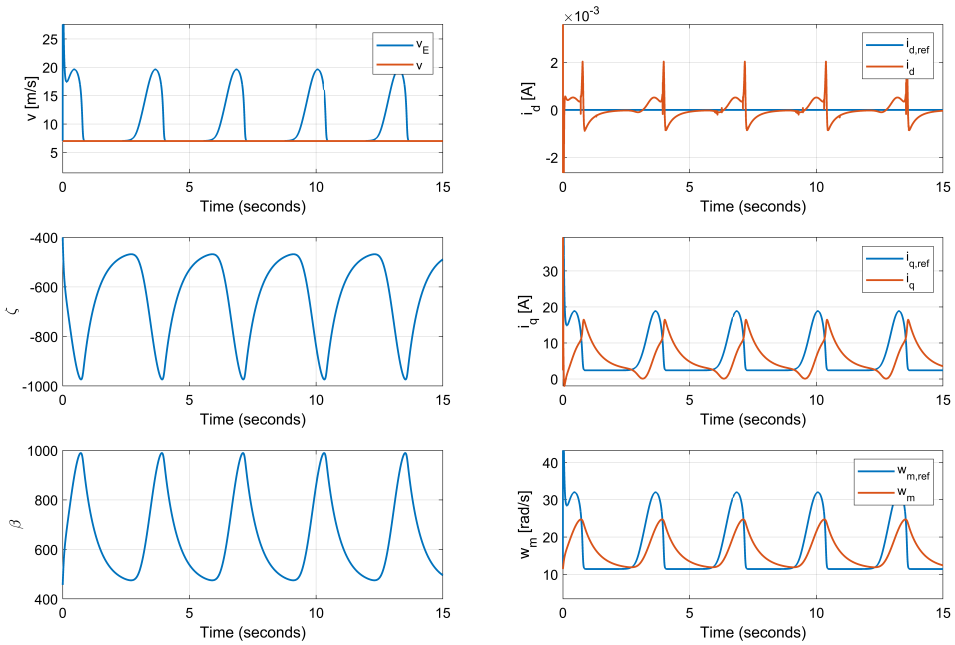

Figure 3.15: When K-condition is not satisfied.

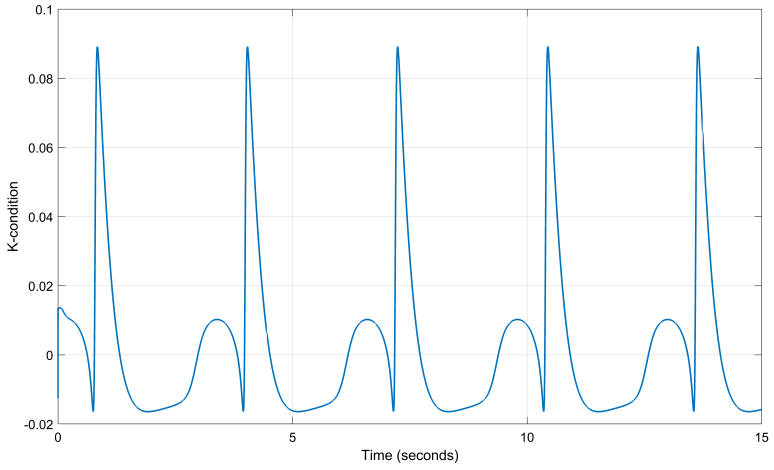

Figure 3.16: K-condition.

What is observed in the figure presented is that once the κ-condition is no longer fulfilled, the system starts on the track of instability. However, due to the mechanical rotor speed being unable to follow the reference speed perfectly, the tip speed ratio at some point gets into the range of λs giving stable solutions. Consequently, the system may look marginally stable but is, in reality switching between the stable region and the unstable region.

3.6 Boundness of I&I

The only thing the I&I estimator requires from the system, except from having a uniformly globally asymptotically stable equilibrium point, is that none of the trajectories of the system goes to infinity. In return, the system requires the I&I estimator to give an estimate different from infinity. One way to ensure this is to bound one of the variables.

3.6.1 Bounding the Controller Output

A possibility may be to bound the output of the controller. This is investigated below, starting with the Lyapunov candidate presented in (3.6.1).

$$\mathcal{W}_2(x, x_c) := \underbrace{\frac{1}{2}\tilde{x}^\top Q\tilde{x}}_{\mathcal{V}(x)} + \frac{1}{2}\tilde{x}_c^\top K_I \tilde{x}_c, \tag{3.6.1}$$

For a PI controller, v can be defined as in (3.6.2), while $\bar{v}$ will be given by (3.6.3). Now, a new function w is introduced, which takes into account the saturation of the control signal to guarantee that the signal will never go to infinity. This is done to ensure that the estimator from I&I will be guaranteed to work.

$$v = -K_p y + K_I x_c, \tag{3.6.2}$$

$$\bar{v} = -K_p \bar{y} + K_I \bar{x}_c. \tag{3.6.3}$$

$$\tilde{u} = w(v) - w(\bar{v}) = [\frac{w(v) - w(\bar{v})}{v - \bar{v}}]\tilde{v} = l(v)\tilde{v} \tag{3.6.4}$$

where $l(v)$ is closely related to the derivative of w, and $\dot{x}_c$ is defined as in (3.6.5).

$$\dot{x}_c = -(y - y^{\text{ref}}) \tag{3.6.5}$$

The term in brackets in Equation (3.6.4) is bounded and positive definite for a monotonically increasing function $w(v)$ as described in definition 1, and practically, a bounded, positive function can be viewed as the second best thing to a constant.

With the new Lyapunov candidate introduced in (3.6.1), the time derivative can be established.

$$\dot{\mathcal{W}}_2 = \dot{\mathcal{V}} + \nabla^\top (\frac{1}{2}\tilde{x}_c^\top K_I \tilde{x}_c) \begin{bmatrix} \dot{\tilde{x}} \\ \dot{\tilde{x}}_c \end{bmatrix} = \dot{\mathcal{V}} + \frac{\partial}{\partial \tilde{x}_c}(\frac{1}{2}\tilde{x}_c^\top K_I \tilde{x}_c)\dot{\tilde{x}}_c = \dot{\mathcal{V}} - \tilde{x}_c^\top K_I \tilde{y} \tag{3.6.6}$$

Rewritten, knowing that each term is a scalar, Equation (3.6.7) is obtained.

$$\dot{\mathcal{W}}_2 = \dot{\mathcal{V}} - \tilde{y}^\top [K_I x_c - K_I \bar{x}_c] \tag{3.6.7}$$

Using Equation (3.6.3) and solving Equation (3.6.2) for $K_I x_c$, Equation (3.6.8) is found.

$$\dot{\mathcal{W}}_2 = \dot{\mathcal{V}} - \tilde{y}^\top [\frac{u}{l(v)} + K_p \tilde{y} - \frac{\bar{u}}{l(v)}] \tag{3.6.8}$$

If now, Equation (3.2.24) is inserted into the above equation and rearranged:

$$\begin{aligned}\dot{\mathcal{W}}_2 &\leq \tilde{y}^\top \tilde{u} + \gamma \tilde{y}^\top \tilde{y} - \tilde{y}^\top \frac{\tilde{u}}{l(v)} - \tilde{y}^\top K_p \tilde{y} \\ &= \tilde{y}^\top l(v)[-K_p y + K_I x_c](1 - \frac{1}{l(v)}) - \tilde{y}^\top (K_p - \gamma)\tilde{y} \\ &= -\tilde{y}^\top K_p l(v) y + \tilde{y}^\top K_I x_c (l(v) - 1) + \tilde{y}^\top \gamma y \\ &= -\tilde{x}^\top Q G [K_p l(v) - \gamma] G^\top Q \tilde{x} - \tilde{x}^\top Q G (1 - l(v)) K_I x_c \\ &= -\begin{bmatrix} Q\tilde{x} \\ K_I \tilde{x}_c \end{bmatrix}^\top \begin{bmatrix} K_p l(v) - \gamma & -\frac{G - G l(v)}{2} \\ -\frac{G^\top - G^\top l(v)}{2} & 0 \end{bmatrix} \begin{bmatrix} Q\tilde{x} \\ K_I \tilde{x}_c \end{bmatrix}\end{aligned} \tag{3.6.9}$$

As can be noticed from the matrix shown in (3.6.9), it now contains off-diagonal elements that create a nonsingular matrix when one diagonal element is zero. This issue will be tried to be resolved, where a form of anti-windup will be implemented. The key is to stop integrating when the parameter value has saturated. If now, the integrator channel in the controller also contains the bounded, positive function $l(v)$, as presented in (3.6.10), then the derivative of the Lyapunov candidate takes the form in (3.6.11).

$$\dot{x}_c = l(v) g^\top Q x \tag{3.6.10}$$

$$\dot{\mathcal{W}}_2 = \dot{\mathcal{V}} + \nabla^\top (\frac{1}{2} \tilde{x}_c^\top K_I \tilde{x}_c) \begin{bmatrix} \dot{\tilde{x}} \\ \dot{\tilde{x}}_c \end{bmatrix} = \dot{\mathcal{V}} + \frac{\partial}{\partial \tilde{x}_c} (\frac{1}{2} \tilde{x}_c^\top K_I \tilde{x}_c) \dot{\tilde{x}}_c = \dot{\mathcal{V}} - \tilde{x}_c^\top K_I l(v) \tilde{y} \tag{3.6.11}$$

Using the fact that each term is a scalar, and rewriting using the incremental dynamics, the following equation is obtained.

$$\dot{\mathcal{W}}_2 = \dot{\mathcal{V}} - \tilde{y}^\top l(v)[K_I x_c - K_I \bar{x}_c] \tag{3.6.12}$$

Then again using the expression in (3.6.2), (3.6.3) and (3.6.4), we get:

$$\begin{aligned}\dot{\mathcal{W}}_2 &= \dot{\mathcal{V}} - \tilde{y}^\top l(v)[\frac{u}{l(v)} + K_p \tilde{y} - \frac{\bar{u}}{l(v)}] \\ &\leq \tilde{y}^\top \tilde{u} + \gamma \tilde{y}^\top \tilde{y} - \tilde{y}^\top \tilde{u} - \tilde{y}^\top K_p l(v) \tilde{y} \\ &= -\tilde{y}^\top [K_p l(v) - \gamma] \tilde{y}.\end{aligned} \tag{3.6.13}$$

Requiring the derivative of the Lyapunov candidate to be negative, the condition $K_p l(v) > \gamma$ is introduced. Hence, when closing in on the equilibrium, the term $K_p l(v)$ diminishes in magnitude. However, in order to satisfy the condition in (3.2.20), it is advantageous to choose a sufficiently large γ to avoid the need for high damping. As a result, while this solution may not be practically beneficial since it only guarantees regional asymptotic stability, it could be worth exploring whether an alternative Lyapunov candidate could yield more promising outcomes.

Other solutions to prevent the system from going unstable could be to bound the estimator output. However, in this thesis, we will rely on the assumption that the estimator does not yield infinite values as a means to ensure stability and avoid the need for additional bounding measures.

Chapter 4

Stability Certificate for the follower subsystem

In this section, the secondary side of the system is analysed by means of the second method of Lyapunov. A stability certificate will be derived for the nonlinear model of the grid-side 2L-VSC, first by only including its passive output in the integral channel of the controller, which leads to a globally asymptotically stable system when controlled with a PI. However, since this passive output requires perfect knowledge of current and voltage references for tight regulation, we would need to rely on having a perfect model of a real system for the load flow to achieve our control objectives, which is not a realistic assumption. As an alternative solution, a "leaky integrator" is therefore investigated, giving the opportunity to indirectly control the voltage in the inner control loop. We show that the leakage term allows to *approximately* regulate the voltage as it significantly limits voltage deviations caused by imperfect equilibrium knowledge, while preserving stability guarantees.

4.1 System Modeling of Secondary Side

For a 2L-VSC connected to the grid, where the motor side is viewed as a power source when the system is decoupled, the equations in (2.2.5) can be written on matrix form:

$$\dot{x} = \begin{bmatrix} \dot{q}_{dc} \\ \dot{\psi}_d^G \\ \dot{\psi}_q^G \end{bmatrix} = \underbrace{\begin{bmatrix} 0 \\ -V_d^G \\ -V_q^G \end{bmatrix}}_{E} + \left(u_1^{(2)} \underbrace{\begin{bmatrix} 0 & -1 & 0 \\ 1 & 0 & 0 \\ 0 & 0 & 0 \end{bmatrix}}_{\mathcal{J}_1} + u_2^{(2)} \underbrace{\begin{bmatrix} 0 & 0 & -1 \\ 0 & 0 & 0 \\ 1 & 0 & 0 \end{bmatrix}}_{\mathcal{J}_2} + L_G \omega_G \underbrace{\begin{bmatrix} 0 & 0 & 0 \\ 0 & 0 & 1 \\ 0 & -1 & 0 \end{bmatrix}}_{\mathcal{J}_3} - \underbrace{\begin{bmatrix} G - \frac{P(t)}{v_{dc}^2} & 0 & 0 \\ 0 & r_G & 0 \\ 0 & 0 & r_G \end{bmatrix}}_{\mathcal{R}(v_{dc})} \right) \underbrace{\begin{bmatrix} v_{dc} \\ i_d^{(2)} \\ i_q^{(2)} \end{bmatrix}}_{\nabla \mathcal{H}(x)} \tag{4.1.1}$$

The form above is the port-Hamiltonian matrix form, and in compact form, the equation can be written as

$$\dot{x} = (u_1^{(2)}\mathcal{J}_1 + u_2^{(2)}\mathcal{J}_2 + L_G\omega_G\mathcal{J}_3 - \mathcal{R}_1)\nabla\mathcal{H}(x) + E + \mathcal{R}_2(v_{dc}), \tag{4.1.2}$$

where

$$\mathcal{R}(v_{dc}) = \underbrace{\begin{bmatrix} G & 0 & 0 \\ 0 & r_G & 0 \\ 0 & 0 & r_G \end{bmatrix}}_{\mathcal{R}_1} - \underbrace{\begin{bmatrix} \frac{P(t)}{v_{dc}} \\ 0 \\ 0 \end{bmatrix}}_{\mathcal{R}_2(v_{dc})}, \tag{4.1.3}$$

and u denoting the modulation indices. Remembering the common form for writing nonlinear equations:

$$\begin{aligned} \dot{x} &= f(x) + g(x)u \\ y &= h(x) + j(x)u, \end{aligned} \tag{4.1.4}$$

it is evident that for this system;

$$\begin{aligned} f(x) &= (L_G\omega_G\mathcal{J}_3 - \mathcal{R})\nabla\mathcal{H}(x) + E + \mathcal{R}_2(v_{dc}) \\ g(x) &= \begin{bmatrix} \mathcal{J}_1\nabla\mathcal{H}(x) & \mathcal{J}_2\nabla\mathcal{H}(x) \end{bmatrix} \\ u &= \begin{bmatrix} u_1^{(2)} \\ u_2^{(2)} \end{bmatrix} \end{aligned} \tag{4.1.5}$$

The non-linear incremental model is used to make the Lyapunov function converge to zero when reaching the desired operating point.

$$\begin{aligned} \dot{\tilde{x}} &= \dot{x} - \dot{\bar{x}} = (f(x) + g(x)u) - (f(\bar{x}) + g(\bar{x})\bar{u}) \\ &= (L_G\omega_G\mathcal{J}_3 - \mathcal{R}_1)\nabla\mathcal{H}(\tilde{x}) + g(x)u - g(\bar{x})\bar{u} + \mathcal{R}_2(v_{dc}) - \mathcal{R}_2(\bar{v}_{dc}) \end{aligned} \tag{4.1.6}$$

It is interesting to note that we are now dealing with several non-linearity's. The first is the control variables which is multiplied with the gradient of $\mathcal{H}$, while the other is the inverse of the voltage. These terms will therefore be investigated further in the analysis below. We start by investigating the term $g(x)u - g(\bar{x})\bar{u}$:

$$\begin{aligned} g(x)u - g(\bar{x})\bar{u} &= g(\tilde{x} + \bar{x})u - g(\bar{x})\bar{u} \\ &= g(\tilde{x})u + g(\bar{x})u - g(\bar{x})\bar{u} \\ &= g(\tilde{x})u + g(\bar{x})\tilde{u} \end{aligned} \tag{4.1.7}$$

By rewriting the expression as above, it enables us to express the system dynamics as in (4.1.8).

$$\dot{\tilde{x}} = \left(\sum_{i=1}^{2}\mathcal{J}_i u_i + L_G\omega_G\mathcal{J}_3 - \mathcal{R}_1\right)\nabla\mathcal{H}(\tilde{x}) + g(\bar{x})\tilde{u} + \mathcal{R}_2(v_{dc}) - \mathcal{R}_2(\bar{v}_{dc}) \tag{4.1.8}$$

4.2 Lyapunov Function Candidate for the Incremental Model

Having obtained the dynamics of the incremental state variables, the Lyapunov stability analysis can be performed. Choosing the Lyapunov candidate as equal to the Hamiltonian, but as a function of the incremental states, the candidate takes the form in (4.2.1)

$$
\begin{aligned}
\mathcal{V}(x) &= \frac{1}{2}\tilde{x}^\top Q\tilde{x} \\
&= \frac{1}{2}\begin{bmatrix}\tilde{q}_{dc} & \tilde{\psi}_d & \tilde{\psi}_q\end{bmatrix}\begin{bmatrix}\frac{1}{C} & 0 & 0\\ 0 & \frac{1}{L} & 0\\ 0 & 0 & \frac{1}{L}\end{bmatrix}\begin{bmatrix}\tilde{q}_{dc}\\ \tilde{\psi}_d\\ \tilde{\psi}_q\end{bmatrix} \\
&= \frac{1}{2}\left(\frac{\tilde{q}_{dc}^2}{C} + \frac{\tilde{\psi}_d^2}{L} + \frac{\tilde{\psi}_q^2}{L}\right)
\end{aligned}
\tag{4.2.1}
$$

It is obvious that both condition i and ii in Lyapunov analysis is fulfilled. This is because the candidate is a quadratic function, and $\mathcal{V}(\bar{x}) = 0$, resulting in the equilibrium being reached when $x = \bar{x}$. To investigate the remaining conditions, the time derivative of the candidate is obtained:

$$
\begin{aligned}
\dot{\mathcal{V}}(x) &= \nabla^\top\mathcal{V}\dot{x} \\
&= \underbrace{\nabla^\top\mathcal{V}\left(\sum_{i=1}^{2}\mathcal{J}_i u_i + L_G\omega_G\mathcal{J}_3\right)\nabla\mathcal{V}}_{=0} - \nabla^\top\mathcal{V}\mathcal{R}_1\nabla\mathcal{V} + \nabla^\top\mathcal{V}\mathcal{R}_2(v_{dc}) - \nabla^\top\mathcal{V}\mathcal{R}_2(\bar{v}_{dc}) + \underbrace{\nabla^\top\mathcal{V}g(\bar{x})}_{\tilde{y}^\top}\tilde{u} \\
&= -\nabla^\top\mathcal{V}\mathcal{R}_1\nabla\mathcal{V} + \nabla^\top\mathcal{V}\mathcal{R}_2(v_{dc}) - \nabla^\top\mathcal{V}\mathcal{R}_2(\bar{v}_{dc}) + \tilde{y}^\top\tilde{u}
\end{aligned}
\tag{4.2.2}
$$

In the above expression, one part is cancelled due to skew symmetry, and the passive output is defined as $\nabla^\top\mathcal{V}g(\bar{x})$. One of the conditions for the system to be stable is for $\dot{\mathcal{V}}(\bar{x}) = 0$. It is therefore necessary to take a closer look at the terms above. Knowing that $\nabla^\top\mathcal{V}(\bar{x}) = 0$, and that at $\tilde{x} = 0$, $x = \bar{x}$, then all terms containing $\mathcal{R}_2$ and $\mathcal{R}_1$ will be zero when reaching the equilibrium. Further, the passive output is calculated below.

$$
\begin{aligned}
\tilde{y}^\top = &\nabla^\top\mathcal{V}g(\bar{x}) = \begin{bmatrix}\nabla^\top\mathcal{V}\mathcal{J}_1\nabla\mathcal{H}(\bar{x}) & \nabla^\top\mathcal{V}\mathcal{J}_2\mathcal{H}(\bar{x})\end{bmatrix} \\
&\nabla^\top\mathcal{V}\mathcal{J}_1\nabla\mathcal{H}(\bar{x}) = \begin{bmatrix}\tilde{v}_{dc} & \tilde{i}_d^{(2)} & \tilde{i}_q^{(2)}\end{bmatrix}\begin{bmatrix}0 & -1 & 0\\ 1 & 0 & 0\\ 0 & 0 & 0\end{bmatrix}\begin{bmatrix}\bar{v}_{dc}\\ \bar{i}_d^{(2)}\\ \bar{i}_q^{(2)}\end{bmatrix} = \begin{bmatrix}-\tilde{v}_{dc}\bar{i}_d^{(2)} + \tilde{i}_d^{(2)}\bar{v}_{dc}\end{bmatrix} \\
&\nabla^\top\mathcal{V}J_2\nabla\mathcal{H}(\bar{x}) = \begin{bmatrix}\tilde{v}_{dc} & \tilde{i}_d^{(2)} & \tilde{i}_q^{(2)}\end{bmatrix}\begin{bmatrix}0 & 0 & -1\\ 0 & 0 & 0\\ 1 & 0 & 0\end{bmatrix}\begin{bmatrix}\bar{v}_{dc}\\ \bar{i}_d^{(2)}\\ \bar{i}_q^{(2)}\end{bmatrix} = \begin{bmatrix}-\tilde{v}_{dc}\bar{i}_q^{(2)} + \tilde{i}_q^{(2)}\bar{v}_{dc}\end{bmatrix} \\
\Rightarrow \tilde{y} = &\begin{bmatrix}-\tilde{v}_{dc}\bar{i}_d^{(2)} + \tilde{i}_d^{(2)}\bar{v}_{dc}\\ -\tilde{v}_{dc}\bar{i}_q^{(2)} + \tilde{i}_q^{(2)}\bar{v}_{dc}\end{bmatrix} = \begin{bmatrix}-v_{dc}\bar{i}_d^{(2)} + i_d^{(2)}\bar{v}_{dc}\\ -v_{dc}\bar{i}_q^{(2)} + i_q^{(2)}\bar{v}_{dc}\end{bmatrix}
\end{aligned}
\tag{4.2.3}
$$

It is obvious that when $\tilde{x} = 0$, $\tilde{y}^\top = 0$, and the last term in (4.2.2) is also zero. Condition iii is therefore satisfied. It will now be explored if the terms containing $\mathcal{R}_2$ contributes to a decrease in the Lyapunov candidate. To investigate, the definition 1 for monotonicity will be used. Defining $z := \nabla\mathcal{H}(x) = Qx$, and a function $M(z) := \mathcal{R}_2(z)$, the following is obtained:

$$
\begin{aligned}
\nabla^\top\mathcal{V}\mathcal{R}_2(v_{dc}) - \nabla^\top\mathcal{V}\mathcal{R}_2(\bar{v}_{dc}) &= \tilde{x}^\top Q\left(\mathcal{R}_2(v_{dc}) - \mathcal{R}_2(\bar{v}_{dc})\right) \\
&= (z - \bar{z})^\top\left(M(z) - M(\bar{z})\right)
\end{aligned}
\tag{4.2.4}
$$

Now having the expression on the same form as in definition 1, it is evident that its only required to check if $M(z)$ is monotonically decreasing, or equivalently, $\frac{\partial M(z)}{\partial z} < 0$.

$$\frac{\partial M(z)}{\partial z} = \frac{\partial}{\partial z}\begin{bmatrix} \frac{P(t)}{v_{dc}} \\ 0 \\ 0 \end{bmatrix} = \begin{bmatrix} -\frac{P+\delta_P(t)}{v_{dc}^2} & 0 & 0 \\ 0 & 0 & 0 \\ 0 & 0 & 0 \end{bmatrix} \tag{4.2.5}$$

The above expression is negative definite as long as $P + \delta_P(t) > 0$, which is true for $P(t)$ being a power source. In addition, the dissipation matrix is negativ semideifinite, and the Lyapunov function can therefore be further simplified to the following.

$$\dot{\mathcal{V}}(x) \leq \tilde{y}^\top \tilde{u} - \tilde{x}^\top Q\mathcal{R}_1 Q\tilde{x} \leq \tilde{y}^\top \tilde{u} \tag{4.2.6}$$

As discussed in the theory regarding passive systems in 2.1.1, the expression above is the definition for a passive system. Having an expression dependent on the incremental control variables enables for the use of passivity based control, making the term $\tilde{y}^\top \tilde{u}$ always less than 0, hence fulfilling condition *iv* of the Lyapunov analysis. The candidate is therefore a Lyapunov function.

4.3 Lyapunov Analysis Using PI-PBC

Having the same equation describing the system dynamics as in (4.1.8), a new state is defined as in Equation (4.3.1). In addition, the control variable for a PI-controller can be defined as in Equation (4.3.2).

$$\dot{x}_c = -y = -g(\bar{x})^\top Qx \tag{4.3.1}$$

$$u = -K_p y + K_I x_c \tag{4.3.2}$$

When introducing the new state, this also needs to be represented in the Lyapunov candidate function, and this will therefore be updated. The candidate is shown in (4.3.3), and its derivative in (4.3.4)

$$\mathcal{W}_1(x, x_c) = \mathcal{V} + \frac{1}{2}\tilde{x}_c^\top K_I \tilde{x}_c \tag{4.3.3}$$

$$\dot{\mathcal{W}}_1(x, x_c) = \dot{\mathcal{V}} + \tilde{x}_c^\top K_I \dot{\tilde{x}}_c \tag{4.3.4}$$

Having already obtained an expression for $\dot{\mathcal{V}}$ in (4.2.6), this can be used directly. Inserting for $\dot{\tilde{x}}_c$, and using (4.3.2):

$$\begin{aligned} \dot{\mathcal{W}}_1(x, x_c) &\leq \tilde{y}^\top \tilde{u} - \tilde{x}_c^\top K_I \tilde{y} \\ &= \tilde{y}^\top \tilde{u} - \tilde{y}^\top [K_I x_c - K_I \bar{x}_c] \\ &= \tilde{y}^\top \tilde{u} - \tilde{y}^\top [u + K_p \tilde{y} - \bar{u}] \\ &= -\tilde{y}^\top K_p \tilde{y} \end{aligned} \tag{4.3.5}$$

It is obvious that $\dot{\mathcal{W}}_1(0,0) = \mathcal{W}_1(0,0) = 0$, and both Lyapunov condition *i* and *iii* are therefore satisfied. In addition, since both $\mathcal{W}_1$ and $\dot{\mathcal{W}}_1(x, x_c)$ are quadratic functions, Lyapunov condition *ii* and *iv* are also fulfilled.

4.4 Including a Leaky Integrator

Since it is expected to not have perfect information of the system, a deviation in the expected equilibrium point and the actual equilibrium point may occur. In some cases, different adaptive control schemes to estimate the parameters can be used to circumvent this issue. In [49] one standard model reference estimator, and two methods based on the I&I methodology, are proposed for a single power converter. Also in [50] they prove that the I&I observer can be combined with a PI controller to preserve the GAS properties of closed loop system containing a single-ended primary inductor converter (SEPIC). However, such solutions require full information of the total system, which in our case includes the primary side of the system as well. This leads to quite complicated and complex designs.

Instead, this thesis will attempt to implement a "leaky integrator". In [51], they show that the PI passivity based control (PBC) in [49] for a DC/DC boost converter can be modified by including leakage in the integral action in order to still guarantee global asymptotic stability for the closed loop system. The proposed modification is valid also for inaccurate knowledge of the systems equilibrium. Inspired by this paper, the proportional term will include the calculated passive output, and the integrator channel will be modified with a leakage term, as shown in (4.4.2). In principle, by adding such a term, one does not guarantee that the passive output is zero at the point of reaching the equilibrium but rather that the sum of the passive output and the leakage term becomes zero. Anyhow, in this section, it will be attempted to design the integral channel in such a way that when having a high leakage, one actually moves closer toward the desired equilibrium.

The same equation describing the incremental system dynamics in (4.1.8) is used, but now defining the control law as in (4.4.1) and the integral action as in (4.4.2).

$$u = -K_p y^* + K_I x_c \tag{4.4.1}$$

$$\dot{x}_c = -y^* - \varepsilon(K_I x_c - \underbrace{K_I x_c^{\text{ref}}}_{u^{\text{ref}}}) \tag{4.4.2}$$

y^* is defined as in Equation (4.4.3), and represent the passive output as a result of the inaccurate calculations in the load flow.

$$y^* = g^\top(x^*)Qx, \tag{4.4.3}$$

where

$$g(x^*) = \begin{bmatrix} J_1 \nabla \mathcal{H}(x^*) & J_2 \nabla \mathcal{H}(x^*) \end{bmatrix} \tag{4.4.4}$$

If now, the Lyapunov candidate takes the form as in (4.4.5), its derivative can be found in (4.4.6), subsequently written on matrix form. The open loop dynamics for $\mathcal{V}$ are known from (4.2.6), while for the system in closed loop the equations for the controller in (4.4.1), (4.4.2) and (4.4.3) are utilized.

$$\mathcal{W}_2(x) = \mathcal{V} + \frac{1}{2}\tilde{x}_c^\top K_I \tilde{x}_c = \frac{1}{2}\tilde{x}^\top Q \tilde{x} + \frac{1}{2}\tilde{x}_c^\top K_I \tilde{x}_c \tag{4.4.5}$$

$$
\begin{aligned}
\dot{\mathcal{W}}_2(x) &= \dot{\mathcal{V}} + \tilde{x}_c^\top K_I \dot{\tilde{x}}_c \leq \tilde{y}^\top \tilde{u} - \tilde{x}^\top Q\mathcal{R}Q\tilde{x} + \tilde{x}_c^\top K_I \dot{\tilde{x}}_c \\
&= \tilde{y}^\top \tilde{u} - \tilde{x}^\top Q\mathcal{R}Q\tilde{x} + \tilde{x}_c^\top K_I(-\tilde{y}^* - \varepsilon K_I \tilde{x}_c) \\
&= \tilde{y}^\top(-K_p\tilde{y}^* + K_I x_c) - \tilde{x}^\top Q\mathcal{R}Q\tilde{x} + \tilde{x}_c^\top K_I(-\tilde{y}^* - \varepsilon K_I\tilde{x}_c) \\
&= -\begin{bmatrix} Q\tilde{x} \\ K_I\tilde{x}_c \end{bmatrix}^\top \underbrace{\begin{bmatrix} \bar{\mathcal{K}}_p + \mathcal{R} & -\frac{g(\bar{x})-g(x^*)}{2} \\ -\frac{g^\top(\bar{x})-g^\top(x^*)}{2} & \varepsilon \end{bmatrix}}_{O-matrix} \begin{bmatrix} Q\tilde{x} \\ K_I\tilde{x}_c \end{bmatrix}
\end{aligned}
\tag{4.4.6}
$$

where $\overline{\mathcal{K}}_p$ is the symmetrical matrix

$$
\overline{\mathcal{K}}_p := \frac{1}{2}\left(g(\bar{x})K_p g^\top(x^*) + g(x^*)K_p g^\top(\bar{x})\right)
$$

Since one of the Lyapunov conditions are for the derivative of $\mathcal{W}_2$ to be less than 0, it will be investigated if the O-matrix above is positive definite. The first requirement is for $\overline{\mathcal{K}}_p + \mathcal{R}$ to be bigger than 0, and the second requirement is obtained by calculating the schur element O/A:

$$
O/A = \varepsilon - \frac{1}{4}(g^\top(\bar{x}) - g^\top(x^*))(\overline{\mathcal{K}}_p + \mathcal{R})^{-1}(g(\bar{x}) - g(x^*)). \tag{4.4.7}
$$

However, the resulting schur complement above is a 2×2 matrix, which is positive if the schur complement of the new matrix is positive definite. From trial and error, the leakage matrix is chosen as in (4.4.8), and from Figure 4.1, it can be observed that the O-matrix will then be positive definite for any $\varepsilon_{1,1} > 0$.

$$
\varepsilon = \begin{bmatrix} \varepsilon_{1,1} & 0 \\ 0 & \varepsilon_{2,2} \end{bmatrix} = \begin{bmatrix} \varepsilon_{1,1} & 0 \\ 0 & 0.0052 \end{bmatrix} \tag{4.4.8}
$$

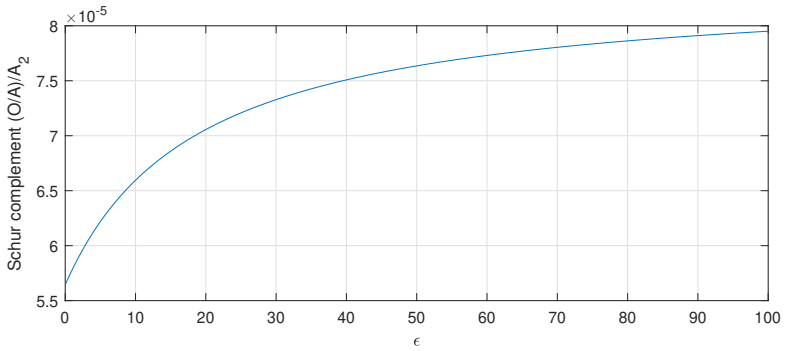

Figure 4.1: The schur complement in $(O/A)/A_{new}$ as a function of different $\varepsilon_{1,1}$ values.

If both of the requirements hold by assumption, the equilibrium $(\bar{x}, \bar{x}_c)$ is globally exponentially stable. It should be mentioned that when the state reaches its equilibrium point where $x = \bar{x}$, the passive output y for the physical system becomes zero, typical for a nonlinear system. A reference term y^{ref} is therefore not included as done in section 3.3. This will result in $K_I x_c = K_I x_c^{\text{ref}}$ at the equilibrium. It is also worth noticing that with a bigger ε, the last term in (4.4.2) will be of greater significance. For a simplified and practical interpretation, Equation (2.2.5b) can be investigated. If it is assumed that both r_G and i_q are relatively small, then, at steady state, Equation (4.4.9) is obtained.

$$
u_1^{(2)} = \frac{r_G\bar{i}_d^{(2)} - L_G\bar{i}_q^{(2)}\omega_G + V_d^G}{\bar{v}_{dc}} \approx \frac{V_d^G}{\bar{v}_{dc}} \tag{4.4.9}
$$

If then, ε is sufficiently large, the term $K_I x_c$ will be forced equal to u^{ref}, and the possibility of indirectly controlling the voltage in the dc-link arises, as seen from Equation (4.4.9).

It can further be emphasized that in the case of perfect knowledge of the equilibrium, where $x^* = \bar{x}$, it can be shown that it is possible to regulate the system to x^* using an arbitary small leakage ε. Having x^* in the set of assignable equilibria, the point $(x^*, K_i^{-1}u(x^*))$ is an equilibrium for the system. Then, $\overline{\mathcal{K}}_p > 0$ and $x^* - \bar{x} = 0$, and consequently the expression in (4.4.7) is satisfied for all $\varepsilon > 0$. If $\varepsilon = 0$, the controller reduces to the same PI-PBC controller as in section 4.3 where global asymptotic stability also holds.

4.5 Control of the System

For the secondary side, the system has two degrees of freedom. The first control objective will be to control the DC-link voltage in order to have the voltage source converter operate as desired.

The second control objective is to control the q-axis current, hence controlling the reactive power flow to the grid. It is assumed that the synchronous reference frame is used to align the d-axis with the voltage vector; hence V_q^G is zero [8]. The reactive power can then be expressed as shown below:

$$Q = \frac{3}{2}(-v_d i_q + v_q i_d) = -\frac{3}{2} v_d i_q \tag{4.5.1}$$

The expression above shows that by controlling the q-axis current, the reactive power is indirectly controlled. The possibility of controlling the reactive power is important in order to maintain the desired power quality. [52]

For simulations conducted on the secondary side, the parameter values used are inspired by the former master thesis in [22] and are shown in Table 4.1. At the time of simulation, it is assumed that it is not required to deliver any reactive power to the grid, and the current, $i^{(2)}_{q,\text{ref}}$ is set to $0[A]$. This choice will be further reasoned later in this chapter.

Parameters	Symbol	Nominal values
DC-link capacitance	C	3.3 $[mF]$
Grid resistance	r_G	$0.2[\Omega]$
Grid inductance	L_G	2 $[mH]$
DC-link conductance	G	10 $[\mu S]$
Number of poles	p	28
Grid angular frequency	ω_G	$2\pi 50$ $[rad/s]$
Grid d-axis voltage	V_d^G	$230\sqrt{2}$ $[V]$
Grid q-axis voltage	V_q^G	0 $[V]$
Gird q-axis current	$i^{(2)}_{q,ref}$	0 $[A]$

Table 4.1: Model parameters and input values for the secondary side.

The control structure that will be used to simulate the follower subsystem is shown in the figure below.

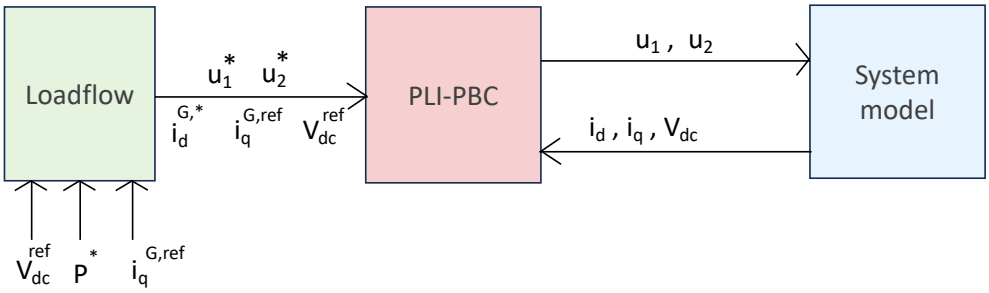

Figure 4.2: Control structure of secondary side with a PLI-PBC.

4.5.1 Equilibrium Analysis

For the secondary side, the coenergy variables are v_{dc}, $i_d^{(2)}$, and $i_q^{(2)}$, and the control variables are $u_1^{(2)}$, $u_2^{(2)}$. The system has two known inputs, namely V_d^G and V_q^G, and the two coenergy variables $i_q^{(2)}$ and v_{dc} are also known at equilibrium. The missing coenergy variable $i_d^{(2)}$ and the control variables can be calculated for the system using the equations in (2.2.5).

As elaborated earlier, when deriving the stability certificates, it is dependent on the fact that an equilibrium point exists for the system to obtain. There are several ways to find the equilibrium point for the d-component current in the grid connection. One way would be to combine multiple equations in (2.2.5) and solve for i_d^G. Another way is to use power conservation and the Hamiltonian of the system, as will be done below. Starting from the system equation in (4.1.2), the derivative of the Hamiltonian is calculated in (4.5.2).

$$\begin{aligned}\dot{\mathcal{H}}(x) &= \underbrace{\nabla^\top \mathcal{H}\left(\sum_{i=1}^{2} \mathcal{J}_i u_i + L_G \omega_G \mathcal{J}_3\right)\nabla\mathcal{H}}_{=0} - \nabla^\top \mathcal{H}\mathcal{R}_1 \nabla\mathcal{H} + \nabla^\top \mathcal{H}\mathcal{R}_2(v_{dc}) + \nabla\mathcal{H}E \\ &= -\nabla^\top \mathcal{H}\mathcal{R}_1 \nabla\mathcal{H} + \nabla^\top \mathcal{H}\mathcal{R}_2(v_{dc}) + \nabla\mathcal{H}E\end{aligned} \tag{4.5.2}$$

At the equilibrium, $x = \bar{x}$ such that

$$0 = \underbrace{-r_G \bar{i}_d^{(2)^2} - r_G \bar{i}_q^{(2)^2} - G\bar{v}_{dc}^2}_{P_{loss}} \underbrace{-\bar{i}_d^{(2)} V_d^G - \bar{i}_q^{(2)} V_q^G}_{P_{out}} \underbrace{+\bar{P}}_{P_{in}}. \tag{4.5.3}$$

Lastly, solving for the direct current in the grid connection, we obtain:

$$i_d^{(2)^*} = -\frac{V_d^G}{2r_G} + \sqrt{\frac{(V_d^G)^2}{4r_G^2} - \frac{1}{r_G}\left(r_G\left(i_q^{(2),\mathrm{ref}}\right)^2 + G\left(v_{dc}^{\mathrm{ref}}\right)^2 + V_q^G i_q^{(2),\mathrm{ref}} - \bar{P}\right)} \tag{4.5.4}$$

It will further be investigated if the term inside the square root is positive, which is required in order for an equilibrium point to exist. Assuming that the reference frame for the d-axis is aligned with the voltage vector, $V_q^G = 0$, the following expression is obtained.

$$\underbrace{\frac{(V_d^G)^2}{4r_G}}_{\hat{P}} \underbrace{- r_G\left(i_q^{(2),\mathrm{ref}}\right)^2 - G\left(v_{dc}^{\mathrm{ref}}\right)^2}_{P_{loss}^*} + \underbrace{\bar{P}}_{P_{in}} > 0 \tag{4.5.5}$$

Knowing that a Hamiltonian system is a passive system, the power into the system, added by an additional positive power, will always be bigger than the losses in the system. Hence, an equilibrium point exists for all possible operating points.

The equations in (2.2.5b) and (2.2.5c) are utilized and rearranged to derive the values of u_1 and u_2 at equilibrium, respectively. The resulting equations describing the variables at steady state are presented below.

$$u_1^* = \frac{1}{v_{dc}^{\text{ref}}}(V_d^G + r_G i_d^{(2),*} - L_G i_q^{(2),\text{ref}} \omega_G) \tag{4.5.6}$$

$$u_2^* = \frac{1}{v_{dc}^{\text{ref}}}(V_q^G + r_G i_q^{(2),\text{ref}} + L_G i_d^{(2),\text{ref}} \omega_G) \tag{4.5.7}$$

4.6 Further Analysis and Simulations of the Secondary System

If the controller is an ordinary passivity controller based on Equation (4.3.1) and (4.3.2), reproduced below for convenience, the response to a step in power from 3kW to 4kW is given in Figure 4.3. The controller parameters used to obtain this result is listed in Table 4.2, and the rest of the parameters are under the assumption of perfect information of the equilibrium to be stabilized.

$$\dot{x}_c = -y = -g(\bar{x})^\top Q x \tag{4.6.1}$$

$$u = -K_p y + K_I x_c \tag{4.6.2}$$

Parameters	value
$k_{p,1} = k_{p,2}$	0.0006
$k_{i,1} = k_{i,2}$	10
step in P	3-4 [kW]

Table 4.2: Control parameters corresponding to the response in Figure 4.3 and 4.4.

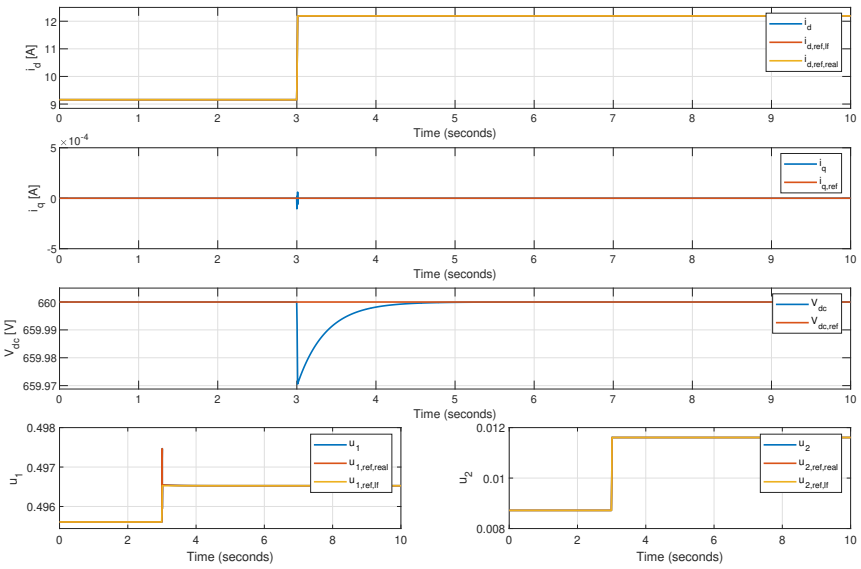

Figure 4.3: Response to a step in power with PI-passivity based control while having a perfect model of the system.

It can be observed that all the states reaches their calculated equilibrium references, and the control objectives are met. This would therefore be a viable solution in the case of perfect knowledge of the system, but such a condition is rarely ever satisfied in practice. If however, we are left with an imperfect model of the system, resulting in the load flow calculations asking for the wrong equilibrium reference, there may be significant deviations between the obtained equilibrium and the optimal equilibrium point. Using the same controller parameters as before, a step in input power from 3000W to 4000W is performed. However, unlike before, the updated value for the input power is not given to the load flow. As a result, Figure 4.4 is obtained.

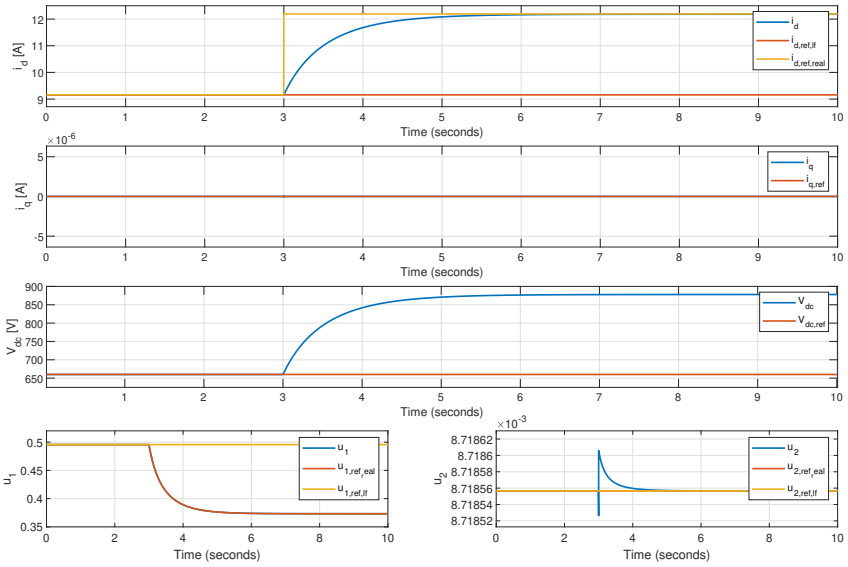

Figure 4.4: Response to a step in power when having an imperfect model without the inclusion of leakage in the integral channel.

For the quadrature current, the obtained steady state value is $0A$, which is the same as we asked for. However, for the voltage, large deviations from the optimal equilibrium to be stabilized are now observed. The voltage over the capacitor is observed to be stabilizing at $872V$ while asking for $660V$. This is clearly not an acceptable situation in practice and poses a serious risk to the safe and uninterrupted operation of the grid. We, therefore, propose to include a leakage term in the integral action. If now, the controller dynamics are described by Equation (4.4.1) and (4.4.2), and the controller parameters are given in Table 4.3, the resulting response is observed in Figure 4.5.

$$u = -K_p y^* + K_I x_c \tag{4.6.3}$$

$$\dot{x}_c = -y^* - \varepsilon(K_I x_c - \underbrace{K_I x_c^{\text{ref}}}_{u^{\text{ref}}}) \tag{4.6.4}$$

Parameters	value
$k_{p,1} = k_{p,2}$	0.0006
$k_{i,1} = k_{p,2}$	10
$\varepsilon_{1,1}$	10^{20}
$\varepsilon_{2,2}$	0.0052
step in P	3-4 [kW]

Table 4.3: Control parameters corresponding to the response in Figure 4.5 and 4.6.

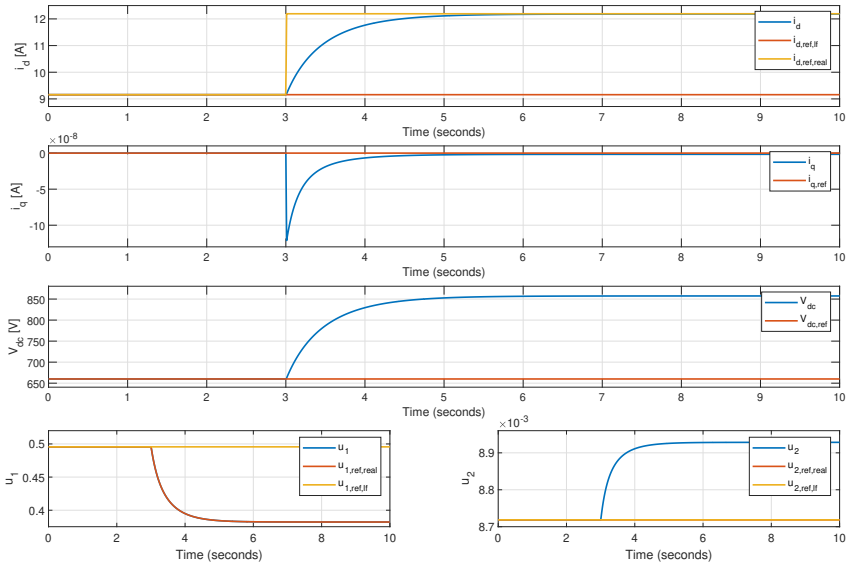

Figure 4.5: Response to a step in power when having an imperfect model with the inclusion of leakage in the integral channel.

In accordance with the discussion in subsection 4.4, the leakage term was designed so that voltage control should be indirectly obtained. As can be noticed by comparing the figure presented above and the response shown in Figure 4.4, it reveals relatively small improvements. Using a leakage of 10^{20} resulted in moving only $14V$ closer to the desired equilibrium. This is due to the leakage term not being significantly big to override the other term containing the passive output. Initially, the thought, following the paper in [51], was to increase ε. However, increasing the leakage even more resulted in a poor performance characterized by high peaks and oscillations, ultimately leading to simulation failure. It becomes apparent that the passive output is influencing in a non-negligible way, hence significantly hindering the achievement of the desired control. Consequently, we opted to attempt to remove the passive output from both the proportional and integral terms, thereby simplifying the controller implementation. The same proof as already preformed in section 4.4 still applies, under the modification that $g(x^*)$ is zero ($v_{dc}^* = i_d^* = i_q^* = 0$). Upon examining the matrix presented in Equation (4.4.6), it becomes evident that the off-diagonal terms now contains $-g(\bar{x})/2$ and its transposed. However, the leakage remains to compensate for those off-diagonal terms. It is clear that $\overline{\mathcal{K}}_p = 0$, and the new condition for ε to guarantee stability is calculated in (4.6.5). While fulfilling this criteria, the response in Figure 4.6 is obtained.

$$\varepsilon - \frac{1}{4} g^\top(\bar{x}) \mathcal{R}^{-1} g(\bar{x}) > 0. \tag{4.6.5}$$

The gain values used is still the same as presented in Table 4.3, but now $\epsilon_{1,1} = \epsilon_{2,2} = 100$.

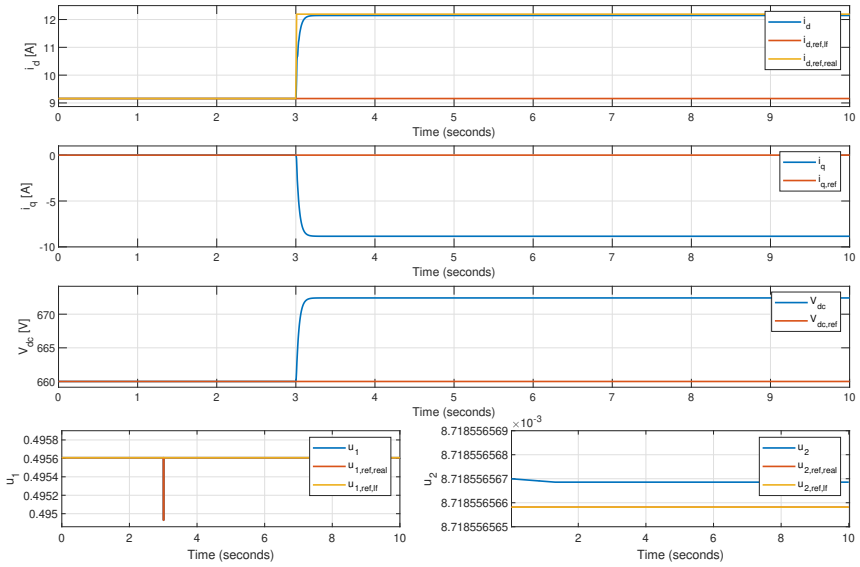

Figure 4.6: Response to a step in power when having an imperfect model with $y^* = 0$ and including leakage in the integral channel.

The voltage in the dc-link is now stabilizing at $672.5V$ instead of $872V$ as before. The attempt to remove the passive output from the controller has made a significant impact on the objective to control the voltage indirectly, and the deviation from the desired steady state value is closing in on reasonable limits. Nevertheless, i_q deviates relatively much from the desired steady state value, now being $-8.9A$ instead of $0A$ which was asked for.

Considering that it is only necessary to indirectly control the voltage in one of the controllers, the possibility of achieving the second control objective arises. We now consider only removing the passive output terms from the controller that contains the d-component of the current, while preserving the original plan for the other controller. If the first controller effectively regulates the dc-link voltage close to the desired equilibrium, consequently the second part of the controller will indirectly control the current when the leakage is relatively small. This emerges from the expression for the passive output, where in order to make y^* approximately zero when v_{dc} is approximately v_{dc}^*, i_q must be approximately i_q^*.

In the case of integrating the passive output related to i_q only, a co-linearity analysis will be of great interest. It is possible to write the q-component of the passive output at equilibrium as:

$$0 = \underbrace{\begin{bmatrix} v_{dc}^* \\ i_q^* \end{bmatrix}^\top}_{A} \underbrace{\begin{bmatrix} 0 & 1 \\ -1 & 0 \end{bmatrix}}_{B} \underbrace{\begin{bmatrix} \bar{v}_{dc} \\ \bar{i}_q \end{bmatrix}}_{C}. \tag{4.6.6}$$

Because matrix B is skew-symmetric, and the right side is equal to zero, the two vectors A and C have to be either the same vectors or, multiplied by a scalar γ. Consequently, the vectors exhibit collinearity. If now, i_q^* is set to zero, and γ is a constant, multiplying a constant with zero results in zero. It will therefore be beneficial to choose a reference for the quadrature current as zero since it is the only value that will guarantee the same equilibrium as requested. However, for the voltage, the resulting steady-state value will be the voltage requested multiplied by a constant;

$$\begin{bmatrix} v_{dc}^* \\ 0 \end{bmatrix} = \varsigma \begin{bmatrix} \bar{v}_{dc} \\ 0 \end{bmatrix}. \tag{4.6.7}$$

With the motivation above in mind, a stability analysis for such a control scheme will be conducted. If the controller is now defined based on the two expressions below,

$$\begin{bmatrix} u_1^{(2)} \\ u_2^{(2)} \end{bmatrix} = \begin{bmatrix} k_{i,1}x_{c,d} \\ -k_{p,2}y_q^* + k_{i,2}x_{c,q} \end{bmatrix} \tag{4.6.8}$$

$$\begin{bmatrix} \dot{x}_{c,d} \\ \dot{x}_{c,q} \end{bmatrix} = \begin{bmatrix} -\varepsilon_d(k_{i,1}x_{c,d} - u_1^{(2),\text{ref}}) \\ -y_q^* \end{bmatrix} \tag{4.6.9}$$

where $y^\top = \begin{bmatrix} y_d & y_q \end{bmatrix}$, and $g(\bar{x}) = \begin{bmatrix} g_d(\bar{x}) & g_q(\bar{x}) \end{bmatrix}$. Additionally, $K_I = \begin{bmatrix} k_{i,1} & 0 \\ 0 & k_{i,2} \end{bmatrix}$ and $K_p = \begin{bmatrix} k_{p,1} & 0 \\ 0 & k_{p,2} \end{bmatrix}$. If modifying the Lyapunov candidate in (4.3.3) by multiplying the term containing the state variable $\tilde{x}_{c,q}$ with a factor of $\frac{1}{\varsigma}$, the expression in (4.6.10) is obtained. Notice that for the first and second Lyapunov criteria to be fulfilled, ς is required to be a positive constant. Using the result obtained in (4.2.6) for $\dot{\mathcal{V}}$, the time derivative of the candidate can be calculated as in (4.6.11).

$$\mathcal{W}(\tilde{x}, \tilde{x}_{c,d}, \tilde{x}_{c,q}) \triangleq \frac{1}{2}\tilde{x}^\top Q\tilde{x} + \frac{1}{2}k_{i,1}\tilde{x}_{c,d}^2 + \frac{1}{2\varsigma}k_{i,2}\tilde{x}_{c,q}^2 \tag{4.6.10}$$

$$\begin{aligned}
\dot{\mathcal{W}} &= \dot{\mathcal{V}} + \tilde{x}_{c,d}^\top k_{i,1}\dot{\tilde{x}}_{c,d} + \frac{1}{\varsigma}\tilde{x}_{c,q}^\top k_{i,2}\dot{\tilde{x}}_{c,q} \leq \tilde{y}^\top\tilde{u} - \tilde{x}^\top Q\mathcal{R}Q\tilde{x} + \tilde{x}_{c,d}^\top K_{i,1}\dot{\tilde{x}}_{c,d} + \frac{1}{\varsigma}\tilde{x}_{c,q}^\top K_{i,2}\dot{\tilde{x}}_{c,q} \\
&= \tilde{y}^\top \begin{bmatrix} k_{i,1}\tilde{x}_{c,d} \\ -k_{p,2}\tilde{y}_q^* + k_{i,2}\tilde{x}_{c,q} \end{bmatrix} - \tilde{x}^\top Q\mathcal{R}Q\tilde{x} - \tilde{x}_{c,d}^\top k_{i,1}\varepsilon_d k_{i,1}\tilde{x}_{c,d} - \frac{1}{\varsigma}\tilde{x}_{c,q}^\top k_{i,2}\tilde{y}_q^* \\
&= \tilde{y}_d^\top k_{i,1}\tilde{x}_{c,d} - \tilde{y}_q^\top k_{p,2}\tilde{y}_q^* + \tilde{y}_q^\top k_{i,2}\tilde{x}_{c,q} - \tilde{x}^\top Q\mathcal{R}Q\tilde{x} - \tilde{x}_{c,d}^\top k_{i,1}\varepsilon_d k_{i,1}\tilde{x}_{c,d} - \frac{1}{\varsigma}\tilde{x}_{c,q}^\top k_{i,2}\tilde{y}_q^* \\
&= \tilde{x}^\top Q g_d(\bar{x})k_{i,1}\tilde{x}_{c,d} - \tilde{x}^\top Q g_q(\bar{x})k_{p,2}g_q^\top(x^*)Q\tilde{x} + \tilde{x}^\top Q g_q(\bar{x})k_{i,2}\tilde{x}_{c,q} - \tilde{x}^\top Q\mathcal{R}Q\tilde{x} \\
&- \tilde{x}_{c,d}^\top k_{i,1}\varepsilon_d k_{i,1}\tilde{x}_{c,d} - \tilde{x}_{c,q}^\top k_{i,2}\underbrace{\frac{1}{\varsigma}g_q^\top(x^*)}_{g_q^\top(\bar{x})}Q\tilde{x}
\end{aligned} \tag{4.6.11}$$

In the second line $\tilde{u}$, $\dot{\tilde{x}}_{c,d}$ and $\dot{\tilde{x}}_{c,q}$ are replaced, then some basic matrix calculations are performed, and in the last equality the expression for the passive output is inserted. The candidate can further be written in matrix form as

$$\dot{\mathcal{W}} \leq \begin{bmatrix} Q\tilde{x} \\ k_{i,1}\tilde{x}_{c,d} \\ k_{i,2}\tilde{x}_{c,q} \end{bmatrix}^\top \begin{bmatrix} -g_q(\bar{x})k_{p,2}g_q^\top(x^*) - \mathcal{R} & g_d(\bar{x}) & g_q(\bar{x}) \\ 0 & -\varepsilon_d & 0 \\ -g_q^\top(\bar{x}) & 0 & 0 \end{bmatrix} \begin{bmatrix} Q\tilde{x} \\ k_{i,1}\tilde{x}_{c,d} \\ k_{i,2}\tilde{x}_{c,q} \end{bmatrix}. \tag{4.6.12}$$

Notice that because of co-linearity, as discussed earlier in this section, we have that $i_q^* = \varsigma\bar{i}_q$, $v_{dc}^* = \varsigma\bar{v}_{dc}$ for a constant scalar ς, and thus $g_q(x^*) = \varsigma g_q(\bar{x})$. The symmetrical part of the matrix can then be written as

$$\dot{\mathcal{W}} \leq \begin{bmatrix} Q\tilde{x} \\ k_{i,1}\tilde{x}_{c,d} \\ k_{i,2}\tilde{x}_{c,q} \end{bmatrix}^\top \begin{bmatrix} -\overline{\mathcal{K}}_p - \mathcal{R} & \frac{1}{2}g_d(\bar{x}) & 0 \\ \frac{1}{2}g_d^\top(\bar{x}) & -\varepsilon_d & 0 \\ 0 & 0 & 0 \end{bmatrix} \begin{bmatrix} Q\tilde{x} \\ k_{i,1}\tilde{x}_{c,d} \\ k_{i,2}\tilde{x}_{c,q} \end{bmatrix} \tag{4.6.13}$$

with $\overline{\mathcal{K}}_p$ as the symmetrical matrix

$$\overline{\mathcal{K}}_p := \frac{1}{2}\left(g_q(\bar{x})k_{p,2}g_q^\top(x^*) + g_q(x^*)k_{p,2}g_q^\top(\bar{x})\right).$$

Consequently, for the system to be stable with the new control scheme, the criteria

$$\overline{\mathcal{K}}_p + \mathcal{R} > 0 \tag{4.6.14}$$

and

$$\varepsilon_d - \frac{1}{4} g_d(\bar{x})^\top (\overline{\mathcal{K}}_p + \mathcal{R}) g_d(\bar{x}) > 0 \tag{4.6.15}$$

are required. Due to the collinearity relationship, we can simplify $\overline{\mathcal{K}}_p$ as:

$$\overline{\mathcal{K}}_p = \frac{1}{2}\left(\frac{1}{\varsigma} g_q(\bar{x}) k_{p,2} g_q^\top(\bar{x}) + \frac{1}{\varsigma} g_q(\bar{x}) k_{p,2} g_q^\top(\bar{x})\right) = \frac{1}{\varsigma} g_q(\bar{x}) k_{p,2} g_q^\top(\bar{x}).$$

Since $\overline{\mathcal{K}}_p$ will always be positive as long as ς remains a positive constant, and considering that $\mathcal{R}$ is positive semi-definite, it is evident that the condition in (4.6.14) will always be satisfied.

However, fulfilling the two conditions alone will only provide global stability and not global asymptotic stability since there is no elements containing the state $x_{c,q}$ in $\dot{\mathcal{W}}$ shown in Equation (4.6.13), hence we do not know what the state will converge to. Further analysis is therefore necessary, and La Salle's invariance theorem can be utilized to assess the state variables at the system minimum, corresponding to when $\dot{\mathcal{W}}(x, x_c) = 0$. Since the conditions in (4.6.14) and (4.6.15) are satisfied by assumption, the matrix in (4.6.13) is negative definite, hence the only solution for $\dot{\mathcal{W}}(x, x_c)$ to be zero is for $\tilde{x}$ and $\tilde{x}_{c,d}$ to be zero. Further, we also know that $u = \begin{bmatrix} u_1^{(2)} \\ u_2^{(2)} \end{bmatrix} = \bar{u}$ since this is the control variable controlling x and $x_{c,d}$ to constant values. This can also be proven using the general expression for nonlinear systems, as shown below. At the equilibrium, we know that $\dot{x}$ is equal to to zero, and that $x = \bar{x}$. In the second line, the expression is multiplied with the transposed of g, followed by basic mathematical calculations.

$$\begin{aligned} 0 &= f(\bar{x}) + g(\bar{x})u \\ &= g^\top(\bar{x}) f(\bar{x}) + g^\top(\bar{x}) g(\bar{x}) u \\ &= [g^\top(\bar{x}) g(\bar{x})]^{-1} g^\top(\bar{x}) f(\bar{x}) + u \\ &\Rightarrow u = -g^*(\bar{x}) f(\bar{x}) = \bar{u} \end{aligned} \tag{4.6.16}$$

$g^*(\bar{x})$ is the left pseudo inverse. Since both $g^*(\bar{x})$ and $f(\bar{x})$ are constant, u also have to be constant. Further on, we know that

$$\begin{aligned} u_2^{(2)} = \bar{u}_2^{(2)} &= -K_p(V_c^* i_q - V_c i_q^*) + K_I x_{c,q} \\ &= -K_p(V_c^* \bar{i}_q - \bar{V}_c i_q^*) + K_I x_{c,q} \\ &= -K_p V_c^* \bar{i}_q + K_I x_{c,q}, \end{aligned} \tag{4.6.17}$$

where the third equality is obtained by the assumption that $i_q^* = 0$. It is also evident that v_{dc}^*, $\bar{i}_q$ and $u = \bar{u}$ are constant, giving that the last term, $K_I x_{c,q}$, must also remain constant. Since the derivative of a constant is always zero, we can conclude that the state has stopped moving at the system minimum, and $\dot{x}_{c,q} = 0$, thereby proving the system's achievement of global asymptotic stability.

With this new control scheme, the order of magnitude of ε_d will not have any significant impact on the deviation between the actual and the requested equilibrium point, but do have an impact on the settling time.

Using the parameters from the table below, and doing a step in input power without updating the load flow, the resulting response when adopting the new control method is presented in Figure 4.7.

Parameters	value
$k_{p,1} = k_{p,2}$	1
$k_{i,1} = k_{i,2}$	50
ε_d	100
step in P	3-4 [kW]

Table 4.4: Control parameters used for Figure 4.7, 4.8 and 4.9.

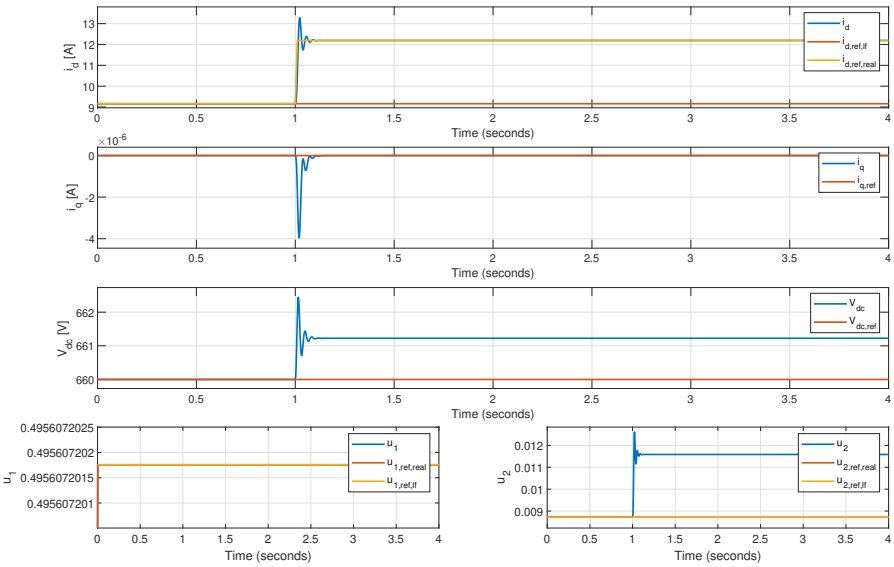

Figure 4.7: Step in input power with imperfect system, $i_q = 0$ and the passive output only included in one part of the control.

The voltage is now observed to only deviate $1.2V$ from the desired steady state value, while the quadrature current reaches the exact requested value. It is evident that the new modification of only including the passive output in one of the controllers have a significant impact on reaching the control objective, where the leakage now acts as a damping term, contributing to compensate for the error introduced due to the inaccurate information provided by the load flow. Observed from the Figure, the deviations are now well within the range of acceptable values. It can further be mentioned that the deviations from the requested equilibrium's will still be within acceptable limits also when $i_q^* \neq 0$, to a certain extent. For a quadrature current of 2A, the response will be given as in Figure 4.8.

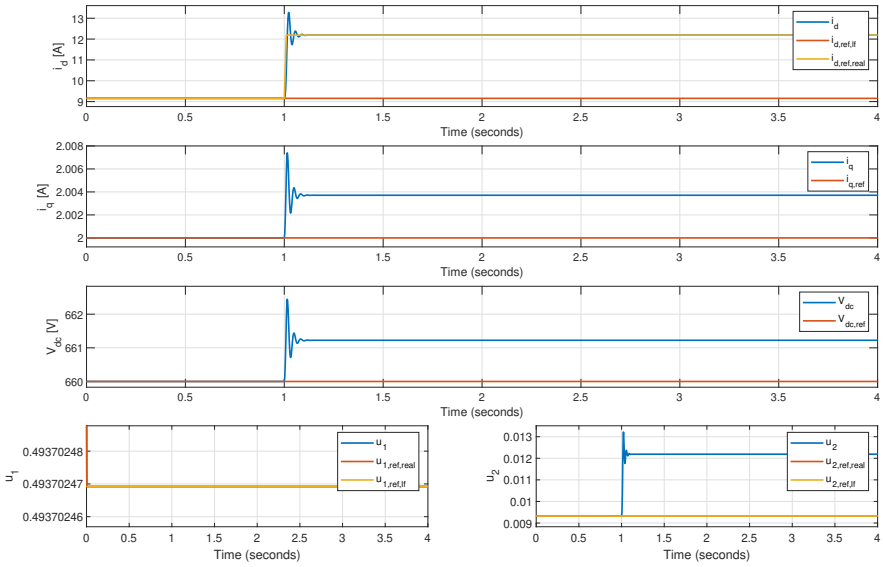

Figure 4.8: Step in input power with an imperfect system, $i_q = 2$ and the passive output only included in one part of the control.

As observed from the figure above, it is evident that a small current would still give reasonable results, whereas the q-axis current now deviates by approximately 4mA. The voltage deviates approximately the same as before. If, on the other hand, the current would be of a higher order, this could impact the equilibrium of the voltage more significantly. From Equation (4.4.9), it is clear that if the term $\frac{L_G \bar{i}_q^{(2)} \omega_G}{\bar{v}_{dc}}$ is not negligible, the voltage in the dc-link and the control variable will no longer be approximately inverse proportional.

It is also of interest to show how the system will react to an oscillating, vanishing perturbation. If the input to the load flow is $3kW$, while the input power P to the model is given as $P(t) = 3000 + 50e^{-10t}sin(2\pi 10t)$, the input will eventually stabilize at $3000W$. The response of the system is given in the figure below.

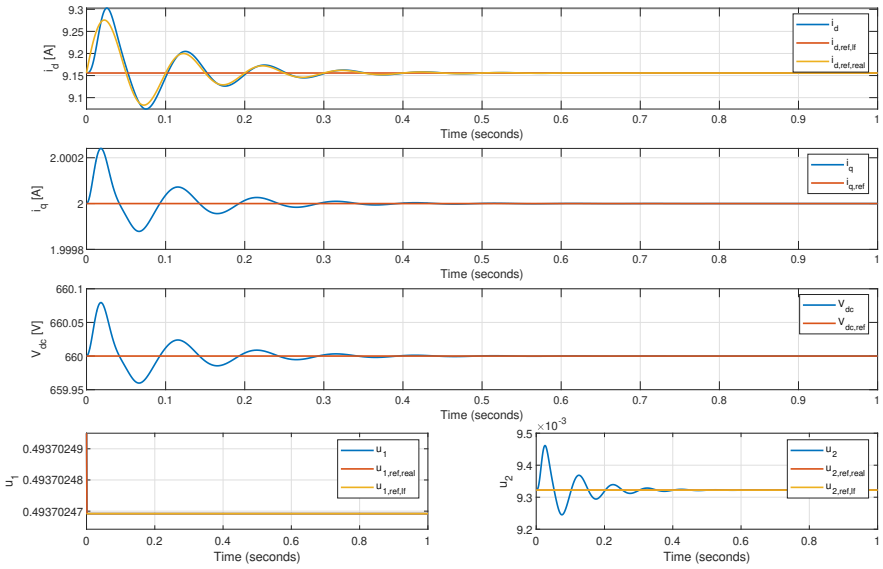

Figure 4.9: Oscillations in power reference.

The system can be observed to be stable, oscillating at start before stabilizing at the requested equilibrium point.

Chapter 5

Simulations on the Full System

5.1 System equations and control

It is now time to assemble the primary and secondary systems and perform simulations of the complete system. The full set of equations describing the system is reproduced below for convenience. In the notation used, $(\cdot)^{(1)}$ refer to the primary side, while $(\cdot)^{(2)}$ refer to the secondary side.

$$\dot{\Psi}_d = L\dot{i}_d^{(1)} = -ri_d^{(1)} + Li_q^{(1)}\frac{P}{2}\omega_m - e_d \tag{5.1.1a}$$

$$\dot{\Psi}_q = L\dot{i}_q^{(1)} = -ri_q^{(1)} - Li_d^{(1)}\frac{P}{2}\omega_m + \phi\frac{P}{2}\omega_m - e_q \tag{5.1.1b}$$

$$\dot{\rho} = J\dot{\omega}_m = T_m - T_e = T_m - \frac{3}{2}\frac{P}{2}\phi i_q^{(1)} + d(\omega_{ref} - \omega_m) \tag{5.1.1c}$$

$$\dot{q}_{dc} = C\dot{v}_{dc} = -Gv_{dc} + \frac{e_d i_d^{(1)}}{v_{dc}} + \frac{e_q i_q^{(1)}}{v_{dc}} - u_1^{(2)}i_d^{(2)} - u_2^{(2)}i_q^{(2)} \tag{5.1.2a}$$

$$\dot{\Psi}_d^G = L_G\dot{i}_d^{(2)} = -r_G i_d^{(2)} + L_G i_q^{(2)}\omega_G + u_1^{(2)}v_{dc} - V_d^G \tag{5.1.2b}$$

$$\dot{\Psi}_q^G = L_G\dot{i}_q^{(2)} = -r_G i_q^{(2)} - L_G i_d^{(2)}\omega_G + u_2^{(2)}v_{dc} - V_q^G \tag{5.1.2c}$$

Next, we provide the expressions governing the control of the system in the following equations:

$$u^{(1)} = -K_p^{(1)}y^{(1)} + K_I^{(1)}x_c^{(1)}, \tag{5.1.3}$$

$$\dot{x}_c^{(1)} = -(y^{(1)} - y^{(1),ref}) \tag{5.1.4}$$

$$\begin{bmatrix} u_1^{(2)} \\ u_2^{(2)} \end{bmatrix} = \begin{bmatrix} k_{i,1}^{(2)}x_{c,d}^{(2)} \\ -k_{p,2}^{(2)}y_q^{(2),*} + k_{i,2}^{(2)}x_{c,q}^{(2)} \end{bmatrix} \tag{5.1.5}$$

$$\begin{bmatrix} \dot{x}_{c,d}^{(2)} \\ \dot{x}_{c,q}^{(2)} \end{bmatrix} = \begin{bmatrix} -\varepsilon_d(k_{i,1}^{(2)} x_{c,d}^{(2)} - u_1^{(2),\text{ref}}) \\ -y_q^{(2),*} \end{bmatrix} \tag{5.1.6}$$

The control parameters that will be used are given in Table 5.1, and a step in wind speed from 10 to $12m/s$ is implemented. The reference value used for the q-axis current is 2A, while the voltage reference in the dc-link is set to 660V.

Parameters	value
$k_{p,1}^{(1)}$	6
$k_{p,2}^{(1)}$	500
$k_{i,1}^{(1)}$	5000
$k_{i,2}^{(1)}$	500
$k_{p,outerloop}$	1.2
$k_{i,outerloop}$	0.005
$k_{p,1}^{(2)} = k_{p,2}^{(2)}$	0.0006
$k_{i,1}^{(2)} = k_{i,2}^{(2)}$	10
$\varepsilon_{1,1}$	10
$\varepsilon_{1,2}$	0

Table 5.1: Control parameters used to control the full system.

5.2 Simulation results

If the adaption gain for the wind speed estimator is equal to 40, the response of the state variables is given in Figure 5.1.

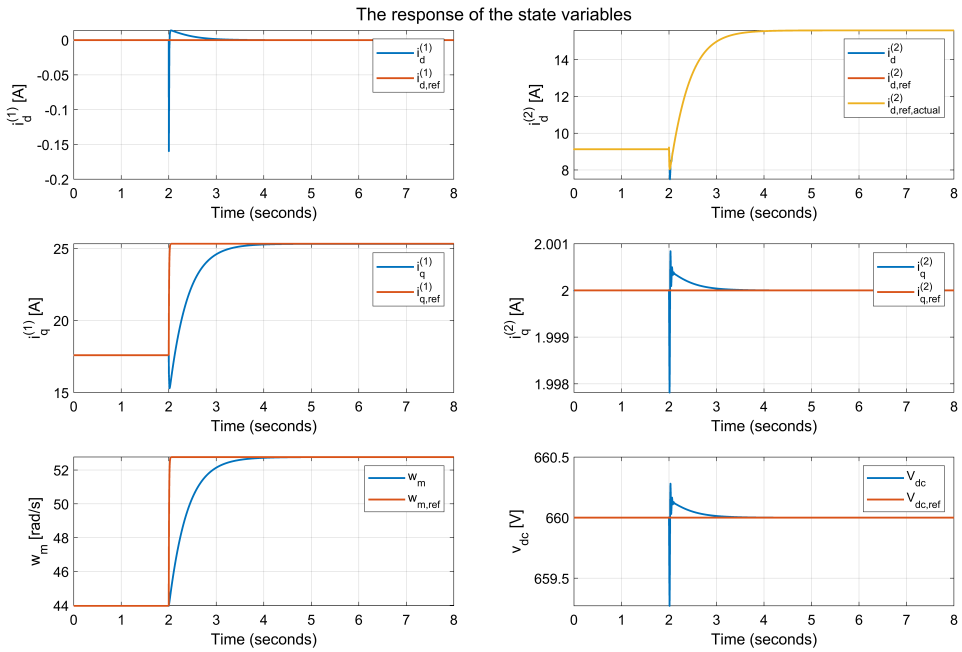

Figure 5.1: The state variable response when doing a simulation of the full system assuming perfect knowledge of the equilibrium

The system is observed to converge to the equilibrium point and achieve stability. As expected, when the system has full knowledge of the equilibrium point, it is observed that $x^* = \bar{x}$. Although some characteristics associated with non-minimum phase systems are still present in Figure 5.1, their impact is relatively small. However, to limit the magnitude of the q-axis current deviation on the primary side, several measures can be considered. These include designing the wind speed estimator to intentionally operate at a slower rate, selecting a generator with an even higher number of pole pairs to reduce the required current, or using a ramp instead of a step in the actual wind speed, which could be argued to be a closer approximation to reality. Since the deviation is already within reasonable limits due to designing the outer loop relatively slow, this thesis will satisfy with the result obtained.

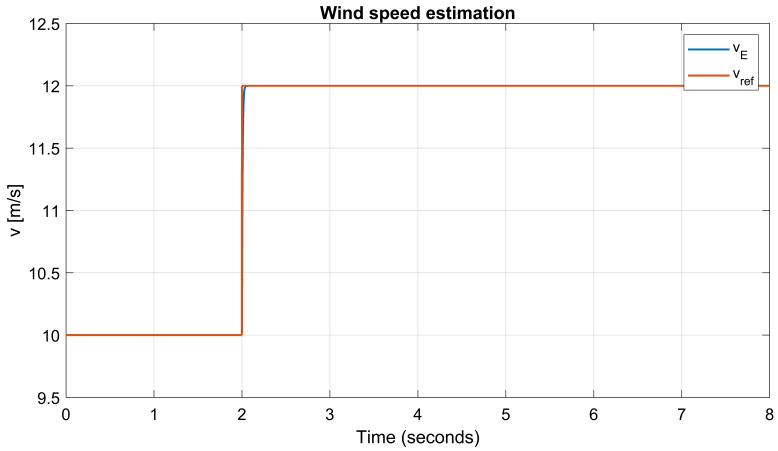

Figure 5.2: The wind speed estimator when doing a simulation of the full system assuming perfect knowledge of the equilibrium

Based on the figure presented above, it is evident that the wind speed estimator exhibits accuracy and achieves the desired results rapidly. Further, both $u_1^{(2)}$ and $u_2^{(2)}$ are observed to be working within their operating range of $[-0.5\ 0.5]$, as seen in Figure 5.3. Both control variables on the secondary side follow their references perfectly and stabilize on a constant value after a short time. The requested voltage is also met for the voltage on the primary side.

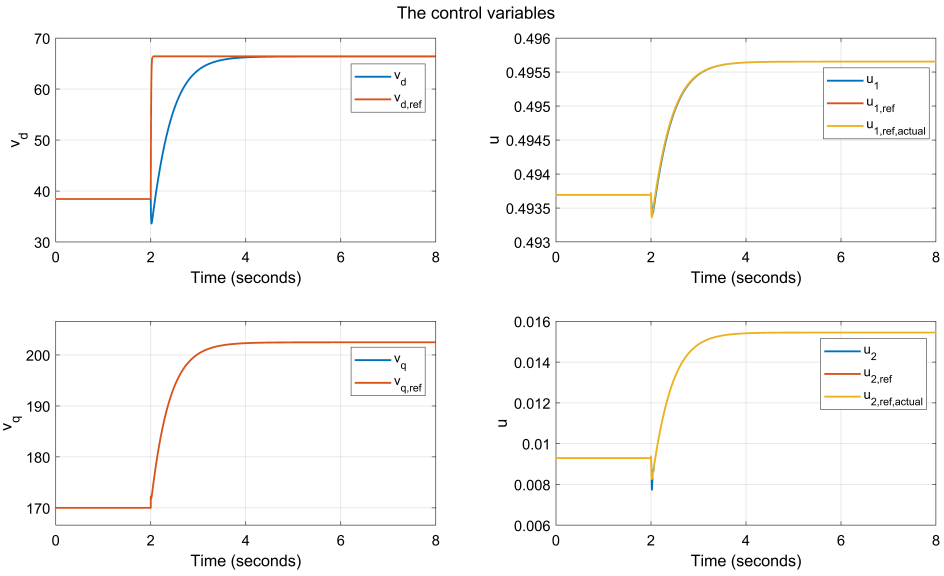

Figure 5.3: The response of the control variables when doing a simulation of the full system assuming perfect knowledge of the equilibrium

Finally, the power from the generator can be found. Using the power formula for $P = \frac{3}{2}(e_d i_d + e_q i_q)$, the following figure is obtained from simulations. The final power is right above 5kW, and consequently, the PMSG will operate just above the rated value for a wind speed of $12m/s$.

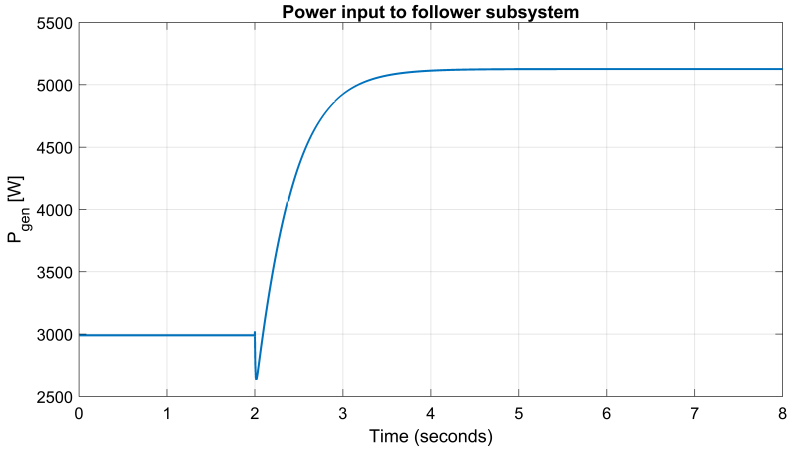

Figure 5.4: The generator power when doing simulation of the full system assuming perfect knowledge of the equilibrium

If, on the other hand, one does not possess perfect information of the system, which often is the case in reality, the requested equilibrium may deviate from the actual equilibrium point. This is the case for the response given in Figure 5.5. In this scenario, the new reference power input from the primary side is not immediately updated when a step in wind speed is performed. This will first happen at t=6s. For the d-axis current and the control variables on the secondary side, $(\cdot)_{\text{ref,actual}}$ refers to what the reference would be if the information were updated, while $(\cdot)_{\text{ref}}$ is the provided reference from the load flow.

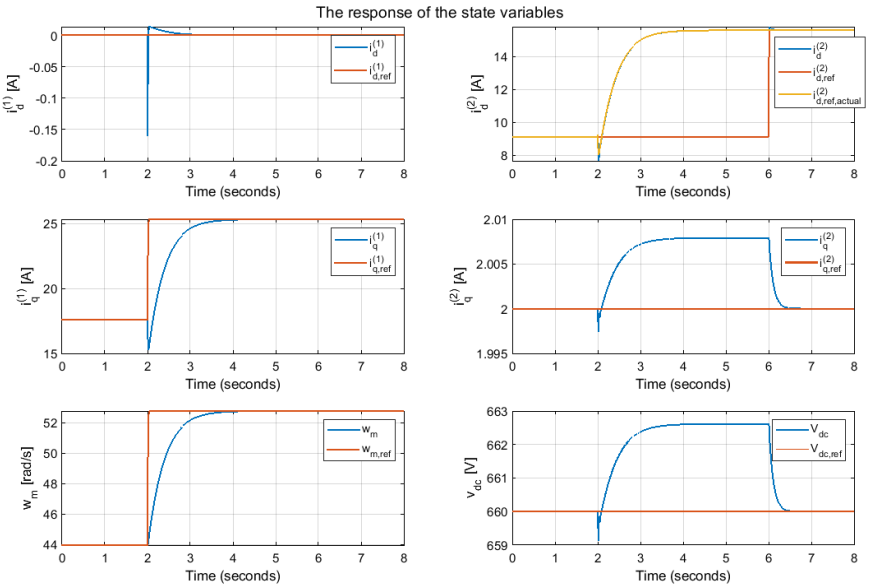

Figure 5.5: The response of the state variables when doing simulation of the full system and not having full knowledge of the equilibrium

As can be observed, $i_d^{(2)}$ follows the actual new reference after the step in input power, and the q-axis current on the secondary side only deviates $0.008A$ from the requested value. The voltage has a deviation

of approximately $2.6V$, which is within a reasonable range, given the inaccuracies provided. The response of the control variables, given in Figure 5.6, also shows that they operate within the limits, and it is observed that $u_1^{(2)}$ follows its original reference, while $u_2^{(2)}$ is now finding the new control reference. This is expected since the integral action for $u_1^{(2)}$ is designed to match the predefined $u_1^{(2),ref}$, while the other control variable is a function of the passive output, as described in (4.6.8) and (4.6.9).

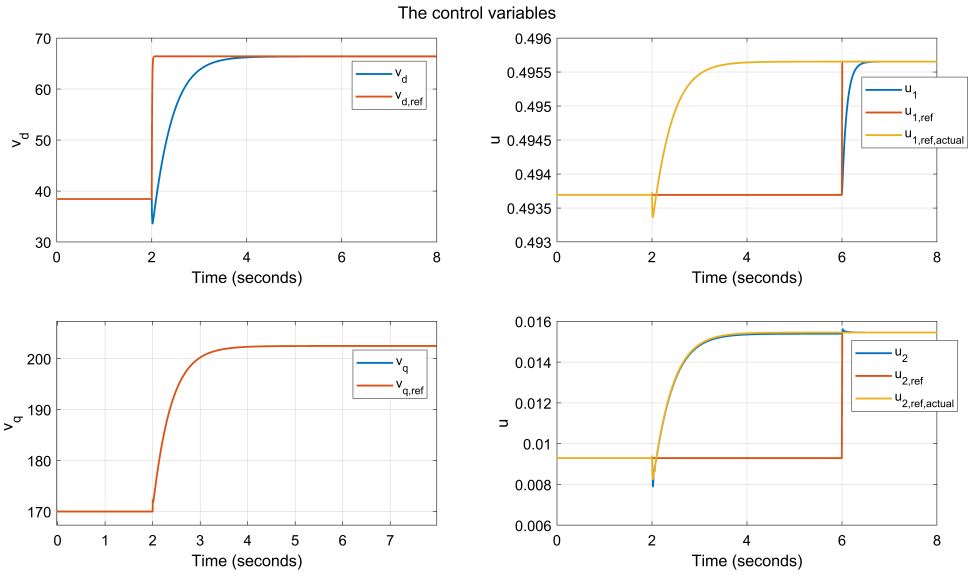

Figure 5.6: The response of the control variables when doing a simulation of the full system and inaccurate knowledge of the equilibrium

In summary, the simulations conducted provide confirmation of the system's stability, effectively mitigating the impact of uncertainties, and the obtained stability certificate presented in this thesis has been successfully validated.

Chapter 6

Conclusion and Further Work

In this master thesis, a comprehensive study was conducted to provide a large-signal stability certificate for a wind energy conversion system consisting of a wind turbine connected to a permanent magnet synchronous generator, followed by a full-scale back-to-back two-level voltage source converter connected to the grid. The main objectives were to analyze the system stability, design effective control strategies, and address the challenges posed by nonlinearities and uncertainties in wind speed and the equilibrium to be stabilized.

The stability analysis and control design are made arguably less complex by *forcing* the system to behave as a cascade connection of two subsystems. The chosen controller for the leader system (WT, PMSG, machine side 2LVSC) is the proportional-integral current controller, which is shown to have prominent plug-and-play features, provided sufficient mechanical damping. Since the leader subsystem is now unaffected by the follower, an adaptive control law based on Immersion and Invariance was designed, only requiring full knowledge of the primary side and thus offering promising scalability properties. Three different I&I estimators were developed to estimate the mechanical torque, mechanical power, and finally, the wind speed. These estimators exhibited high convergence speed and accurate estimation, contributing to the optimal operation of the conversion system. When including all the nonlinearities regarding the wind speed, multiple equilibrium points for the rotor speed were observed, given a specific mechanical torque. To account for this, an outer loop was incorporated into the simulations. However, this additional loop introduces characteristics associated with a non-minimum-phase system, adding complexity to the overall system behavior and compromising the stability analysis to a certain extent.

For the follower subsystem (grid-side 2L-VSC, grid), the goal was to ensure global asymptotic stability, even under the case of inaccurate knowledge of the equilibrium to be stabilized. Initially, a PLI-PBC (a PI with an additional leakage term in the integral channel) was considered, but due to poor performance and its failure to limit voltage deviations within acceptable limits, the controller was modified in the following two ways. First, the passive output is only included in the control input q-channel without any leakage action. Conversely, the control input d-channel had an important leakage term and did not utilize the passive output. These two changes resulted in indirectly controlling the voltage with one control input while regulating the q-axis current to zero with the other. This modification significantly improved the performance, complied with the control objectives while ensuring global asymptotic stability.

Taking all the challenging non-linearities in the generator dynamics, power converters, and between wind speed and mechanical torque, a viable Lyapunov candidate is obtained for both the leader and the follower subsystem. Finally, simulations were performed for the full system, which validated the theoretical results obtained throughout the study, and demonstrated the effectiveness of the method.

The outcomes of this master thesis contribute to the understanding and development of large-signal stability certificates and control strategies for wind energy conversion systems. The proposed techniques, including the cascaded structure, I&I-based adaptive control, and PLI-PBC design for 2L-VSCs, showcase promising results in terms of stability.

6.1 Future work

1. **Enhancement of Damper Windings Model**: It is recommended to explore and develop a more realistic model that effectively describes the behavior of short-circuited copper bars.
2. **Integration of Mechanical Rotor Speed Error**: To avoid the need for an outer loop speed controller, an alternative approach worth investigating is modifying the controller of the leader system to integrate the mechanical speed error into one of the control inputs instead of using the passive output.
3. **Utilization of Singular Perturbation Theory**: Alternatively, the application of singular perturbation theory, a mathematical tool for analyzing systems with multiple time scales, could prove valuable for studying the wind conversion system. Given the time scale separation between the outer loop and the rest of the system, incorporating the outer loop into the stability proof should be explored.
4. **Application of Graph Theory**: In order to extend the model from a single wind turbine to a wind park, the use of graph theory is recommended. This approach enables the investigation of the stability of the entire system, providing valuable insights.
5. **Improved Power Coefficient Curve**: The power coefficient curve $C_p(\lambda)$ used in this thesis guarantees only regional asymptotic stability. Hence, for future work, it is preferable to employ a wind turbine with a power coefficient curve that satisfies the requirements for global asymptotic stability.
6. **Estimation of Multiple Parameters**: Further exploration can be conducted to investigate if I&I can be used to estimate the magnetic flux, and combine this with the estimation of the wind.

Bibliography

1. Chang, V. *et al.* The market challenge of wind turbine industry-renewable energy in PR China and Germany. *Technological Forecasting and Social Change* **166,** 120631 (2021).
2. Sourmehi, C. EIA projects nearly 50% increase in world energy use by 2050, led by growth in renewables. *Today in Energy* (2021).
3. Growing, I. G. E. D. I. *Faster than Renewables, Driving Strong Increase in Generation from Fossil Fuels*
4. Qazi, H., Nolan, S. & Wall, P. Technical shortfalls for pan European power system with high levels of renewable generation (Apr. 2020).
5. Rampokanyo, M. *et al.* Impact of high penetration of inverter-based generation on system inertia of networks. *Electra* (2021).
6. Carrasco, J. *et al.* Power-Electronic Systems for the Grid Integration of Renewable Energy Sources: A Survey. *IEEE Transactions on Industrial Electronics* **53,** 1002–1016 (2006).
7. Muljadi, E. & Butterfield, C. Pitch-controlled variable-speed wind turbine generation. *IEEE Transactions on Industry Applications* **37,** 240–246 (2001).
8. Prabaharan, N., Rini Ann Jerin, A., Najafi, E. & Palanisamy, K. in *Hybrid-Renewable Energy Systems in Microgrids* (eds Fathima, A. H. *et al.*) 97–107 (Woodhead Publishing, 2018). ISBN: 978-0-08-102493-5. https://www.sciencedirect.com/science/article/pii/B9780081024935000066.
9. Surdal, E. *Plug-and-Play control of PMSG-based Wind Turbines* Project report in TET4900 (Department of Electric Power Engineering, NTNU – Norwegian University of Science and Technology, Dec. 2023).
10. Van Der Schaft, A., Jeltsema, D. *et al.* Port-Hamiltonian systems theory: An introductory overview. *Foundations and Trends® in Systems and Control* **1,** 173–378 (2014).
11. Khalil, H. K. Lyapunov stability. *Control Systems, Robotics and AutomatioN* **12,** 115 (2009).
12. Lozano, R., Brogliato, B. & Landau, I. Passivity and global stabilization of cascaded nonlinear systems. *IEEE Transactions on Automatic Control* **37,** 1386–1388 (1992).
13. Astolfi, A. & Ortega, R. Immersion and invariance: a new tool for stabilization and adaptive control of nonlinear systems. *IEEE Transactions on Automatic Control* **48,** 590–606 (2003).
14. Freeman, R. Nonlinear and Adaptive Control with Applications (Astolfi, A.; 2008) [Bookshelf]. *IEEE Control Systems Magazine* **31,** 90–92 (2011).
15. Mosavi, A. H. *et al.* Deep learning fuzzy immersion and invariance control for type-I diabetes. *Computers in Biology and Medicine* **149,** 105975. ISSN: 0010-4825. https://www.sciencedirect.com/science/article/pii/S0010482522007028 (2022).
16. Hu, J. & Zhang, H. Immersion and invariance based command-filtered adaptive backstepping control of VTOL vehicles. *Automatica* **49,** 2160–2167. ISSN: 0005-1098. https://www.sciencedirect.com/science/article/pii/S000510981300188X (2013).

17. Østergaard, K. Z., Brath, P. & Stoustrup, J. **75,** 012082. https://dx.doi.org/10.1088/1742-6596/75/1/012082 (July 2007).

18. Astolfi, A. & Karagiannis, D. *Nonlinear and Adaptive Control with Applications* ISBN: 978-1-84800-065-0 (Jan. 2007).

19. Golestan, S., Joorabian, M., Rastegar, H., Roshan, A. & Guerrero, J. M. *Droop based control of parallel-connected single-phase inverters in D-Q rotating frame* in *2009 IEEE International Conference on Industrial Technology* (2009), 1–6.

20. Freire, N., Estima, J. & Cardoso, A. A Comparative Analysis of PMSG Drives Based on Vector Control and Direct Control Techniques for Wind Turbine Applications. *Przeglad Elektrotechniczny* **88,** 184–187 (Jan. 2012).

21. Cisneros, R., Gao, R., Ortega, R. & Husain, I. *An adaptive passivity-based controller for a wind energy conversion system* in *2019 IEEE 58th Conference on Decision and Control (CDC)* (2019), 4852–4857.

22. Tutturen, T. M. & Nyhus-Solli, J. *Towards Plug-and-Play Control of Wind Power Systems: Scalable stability certificate guaranteeing large signal stability for entire wind parks* MA thesis (NTNU, 2022).

23. Kinnunen, J., Pyrhonen, J., Niemela, M., Liukkonen, O. & Kurronen, P. Design of damper windings for permanent magnet synchronous machines. *INTERNATIONAL REVIEW OF ELECTRICAL ENGINEERING-IREE* **2,** 260–272 (2007).

24. Monshizadeh, N., Monshizadeh, P., Ortega, R. & van der Schaft, A. Conditions on shifted passivity of port-Hamiltonian systems. *Systems & Control Letters* **123,** 55–61 (2019).

25. De La Sen, M. *Dynamic Systems: Passivity and Positivity Properties* in *IOP Conference Series: Materials Science and Engineering* **472** (2019), 012013.

26. Johnson, C. R. Positive definite matrices. *The American Mathematical Monthly* **77,** 259–264 (1970).

27. Sun, T., Wang, J. & Chen, X. Maximum torque per ampere (MTPA) control for interior permanent magnet synchronous machine drives based on virtual signal injection. *IEEE Transactions on Power Electronics* **30,** 5036–5045 (2014).

28. Zhang, F. *The Schur complement and its applications* (Springer Science & Business Media, 2006).

29. Gil, W., Montoya, O. D., Garces, A. *et al.* Direct power control of electrical energy storage systems: A passivity-based PI approach. *Electric Power Systems Research* **175,** 105885 (2019).

30. Ortega, R., Van Der Schaft, A., Mareels, I. & Maschke, B. Putting energy back in control. *IEEE Control Systems Magazine* **21,** 18–33 (2001).

31. Bergna-Diaz, G., Zonetti, D., Sanchez, S., Ortega, R. & Tedeschi, E. PI Passivity-Based Control and Performance Analysis of MMC Multiterminal HVDC Systems. *IEEE Journal of Emerging and Selected Topics in Power Electronics* **7,** 2453–2466 (2019).

32. Cisneros, R., Gao, R. & Husain, I. PI Passivity-Based Control for Maximum Power Extraction of a Wind Energy System with Guaranteed Stability Properties. *International Journal of Emerging Electric Power Systems* **17** (Jan. 2016).

33. Zonetti, D., Ortega, R. & Benchaib, A. Modeling and control of HVDC transmission systems from theory to practice and back. *Control Engineering Practice* **45,** 133–146. ISSN: 0967-0661. https://www.sciencedirect.com/science/article/pii/S096706611530023X (2015).

34. Song, Y., Dhinakaran, B. & Bao, X. Variable speed control of wind turbines using nonlinear and adaptive algorithms. *Journal of wind engineering and industrial aerodynamics* **85,** 293–308 (2000).

35. RHAILI, S. E., ABBOU, A., HICHAMI, N. E. & MARHRAOUI, S. *A New Strategy Based Neural Networks MPPT Controller for Five-phase PMSG Based Variable-Speed Wind Turbine* in *2018 7th International Conference on Renewable Energy Research and Applications (ICRERA)* (2018), 1038–1043.

36. Mendi, B., Pattnaik, M. & Srungavarapu, G. *A Speed Sensorless Modified Perturb and Observe MPPT Scheme for Stand-alone PMSG based Wind Turbine System* in *2022 IEEE IAS Global Conference on Emerging Technologies (GlobConET)* (2022), 338–342.

37. Soltani, M. N. *et al.* Estimation of Rotor Effective Wind Speed: A Comparison. *IEEE Transactions on Control Systems Technology* **21,** 1155–1167 (2013).

38. Ma, X., Poulsen, N. & Bindner, H. *Estimation of Wind Speed in Connection to a Wind Turbine* English (Informatics and Mathematical Modelling, Technical University of Denmark, DTU, 1995).

39. Ortega, R., Mancilla-David, F. & Jaramillo, F. *A globally convergent wind speed estimator for windmill systems* in *2011 50th IEEE Conference on Decision and Control and European Control Conference* (2011), 6079–6084.

40. Cisneros, R., Mancilla-David, F. & Ortega, R. Passivity-Based Control of a Grid-Connected Small-Scale Windmill With Limited Control Authority. *IEEE Journal of Emerging and Selected Topics in Power Electronics* **1,** 247–259 (2013).

41. Mancilla-David, F. & Ortega, R. Adaptive passivity-based control for maximum power extraction of stand-alone windmill systems. *Control Engineering Practice* **20,** 173–181. ISSN: 0967-0661. https://www.sciencedirect.com/science/article/pii/S0967066111002139 (2012).

42. Liu, Y., Pamososuryo, A. K., Ferrari, R. M. G. & van Wingerden, J.-W. The Immersion and Invariance Wind Speed Estimator Revisited and New Results. *IEEE Control Systems Letters* **6,** 361–366 (2022).

43. Ortega, R., Liu, X., Su, H. & chu, J. Immersion and Invariance Adaptive Control of Nonlinearly Parameterized Nonlinear Systems *. *IFAC Proceedings Volumes* **43.** 8th IFAC Symposium on Nonlinear Control Systems, 641–646. ISSN: 1474-6670. https://www.sciencedirect.com/science/article/pii/S1474667015370361 (2010).

44. Liu, X., Ortega, R., Su, H. & Chu, J. *Identification of nonlinearly parameterized nonlinear models: application to mass balance systems* in *Proceedings of the 48h IEEE Conference on Decision and Control (CDC) held jointly with 2009 28th Chinese Control Conference* (2009), 4682–4685.

45. Isidori, A. *Nonlinear control systems: an introduction* (Springer, 1985).

46. Slotine, J.-J. E., Li, W. *et al. Applied nonlinear control* **1** (Prentice hall Englewood Cliffs, NJ, 1991).

47. Hauser, J., Sastry, S. & Meyer, G. Nonlinear control design for slightly non-minimum phase systems: Application to V/STOL aircraft. *Automatica* **28,** 665–679. ISSN: 0005-1098. https://www.sciencedirect.com/science/article/pii/000510989290029F (1992).

48. Ho, D. & Karl Hedrick, J. *Control of nonlinear non-minimum phase systems with input-output linearization* in *2015 American Control Conference (ACC)* (2015), 4016–4023.

49. Hernandez-Gomez, M., Ortega, R., Lamnabhi-Lagarrigue, F. & Escobar, G. Adaptive PI Stabilization of Switched Power Converters. *IEEE Transactions on Control Systems Technology* **18,** 688–698 (2010).

50. Jaafar, A., Alawieh, A., Ortega, R., Godoy, E. & Lefranc, P. PI Stabilization of Power Converters With Partial State Measurements. *IEEE Transactions on Control Systems Technology* **21,** 560–568 (2013).

51. Zonetti, D., Bergna-Diaz, G. & Ortega, R. *P+leaky I passivity-based control of power converters* in *2020 59th IEEE Conference on Decision and Control (CDC)* (2020), 854–859.

52. Hunyár, M. & Veszprémi, K. *Reactive power control of wind turbines* in *2014 16th International Power Electronics and Motion Control Conference and Exposition* (2014), 348–352.

Appendix

A.1 Estimate ϕ

For the estimation of the flux parameter, the differential equation of ρ will be considered first. Let the estimation parameter be defined as in Equation (A.1.1), and the error between the estimated and real value of the parameter as in Equation (A.1.2).

$$\phi^E := \beta(\Psi_q, \rho) + \zeta \tag{A.1.1}$$

$$e_\phi := \phi^E - \phi \tag{A.1.2}$$

This gives:

$$\begin{aligned} \phi &= \phi^E - e_\phi \\ &= \beta(\Psi_q, \rho) + \zeta - e_\phi \end{aligned} \tag{A.1.3}$$

It is desired to have the error converge to zero, and the derivative of the error is therefore calculated. Since the actual value of the parameter is regarded as a constant in the estimation process, the derivative of this will be zero.

$$\begin{aligned} \dot{e}_\phi = \dot{\phi}^E &= \nabla\beta(\Psi_q, \rho) \cdot \begin{bmatrix} \dot{\Psi}_q \\ \dot{\rho} \end{bmatrix} + \dot{\zeta} \\ &= \nabla\beta(\Psi_q, \rho) \cdot \begin{bmatrix} -ri_q - Li_d\frac{P}{2}\omega_m + (\phi^E - e_\phi)\frac{P}{2}\omega_m - v_q \\ T_m - \frac{P}{2}(\phi^E - e_\phi)i_q + d(\omega_{ref} - \omega_m) \end{bmatrix} + \dot{\zeta} \end{aligned} \tag{A.1.4}$$

Since it is now desired to construct ζ in such a way that only the term containing the error remains in the above equation, ζ is defined as in Equation (A.1.5).

$$\dot{\zeta} = -\nabla\beta(\Psi_q, \rho) \cdot \begin{bmatrix} -ri_q - Li_d\frac{P}{2}\omega_m + \phi^E\frac{P}{2}\omega_m - v_q \\ T_m - \frac{P}{2}\phi^E i_q + d(\omega_{ref} - \omega_m) \end{bmatrix} \tag{A.1.5}$$

The error function will then take the form:

$$\begin{aligned} \dot{e}_\phi &= -\nabla\beta(\Psi_q, \rho) \cdot \begin{bmatrix} -e_\phi\frac{P}{2}\omega \\ e_\phi\frac{P}{2}i_q \end{bmatrix} \\ &= -\frac{\partial\beta}{\partial\Psi_q}e_\phi\frac{P}{2}\omega + \frac{\partial\beta}{\partial\rho}e_\phi\frac{P}{2}i_q \end{aligned} \tag{A.1.6}$$

As can be noticed from the above equation, the error dynamics is dependant on the $\beta(\rho)$-function, the mechanical rotor speed, and the quadrature current, which implies a nonlinear behavior where the two latter parameters act as a non-constant disturbance.

The direct Lyapunov method can now be used, and the Lyapunov candidate is chosen as in Equation (A.1.7), and the derivative is given in (A.1.8).

$$V(e_r) = \frac{1}{2} e_\phi^2 \tag{A.1.7}$$

$$\begin{aligned} \dot{V}(e_\phi) &= e_\phi \dot{e}_\phi \\ &= e_\phi^2 (-\frac{\partial \beta}{\partial \Psi_q} \frac{P}{2} \omega + \frac{\partial \beta}{\partial \rho} \frac{P}{2} i_q) \end{aligned} \tag{A.1.8}$$

Requiring the above equation to be negative definite, it was yet not successful to find a β-function that satisfy the requirement.

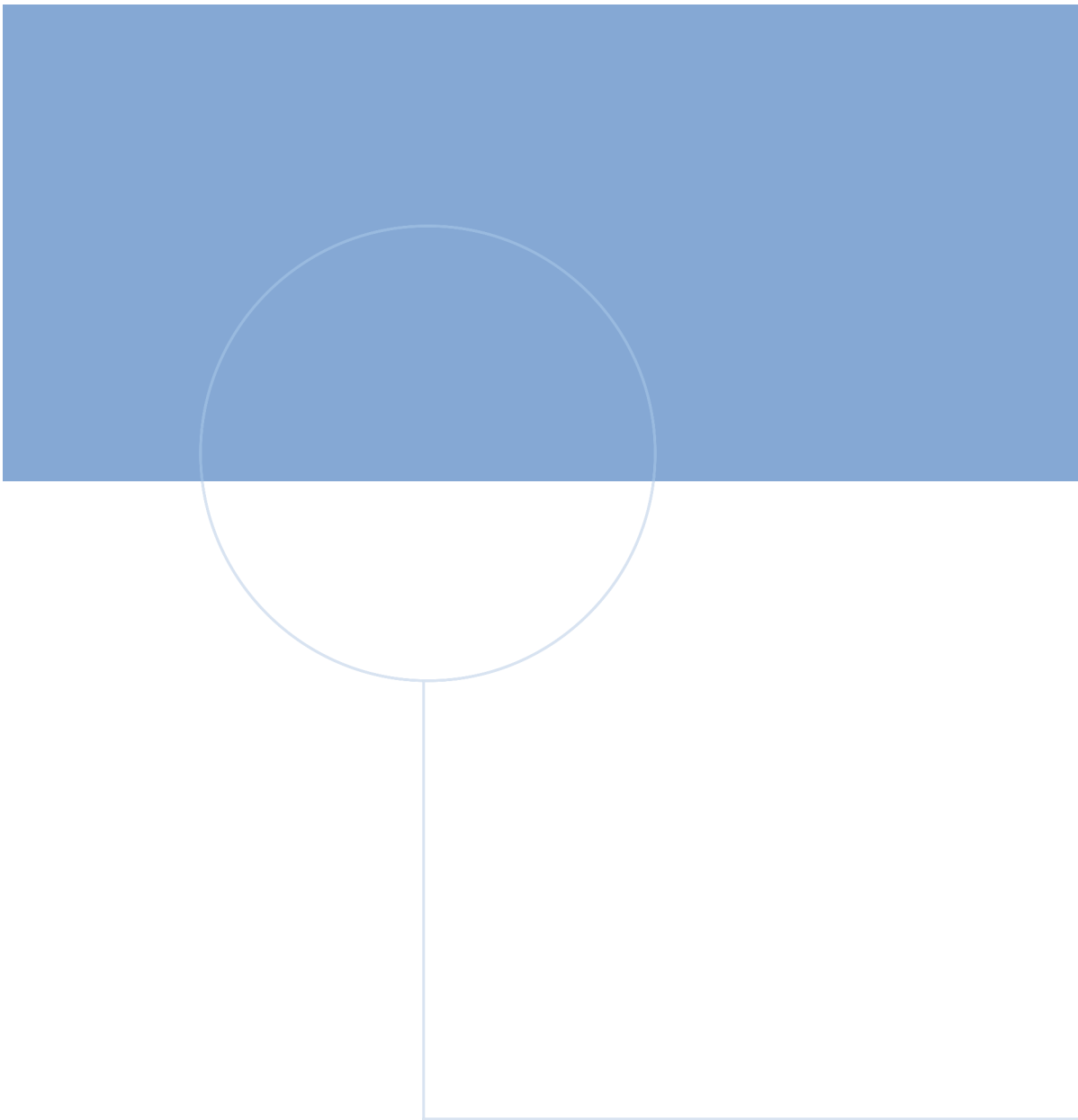

NTNU

Norwegian University of
Science and Technology